CHARACTERIZATION AND MODELING OF SHEAR STRESS DURING MANUFACTURING AND THERMAL PROPERTIES OF STRUCTURAL COMPOSITE MATERIALS

A Dissertation by

Ronald Vicente Joven Pineda

Master of Engineering, Universidad de los Andes, Colombia, 2009

Mechanical Engineer, Universidad de los Andes, Colombia, 2007

Submitted to the Department of Mechanical Engineering
and the faculty of the Graduate School of
Wichita State University
in partial fulfillment of
the requirements for the degree of
Doctor of Philosophy

July 2013

Copyright 2013 by Ronald Vicente Joven Pineda

All Rights Reserved

CHARACTERIZATION OF SHEAR STRESS DURING MANUFACTURING AND THEMRAL PROPERTIES OF STRUCTURAL COMPOSITE MATERIALS

The following faculty members have examined the final copy of this dissertation for form and content, and recommend that it be accepted in partial fulfillment of the requirement for the degree of Doctor of Philosophy with a major in Mechanical Engineering

_____
Bob Minaie, Committee Chair

_____
Krishna Krishnan, Committee Member

_____
Hamid Lankarani, Committee Member

_____
Tiruvadi Ravigururajan, Committee Member

_____
Brian Driessen, Committee Member

Accepted for the College of Engineering

_____
Vishwanath Prasad, Interim Dean

Accepted for the Graduate School

_____
Abu Masud, Interim Dean

DEDICATION

To mom, dad, and my siblings

ACKNOWLEDGEMENTS

I would like to thank my advisor, Dr. Bob Minaie for his years of guidance and support. I would also like to extend my gratitude to the members of my committee, Dr. Krishna Krishnan, Dr. Hamid Lankarani, Dr. Tiruvadi Ravigururajan, and Dr. Brian Driessen for their helpful comments and suggestions for this dissertation. Thanks are also due to all who contributed directly or indirectly to this work, especially to my colleagues Alejandro Rodriguez, Mauricio Guzman, Chee Sern Lim, Pooneh Roozbejavan, Behrouz Tavakol, Hoda Koushar, Rony Das, Ashraf Ahmed, Joseph Schaefer, Khalil Vora, Mohammad Habibi, and Amdadul Islam

ABSTRACT

An experimental methodology is presented to determine tool-part frictional interaction of composite parts and the structural integrity of sandwich structures when subjected to temperatures and pressures similar to those of autoclave processing. This methodology includes the development of a testing rig that mimics the deformation mismatch between tools and parts, and quantifies shear stress—that is, tool-part friction or shear stress of sandwich structures. Discrete and continuous friction characterization was performed to validate this testing methodology, and a semiempirical mathematical model was obtained to predict the tool-part frictional interaction as a function of different manufacturing variables including temperature, pressure, and part length. Moreover, a characterization of the shear strength of sandwich structures is presented where results indicate a strength decrease when temperature and pressure increase following an inverse-exponential trend for both cases.

Furthermore, an alternative methodology to measure thermal properties of composite materials by radiation known as light flash analysis (LFA) is used to characterize diffusivity, conductivity, and specific heat of composite materials tested at typical manufacturing temperatures. Accordingly, this research portrays the mathematical considerations required for the testing of anisotropic materials. Thermal properties of cured composite samples with three different fabric weaves and two resin formulations were obtained, and results indicate that conductivity, diffusivity, and density are strongly influenced by testing temperature, fiber configuration, and fiber volume fraction.

TABLE OF CONTENTS

TABLE OF CONTENTS (continued)

Chapter Page

TABLE OF CONTENTS (continued)

LIST OF TABLES

LIST OF FIGURES

LIST OF FIGURES (continued)

LIST OF FIGURES (continued)

Figure Page

LIST OF ABBREVIATIONS/NOMENCLATURE

8HS	Eight-harness satin weave
ASTM	American Society for Testing and Materials (Standard Testing Method)
CFRP	Carbon Fiber-Reinforced Polymers
COF	Coefficient of Friction
CTE	Coefficient of Thermal Expansion
DOE	Design of Experiments
DSC	Differential Scanning Calorimeter
LFA	Light Flash Analyzer
MRCC	Manufacturer's Recommended Cure Cycle
PW	Plain Weave
TFE	Tetrafluoroethylene
TMA	Thermomechanical Analyzer
UD	Unidirectional Tape
UTM	Universal Testing Machine

LIST OF SYMBOLS

A	Area
μ_k	Coefficient of friction, Kinetic
μ_k	Coefficient of Friction, Static
CTE_{part}	Coefficient of Thermal Expansion of the part
CTE_{tool}	Coefficient of Thermal Expansion of the tool
v_{max}	Crosshead pull-out speed
º	Degree
ρ	Density
x	Distance
F'	Frictional force
L	Half of part length
Q	Heat
$\Delta T/\Delta t$	Heat-up ramp
L_{oij}	Length at room temperature
$\Delta L\ (T)_{ij}$	Length change, Thermal expansion
$Tan\ (\delta)$	Loss tangent
G'	Moduli, elastic
G''	Moduli, viscous
F_N	Normal Force
P	Pressure
R_q	Root-mean-squared surface roughness
L	Sample Thickness

w	Sample weight in air
w_w	Sample weight in water
F	Shear Force
t	Shear Stress
C_p	Specific heat
v	Speed of the part relative to the tool
$\varepsilon_{ij}\ (T)$	Strain
T	Temperature
ΔT_r	Temperature change, reference
ΔT_s	Temperature change, sample
k	Thermal Conductivity
α	Thermal Diffusivity
t	Time

CHAPTER 1

INTRODUCTION

1.1 Motivation and Scope

Carbon fiber-epoxy composites and sandwich structures are widely used in the aerospace industry due to their specific strength and stiffness, which represents a considerable weight reduction in airframe structures compared with those made of aluminum. However, one of the major setbacks of using these composites is the geometrical distortion of parts and the crush of sandwich structures that is caused by residual stresses induced during manufacturing. In this context, an important contributor to residual shear stress is the frictional interaction and the mismatch in thermal deformation between tools and parts during autoclave processing. Furthermore, irregular heat flow through parts, which is caused by the anisotropic thermal properties of composite materials, might cause gradients in degree of cure and thermal expansion that can result in residual stresses and uneven mechanical properties. As such, the study of tool-part contact shear stress and thermal properties of composite materials is crucial to predict geometrical distortion in composites.

Composite parts manufacturing has been challenging due to part distortion resulting from different deformation mechanisms and frictional interactions between tools and parts (Figure 1). Deformation mechanisms are typically caused by resin cure shrinkage [1], different coefficients of thermal expansion (CTE) within ply, and CTE mismatch between tools and parts [2], while frictional interactions are developed due to high autoclave pressure. The tools used for composites manufacturing are commonly made of isotropic materials including ferrous alloys and aluminum where their CTE values range from 1.6 (INVAR) to 23.6 μm/(m·ºC) (aluminum) [3]. For anisotropic materials like carbon epoxy composites, the CTE value depends on fiber

orientation since composites have less thermal expansion in fiber direction (-0.5 µm/(m·ºC)) than in transverse direction (32.0 µm/(m·ºC)) [3]. Additionally, thermoset composites develop geometrical changes caused by chemical shrinkage of the resin, layup compaction, and thickness reduction due to resin bleeding. The residual stresses induced by CTE mismatch and cure shrinkage might result in geometrical distortion when the part is removed from the tool.

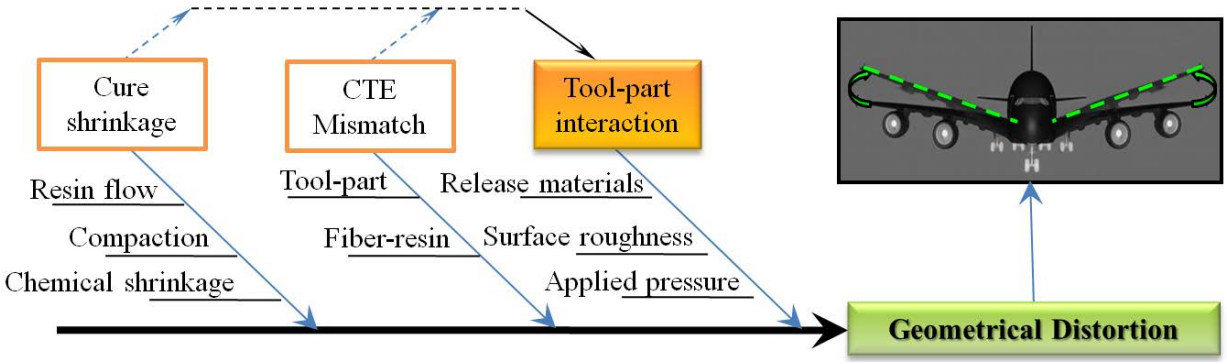

Figure 1. Factors that influence composite distortion caused by tool-part interaction

Friction force between tools and parts is an important source of geometrical distortion, which commonly induces part warpage [2, 4]. Due to the combined effect of elevated consolidation pressure (around 550 kPa), tool-part deformation mismatch, and tool-part friction, warpage is caused by a gradient of shear stress from the bottom layer in contact with the tool to the top layer of the composite part (see Figure 2a). When the autoclave pressure is released, the bottom layer contracts in order to liberate the elastic component of stress induced by the friction force during cure, causing a concave distortion with respect to the bottom layer [5].

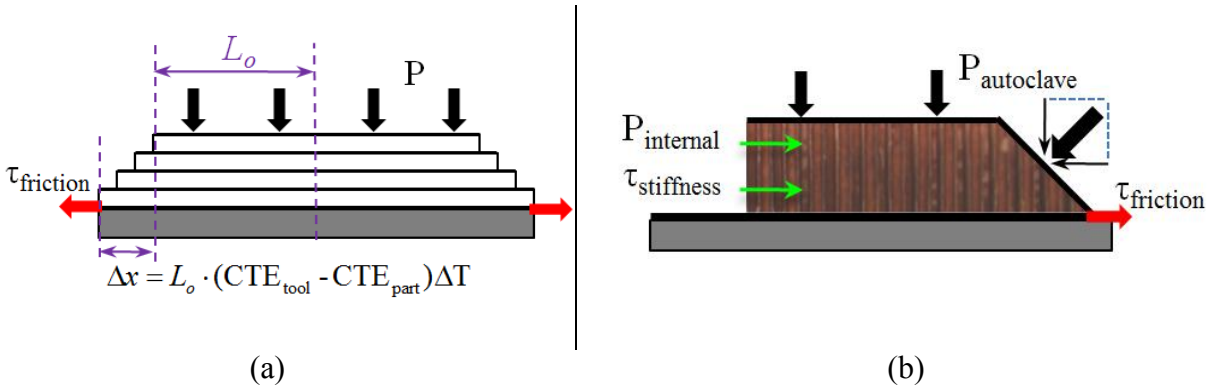

Figure 2. Autoclave force diagram for (a) prepreg and (b) sandwich structure

Additionally, these deformations mechanisms may induce transverse residual stresses during manufacturing of co-cured sandwich structures [6]. As illustrated in the free-body diagram of Figure 2b, residual shear stresses combined with transverse components of autoclave pressure might cause core crush during manufacturing. Opposite forces corresponding to shear stiffness of the sandwich structure and internal pressure of the core uphold the structural integrity of the part [7]. As such, it is crucial to measure the shear strength of cores when subjected to combined conditions of pressure and temperature in order to determine the manufacturing parameters of sandwich structures.

This research is aimed at studying tool-part interaction during the curing of carbon fiber-reinforced polymeric (CFRP) composites utilizing a customized testing rig that was developed to mimic autoclave manufacturing. Using this testing rig, tests were performed to measure the shear stress caused by friction while the rig reproduced the tool-part deformation mismatch phenomenon. Experiments were performed with coupons of CFRP prepreg—carbon-fiber fabric impregnated with epoxy resin—that were tested against an aluminum tool at different temperatures, pull-out speeds, consolidation pressures, and tool surface conditions. These results were used to determine the physical phenomena related to tool-part interaction, and to propose a

semi-empirical friction model. Using the aforementioned testing rig, subsequently, a novel methodology was implemented to determine the shear strength of sandwich structures and aramid honeycomb cores during manufacturing. Lastly, the thermal properties—thermal conductivity, diffusivity, and specific heat—of CFRP samples were measured using a radiation technique known as LFA. These tests were aimed at studying the difference between autoclave and out-of-autoclave prepregs made of different carbon fiber fabrics including plain weave, eight-harness satin weave, and unidirectional tape. Accordingly, the mathematical considerations required for thermal characterization of anisotropic materials by LFA method were portrayed, in which the volumetric thermal expansion was calculated considering the CTE mismatch between fiber and trough-the-thickness directions of the samples. The findings presented in this research will provide a better understanding of the residual stress induced during autoclave manufacturing that can compromise the quality of structural composite materials.

1.2 Objectives

The main objective of this research is to develop a mathematical approach to the frictional interaction caused by tool-part deformation mismatch during autoclave manufacturing of composites, with the aim of generating an expression that can be used in computational simulations to predict process induced distortion.

Two secondary objectives were addressed to study important setbacks of processing composite materials using autoclaves:

- Implementation of a testing methodology to measure shear strength of sandwich structures when subjected to combined conditions of temperature and pressure
- Study of thermal properties of CFRP by the LFA method and the relevance of fiber configuration

These objectives were tackled as follows: In Chapter 1 an introduction and problem definition is presented regarding to residual stresses that are induced in composite parts during autoclave manufacturing, which might cause geometrical distortion or compromise structural properties. Then, in Chapter 2 is provided a literature review, which includes studies related to tool-part interaction, core crush during autoclave processing of sandwich structures, and thermal properties of fiber-reinforced polymeric composites. In Chapter 3 is shown the development of a customized testing rig, which was used to measure the tool-part shear stress of composite samples and the shear strength of sandwich structures when subjected to pressures and temperatures typical of autoclave manufacturing. Using this rig, in Chapter 4 are depicted the findings corresponding to tool-part interaction during the cure cycle of a composite prepreg when subjected to autoclave manufacturing conditions. In addition, this chapter shows the development of a mathematical model to predict tool-part friction force. In Chapter 5 is portrayed the shear strength obtained for sandwich structures when subjected to combined conditions of temperature and pressure. Lastly, the characterization of thermal properties of composite materials at different temperatures was performed in Chapter 6 using the LFA method where composite samples with different fiber architecture and resin formulations were tested. In addition, the experimental considerations required for testing anisotropic materials were depicted.

CHAPTER 2

LITERATURE REVIEW

2.1 Tool-Part Interface

2.1.1 Experimental Methodologies Used to Measure Tool-Part Friction

Previous studies used customized devices to measure friction at pressures and temperatures typical of autoclave manufacturing of composite materials [5, 8-13]. Martin et al. [13] proposed a method to characterize the friction resistance of carbon fiber-epoxy prepregs that are commonly used in sandwich structures. In their approach, a customized device was used to quantify the friction interaction of prepreg-prepreg and prepreg-tool at different temperatures and constant pressure. The authors found that prepregs with high resin content had the lowest friction values and therefore were prone to cause core crush. Ersoy et al. [5] presented a method to characterize friction-induced shear stress at prepreg-prepreg and prepreg-tool interfaces by continuous pulling of overlapping plies during the ramp-up of the cure cycle of carbon-epoxy unidirectional composites. With this method, the authors identified the interfacial shear stress during cure and established a gel point-stress relationship. Kaushik et al. [12] measured the static and dynamic coefficient of friction as a function of degree of cure and implemented a computational model to predict the distortion of composite parts. Furthermore, the researchers studied the failure modes at the tool-part interface in which they identified adhesive bonding and cohesive failure of resin.

Twigg et al. [14] presented an alternative method to quantify the shear interaction at the tool-part interface using a tool instrumented with strain gages. The authors used modulations of temperature in the cure cycle to study changes in tool thermal strain due to interaction with a composite part. By analyzing the strain readings, the static and sliding frictions were identified

since the free thermal expansion of the tool was constrained due to tool-part adhesion when static friction occurred. In a different work, Twigg et al. [15] proposed an analytical model, which was experimentally validated, to predict the maximum part warpage as a function of modulus of elasticity, geometry (length and thickness), and manufacturing conditions (pressure and tool surface conditions) of composite parts. In their approach, they found that the maximum part warpage was affected by geometry, but it was independent of surface conditions when a release agent and a fluorinated ethylene propylene release film were used.

2.1.2 Release Materials

Materials such as fluorocarbon-based release films and polymeric release agents have been used to reduce friction between tools and parts during composite manufacturing [16]. Release films are used for simple geometries such as flat panels, while release agents are utilized in complex geometries where release films are impractical due to wrinkling. These materials reduce frictional interaction because the high rigidity and stability of fluorocarbon-based polymers like PTFE lead to small contact areas with most of the surfaces [17]. Researchers have studied the rigidity and microstructure of PTFE films with respect to temperature, showing that change in the film hardness with respect to temperature could vary the frictional interaction between tool and part [8, 18, 19]. Fote et al. [20] studied the friction behavior of PTFE as a function of temperature and indicated that the friction force decreased as temperature increased due to the change in hardness of the polymer.

2.1.3 Tool-Part Friction Modeling

In another perspective, mathematical models and computational simulations of tool-part interface are commonly used to predict the distortion of composite parts. Due to the complexity of developing a mathematical expression for tool-part contact, researchers have approximated

this frictional interaction using different alternatives. Johnston et al. [21] assumed perfect bonding conditions between tools and parts to simulate composite distortion. Zarrelli et al. [4], in a similar approach, simulated part warpage assuming that deformation mismatch of composites was equivalent to that of a bi-material strip made of resin and aluminum. Ferlund et al. [22] implemented in their simulations a thin body between the tool and the part where the mechanical properties of such body were changed to mimic bonded or sliding conditions. Zeng et al. [23] used a simplified friction model where the pressure-friction relation was assumed linear. Finally, Kaushik et al. [12] preformed simulations of part distortion where the frictional tool-part interaction values were obtained experimentally. Other studies predicted manufacturing-induced distortion of flat, L, and U shaped parts [24-26] where their computational models included a database of diverse properties of composite materials comprising thermal expansion during cure [27], thermal properties of composites and release materials [30], and an analysis of stress relaxation [28, 29].

Note that the modeling of tool-part frictional interaction is an incomplete area of research, which is crucial for computational simulations aimed at predicting process-induced composites distortion [9]. Therefore, herein was included an experimental study of tool-part contact and an analysis of the physics behind this frictional interaction in order to develop a mathematical model of the tool-part frictional phenomena (see Chapters 3 and 4).

2.2 Sandwich Structures

In the literature were found methodologies that can reduce or prevent core crush during autoclave manufacturing of sandwich structures. These studies mainly addressed three design parameters: the formulation of resins and skin-core adhesive layer, the implementation of fabric tie-down systems, and the development of high friction fabrics. Research was also performed to

characterize the shear strength of cores, which is the design parameter that determines what methodologies are required to avoid core crush.

2.2.1 Influence of Resin Formulation on Core Crush

Grove et al. [31] implemented the Taguchi's orthogonal design of experiments (DOE) to study the adhesive properties of a carbon fiber-epoxy prepreg when co-cured with hexagonal cell aramid honeycomb cores. The influence on core-skin adhesive properties of consolidation pressure, temperature profile, dwell temperature, and vacuum pressure was evaluated where temperature was identified as the dominant parameter. In a different approach, Renn et al. [7] utilized a factorial DOE to study core failure when subjected to similar manufacturing conditions presented by Grove et al, but the testing parameters also included different resin formulations and fabric configurations. Their tests indicated that resin formulation was the predominant parameter that affected the integrity of the cores because highly rubberized resins seemed to hold a greater amount of residual shear stress while lower rubberized ones caused higher areas of core crush. These results also agreed with the study presented by Martin et al. [13] who claimed that an important factor contributing to core crush is the shear interaction between prepreg-prepreg and prepreg-tool. Renn et al. also reported that core crush happened before the gel point of the resin, which was the region of the cure cycle where most of the process-induced residual stresses (such as CTE mismatch and resin chemical shrinkage) could be developed.

High performance core-skin adhesives have been used in sandwich structures to avoid resin trickling down to the core. Yuan et al. [32], indicated that this trickling increased air permeability of the skins, which caused a reduction in the internal pressure of the core. Low core pressure could reduce the shear strength of the structure and increase void content since the consolidation pressure on the skins was also reduced. A methodology to overcome this limitation

was presented by Kohli [33] who developed a nano-reinforced epoxy core-skin adhesive layer that reduced resin trickling to the core.

2.2.2 Methodologies to Prevent Core Crush by Fabric Tie-Down

A proper interaction between the layers of composite parts was found as an important factor to reduce core crush during manufacturing since a strong interaction between prepregs might restrain the transverse component of pressure to induce shear stresses on the core. Thus, Corbett et al. [34] and Hopkins et al. [35] developed a tie-down method to increase the prepreg-prepreg and prepreg-tool contact force by placing bonding agents between the trimming line and the edge of the part. Later, Erickson et al. [36] developed a method to reduce part distortion and core crush by gripping composite parts on the tool using a grove or step on the tool and a gripping fixture so that the movement of the layers was restrained.

2.2.3 Influence of Fabric Architecture on Core Crush

Martin et al. [37] studied different manufacturing parameters of prepregs to identify those that could generate a material designed to reduce core crush when utilized in sandwich panels as face sheets. Their findings indicated that prepregs manufactured using low fiber tension during impregnation reduced core failure during autoclave manufacturing. Moreover, it was observed that this prepreg had high prepreg-prepreg frictional interaction, which implied that this contact force reduced the stress transferred to the core. Prepregs manufactured with higher fiber tension, conversely, might squeeze out the resin impregnated in the tow, thus creating a prepreg-prepreg interface rich in resin that lubricated and reduced the frictional interaction among the plies.

Hsiao et al. patented [38] and tested [6] a core-crush resistant woven fabric characterized for its high prepreg-prepreg frictional interaction. This material was developed by optimizing fabric properties such as tow aspect ratio, prepreg thickness, and openness (filament twisting and

roundness) to increase the prepreg-prepreg friction by mechanical interlocking. Moreover, this fabric showed a low amount of resin on its surface (dry fabric) since the tow configuration allowed high viscosity resins to remain inside the tow, thus reducing the interply lubricant effect. Similarly, Schneider et al. [39] developed a fabric where the mechanism to increase friction force was based on a combination of twisted and untwisted fiber tows in the warp and fill directions of the fabric so that prepreg-prepreg friction was increased by tow mechanical interlocking.

2.2.4 Shear Strength of Cores

Pan et al. [40, 41] presented an experimental and analytical study of the shear strength of aluminum honeycomb cores tested at room temperature, following the ASTM C273 [42]. In these tests, the failure modes of the cores were characterized, and four stages during testing were identified corresponding to elastic deformation, plastic deformation, fracture of cell wall, and face sheet debonding. Lee et al. [43] characterized the failure mechanisms and strength of hexagonal aramid honeycomb cores when subjected to compressive and shear forces. The authors tested the cores at temperatures between 25ºC and 300ºC where results indicated a decrease in both shear and compressive strengths as temperature increased.

However, core crush is still a common manufacturing problem, particularly when the aforementioned fabric configurations and resins are not viable. Moreover, previous literature does not include the study of shear strength of cores when subjected to combined conditions of temperature and pressure typical of autoclave manufacturing. As such, Chapter 4 of this research tackled this matter by introducing a customized testing apparatus and a methodology for shear strength characterization of sandwich structures when applying temperature and pressure corresponding to autoclave conditions.

2.3 Thermal Properties of Composite Materials

Previous studies used conduction methods to measure the thermal properties of fiber-reinforced composites by conduction [44]. Yamane et al. [45] proposed a method to characterize thermal diffusivity of a single carbon fiber, which was calculated based on the temperature decay associated to the heat propagation along the fiber. Their results showed that once the thermal properties of the fiber were obtained, the diffusivity and conductivity of CFRP could be calculated based on the rule of mixtures. In a different approach, Sweeting et al. [46] implemented a customized device to measure thermal conductivity under vacuum conditions in which temperature sensors were placed along and through the thickness of CFRP panels. Scott et al. [47] proposed an alternative method to characterize simultaneously volumetric heat flux and thermal conductivity of composite materials during cure. Using modulated heat, the authors found an increase of thermal conductivity as a function of degree of cure. Friis et al. [48] developed a technique to determine thermal properties (specific heat—C_p, diffusivity, and conductivity) of carbon fiber-epoxy composites using the Ångström method [49] . This method consisted in inducing modulated heat in one end of a rectangular sample and measuring the temperature response in the opposite end of the part, as shown in Figure 3. The authors found that thermal properties were related to resin vitrification since their measurements showed an important variation in thermal properties when the degree of cure was higher than 0.7. Garnier et al. [50] proposed a different approach based on the Ångström method, which was used to measure the thermal conductivity during curing of a CFRP. In their study, a signal analysis was performed to identify and correct the effect of internal heat generation where a deconvolution of the measured temperature response was performed to separate the internal heat generation from the temperature response associated with thermal conductivity and diffusivity of the sample.

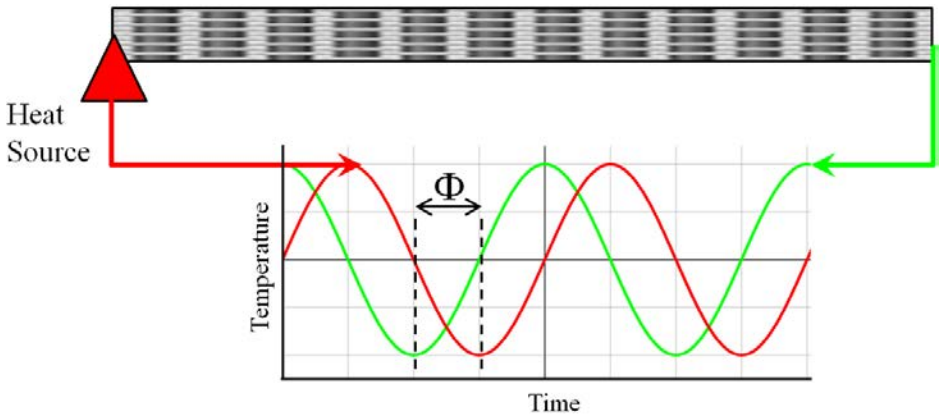

Figure 3. Methodology used to determine thermal conductivity using a modulated heat source

LFA is an alternative methodology used to characterize thermal properties of composites by radiation, which is well known for short experimental times compared to heat conduction methods [51, 52]. In previous studies, LFA has been used to determine the thermal properties of CFRP including an analysis of *boron nitride-carbon fiber-polybutylene terephthalate* composites [53] and carbon fiber-epoxy bipolar plates [54]. However, these studies did not include detailed a validation of LFA method for testing composite materials. As such, Alway-Cooper et al. [55] validated the use of the Parker model [51] for composite samples since this model was developed to determine the thermal diffusivity of homogeneous materials. Their results indicated that the temperature response obtained for CFRP showed a good fit with the Parker model. Moreover, using the rule of mixtures and the fiber volume fraction of the samples, the thermal diffusivity of the carbon fibers and the resin was obtained where those results indicated a negligible error when compared with theoretical values.

Based on these studies, it was found that further research is required to determine the thermal properties of composite materials by the LFA method including thermal diffusivity and conductivity models. Moreover, a detailed analysis of the considerations related to the anisotropy

of fiber-reinforced composites should be included. These topics are addressed in Chapter 6 where a study of the influence of fiber architecture on thermal properties and a comparison between autoclave and out-of-autoclave resins is also included.

CHAPTER 3

DEVELOPMENT OF A CUSTOMIZED TESTING RIG FOR SHEAR STRESS CHARACTERIZATION AT TEMPERATURES AND PRESSURES TYPICAL OF AUTOCLAVE PROCESSING

3.1 Introduction

A customized testing rig was designed to measure the shear stress of composite materials and sandwich structures when subjected to combined conditions of pressure and temperature. Initially, this apparatus was developed to determine the frictional interaction between a composite sample and a metallic tool since, as shown in Table 1, current standard test methods to characterize friction in polymeric materials are limited to temperatures, pressures, and speeds that do not correspond to values required to mimic autoclave manufacturing conditions.

TABLE 1

COMPARISON BETWEEN STANDARD AND REQUIRED TESTING PARAMETERS

Parameter	Standard	Standard Value	Required Values
Temperature (ºC)	ASTM D3028 ASTM D1894	Room temperature	Between room temperature and 177ºC
Test speed (mm/min)	ASTM D3028 ASTMD1894	$0.1\ (10)^3 - 3\ (10)^3$ 120 – 180	~ 0.254
Pressure (kPa)	ASTM D3028 ASTM D1894	Variable 0.44	Up to 700

*ASTM D3028 withdrawn on 2000

Instead, generalized standard test methods for friction (ASTM G115 [56] and ISO 6601 [57]) were used to identify the static and dynamic friction forces obtained with the testing rig. Further, the testing rig was also used to measure the shear strength in the sandwich (chapter 5, pp. 52) since current standard tests for sandwich structures (ASTM C273 [42]) do not include

specifications to measure shear strength when samples are subjected to the combined conditions of pressure and temperature.

3.2 Mechanics of the Testing Rig

Figure 4 illustrates the rig developed to test structural composite materials at different temperatures and pressures typical of autoclave processing. As shown in the figure, a pneumatic piston in the rig (a) applied pressure to a sample lodged between two metallic plates (b), and the mobile plate on the fixed rig (c) was then pulled by a universal testing machine (UTM, MTS Qtest). A load cell (d) was used to measure the sample consolidation pressure, and the use of elastomeric bushings (e) was a particular accessory used only for modulated temperature experiments mentioned in section 4.2.4 (see pp. 31). The force diagram of this system was illustrated in Figure 5a, which was equivalent to the forces exerted during autoclave processing shown in Figure 5b. As such, the corresponding force equations of the testing rig are:

$$\tau = \frac{F}{\mathrm{A}} \qquad (1)$$

$$\mathrm{P} = \frac{F_N}{\mathrm{A}}$$

where τ is the shear stress induced by the tool-part interaction force F, A is the area of the sample, and P is the consolidation pressure generated by the normal force F_N. Notice that according to ASTM G115, the mechanics of this testing rig corresponded to a conforming-surface-tribosystem where the unit of measurement was the pull-out force.

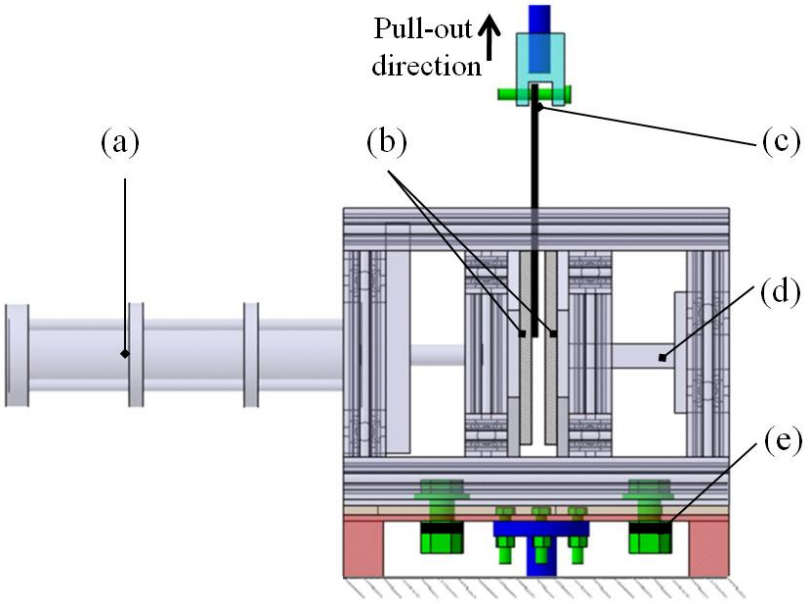

Figure 4. Description of the testing rig: (a) pneumatic piston, (b) heated metallic plates, (c) mobile plate, (d) load cell, and (e) elastomeric bushings

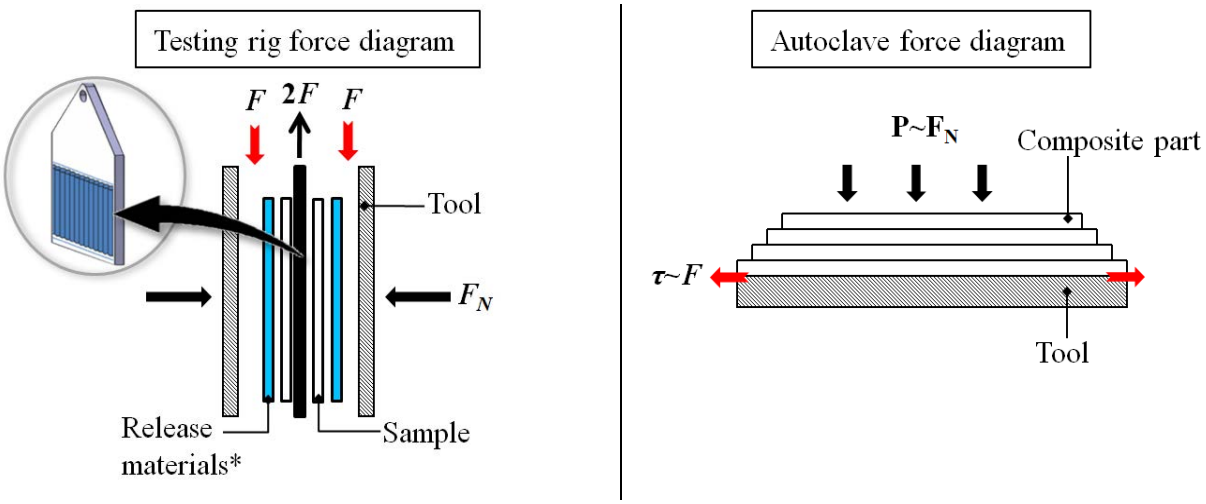

Figure 5. (a) Force diagram of the testing rig and (b) force diagram of autoclave

3.3 Instrumentation and Software Design

PID pressure and temperature controllers were implemented in the testing rig in order to mimic accurately autoclave conditions. These controllers modified the pressure applied by the pneumatic piston (Figure 4a) and the heat supplied by the tools (Figure 4c) based on the feedback signal of different sensors located in the rig, as shown Figure 6. Simultaneously, the data obtained with these sensors was exported to a Visual Basic processing algorithm to synchronize the signals obtained from the testing rig with the force measurements acquired by the UTM. As a result, a spreadsheet was obtained with the data corresponding to temperature, pressure, and pull-out force.

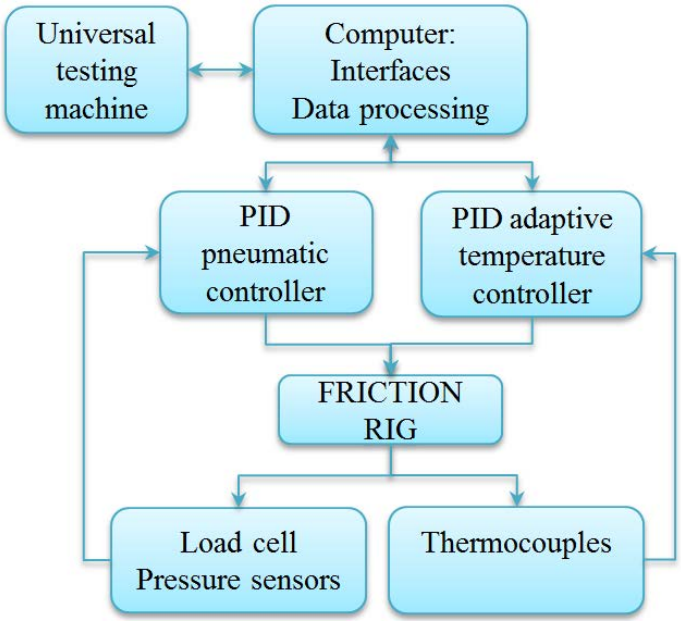

Figure 6. Data processing of the testing rig

Additionally, a LabVIEW control panel (shown in Figure 7) was designed to operate the testing rig using a user-friendly interface. This panel included temperature and pressure monitoring displays, port configuration, temperature and pressure profile setup, data file configuration, and safety buttons to terminate the test.

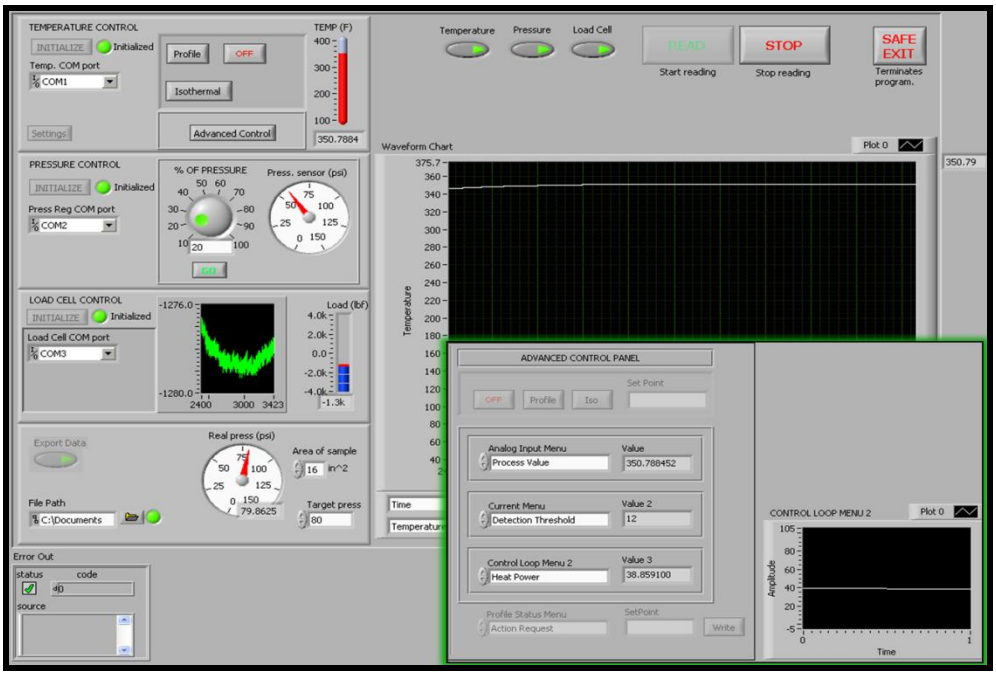

Figure 7. LabVIEW control panel

The testing rig was also equipped with a load cell (Figure 4d) which was used to measure and correct the consolidation pressure applied on the sample. During testing, it was observed that**,** at high temperatures**,** the force applied with the piston (Figure 4a) differed from the desired consolidation force on the sample, which was measured with the load cell. In order to correct this issue, an adaptive controlling routine was implemented using LabVIEW, which followed the sequence illustrated in Figure 8. If the difference between the desired consolidation pressure and the pressure measured with the load cell was higher than 1%, the error signal (load cell force minus target force) was multiplied by an adaptive constant in order to correct the pressure of the pneumatic piston. As a result of implementing this routine, the testing rig was able to correct noise induced by the thermal expansion of the rig, thus guarantying a constant pressure on the sample.

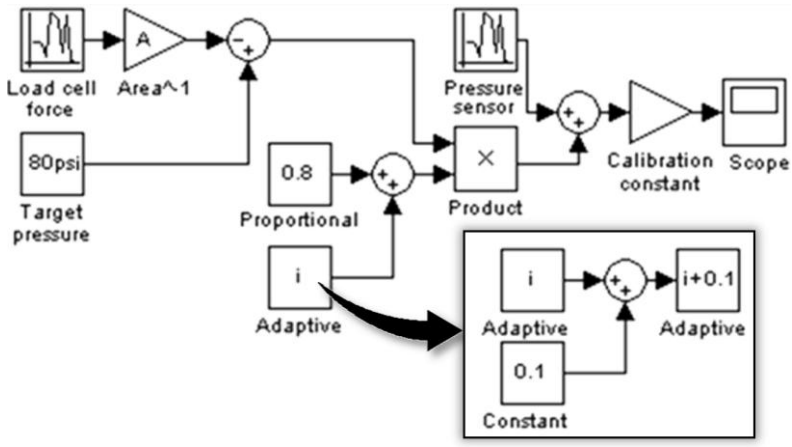

Figure 8. Adaptive pressure control system which operated when the difference between load cell pressure and the desired pressure was more than 1%

3.4 Experimentation

The methodology utilized to determine static and dynamic friction force with the testing rig was portrayed using a point-wise characterization of tool-part interaction during the manufacturer's recommended cure cycle (MRCC) of a carbon fiber-epoxy prepreg. In these experiments, two different methods were utilized to determine static and dynamic friction force where the ASTM G115 [56] was used as a reference.

3.4.1 Materials

Carbon fiber-epoxy unidirectional prepreg (Cytec IM7/977-2 UD) coupons of 10 x 10 cm^2 with a stacking sequence of $[0^o]_2$ were placed on both sides of a stainless steel mobile plate as shown in Figure 5a. The width of this plate was the same as the width of the sample coupon in order to minimize changes in contact area due to resin flow and fiber spreading. According to the MRCC of the prepreg IM7/977-2 UD, samples were cured at a ramp rate of 2.7ºC/min until 177ºC, and then held at this temperature for 4 hours while applying a consolidation pressure of 550 kPa (80 psi).

The heated tools (Figure 4b) were made of aluminum 6061 and the tool surfaces were conditioned with a 400 grit sand paper and cleaned with acetone, which corresponds to typical surface conditions found in industrial applications [16]. Then, the tool roughness was measured using a surface roughness tester (Mitutoyo SJ-201) and the root-mean-squared surface roughness value (R_q) obtained for both tools was ~0.18 µm. Subsequently, tools were treated with mold sealer (Frekote B-15) and then cured inside an oven for one hour at 94ºC. Finally, three coats of polymeric release agent Frekote 770NC were applied on the heated tool and a layer of TFE release film (Airtech WL-5200 blue) was placed between the tool and the sample.

3.4.2 Testing Parameters for Discrete Friction Measurement

The tool-part frictional force was measured at different points of the MRCC of the prepreg IM7/977-2 UD. Samples, summarized in Table 2, were tested during the heat-up and dwell region at the points depicted in Figure 9 using a UTM crosshead speed of 20 mm/min. After testing, the static and dynamic friction forces were identified using the ASTM G115.

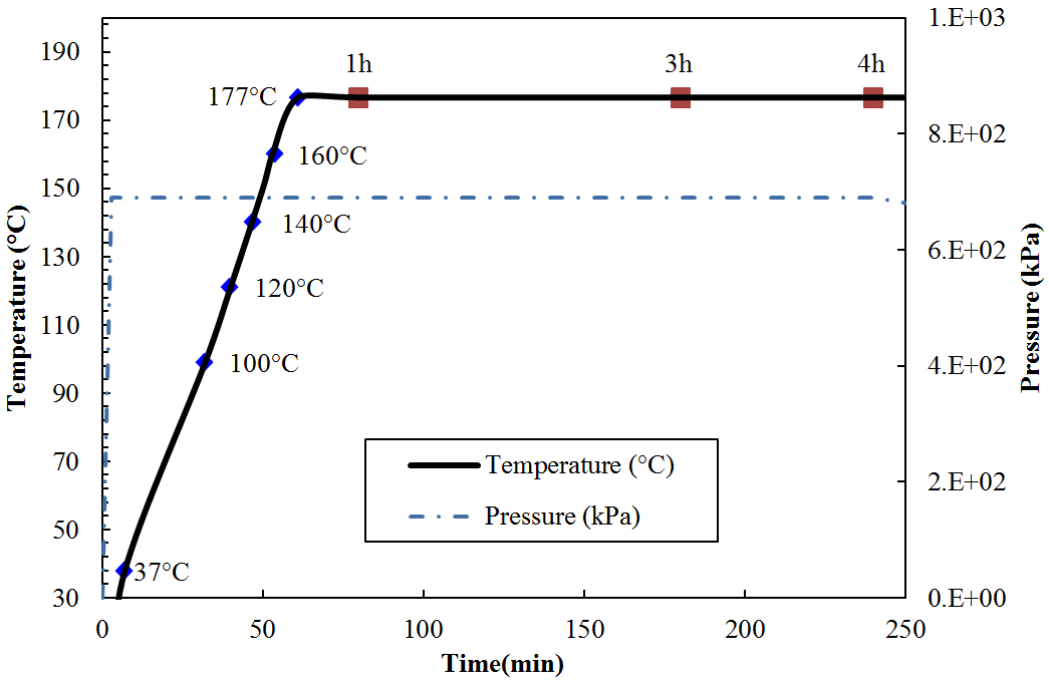

Figure 9. Points during the cure cycle of the prepreg IM7/977-2 UD where discrete friction tests were performed

TABLE 2

SET OF EXPERIMENTS USED FOR DISCRETE FRICTIONAL CHARACTERIZATION

Temperature		Number of Experiments
37ºC		2
100ºC		2
120ºC		2
140ºC		2
160ºC		2
177ºC		1
177ºC	1 hour of MRCC	1
177ºC	3 hours of MRCC	1
177ºC	4 hours of MRCC	1

3.5 Results

Tests were carried out to determine tool-part frictional interaction at different points of the curing cycle shown in Figure 9. During this cure cycle, two friction modes were observed, as shown in Figure 10. The first mode (Figure 10a) showed a breakaway point that was related to the static friction force [56]. Subsequently, force decreased to a value corresponding to the dynamic friction. This friction mode was observed only when samples were tested during the dwell region of the cure cycle (Figure 9), in which the composite coupons had an advanced degree of cure. When samples were tested during the ramp-up region, a second friction mode was identified (Figure 10b) where the force curve did not show a breakaway point. Instead, a continuous increase in friction was measured where a linear behavior was observed at low deformations. The point where the force changed from a linear to a non-linear curve (F') was used to identify the static friction force [56]. Therefore, these two frictional modes implied that during the ramp-up region, the friction force was dominated by the consistency of the epoxy resin**,** while during the dwell region this force could be related to the interaction between tool and part.

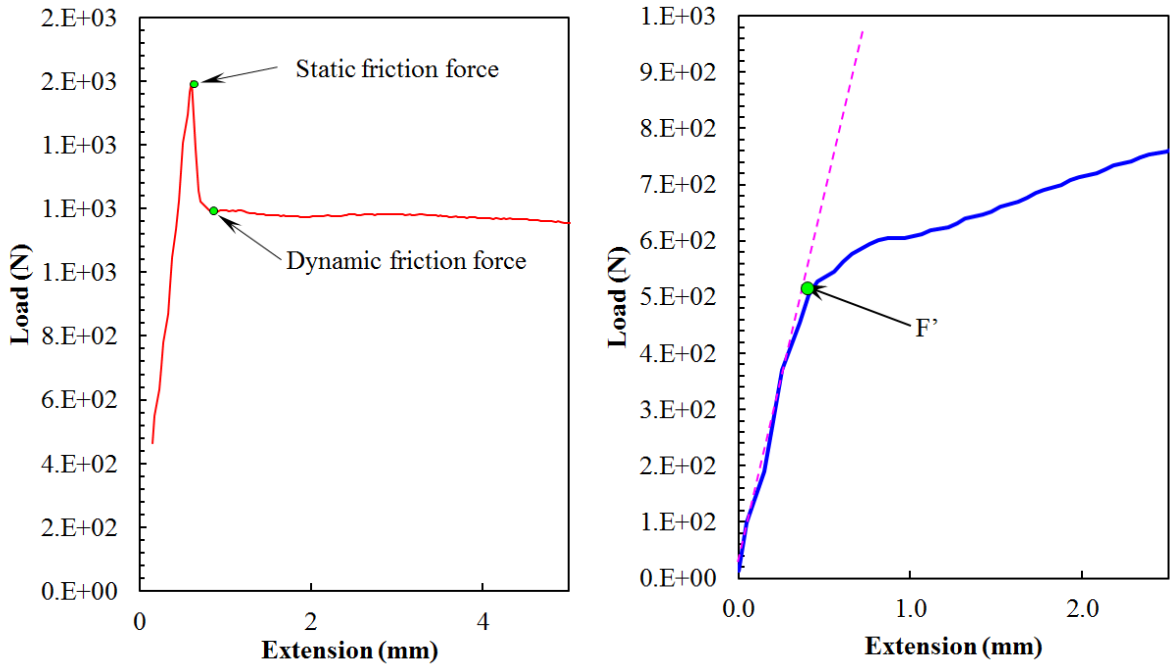

Figure 10. Friction force characterization according to ASTM G115 for IM7/977-2 UD coupons tested during (a) heat-up ramp (120ºC) and (b) dwell region (1 hour of MRCC) using release film (method 1) at the tool-part interface

Figure 11 showed the results corresponding to frictional shear stress during the curing of CFRP prepregs, which were tested at the points indicated in Figure 9. Shear stress was calculated using equation (1) where the frictional force (F') was determined based on the friction characterization modes shown in Figure 10. For samples tested between 37 and 177ºC, shear stress increased as a function of temperature until a value of ~0.1 MPa was reached. Then, samples measured after 1 hour of the cure cycle depicted a negligible variation in frictional stress. Note that the gel point of the prepreg IM7/977-2 UD is reported in the literature at the 70th minute of the MRCC [58]. Furthermore, Ersoy et al. [5] indicated that the friction force after the gel point could be governed by the release materials placed between the tool and the part. As such, the friction force obtained after 1 hour of the cure cycle might correspond to the frictional interaction of the TFE release film since this material was used between the tool and the part.

Therefore, the release material depicted an important role when manufacturing thermoset composite materials since the frictional properties of such release materials could determine the maximum value of tool-part residual shear stress induced during cure.

It was also observed that the values obtained during the dwell region of Figure 11 were in the same order of magnitude of those reported in the literature [5] for tests performed with CFRP samples and release materials similar to those used herein. Thus, these findings indicated that the testing rig was a reliable setup to characterize tool-part shear stress.

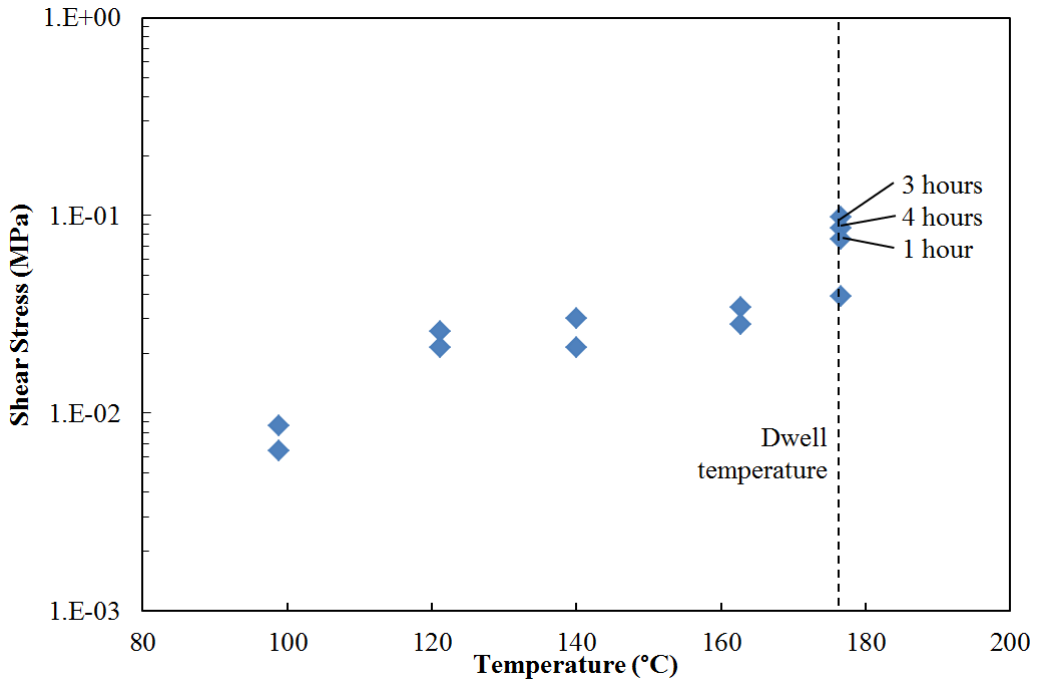

Figure 11. Shear stress corresponding to static frictional force

3.6 Summary

In this chapter was presented the development of a testing rig that was designed to measure the tool-part interaction of carbon fiber-epoxy composite samples and the shear strength of sandwich structures when subjected to temperatures and pressures typical of autoclave processing. This rig was coupled with a universal testing machine that quantifies the shear force required to pull out a sample lodged between two metallic plates, while the rig applies

customized temperature and pressure cycles. For this reason, advanced sensors and control systems were implemented in the rig in order to mimic accurately the autoclave conditions. As well, several VBA and LabVIEW algorithms were developed for data acquisition, processing, and monitoring using a user-friendly interface.

Preliminary experiments were performed utilizing the testing rig to validate its functioning. These tests consisted of measuring the friction force between a CFRP sample and a metallic tool at different points of the cure cycle. Using the ASTM G115 as a reference, two friction modes were identified at the ramp-up region and dwell of the cure cycle. During the ramp-up region, friction force did not depict breakaway points, which indicated that the consistency of the resin was weak due to its low degree of cure. As such, frictional stress increased as the resin gelled because viscosity seemed to increase as crosslinking reactions were developed. Then, during the dwell region, the frictional stress converged to a constant value of ~0.1 MPa where the static and dynamic friction forces were clearly identified. These findings indicated that the composite sample reached an advanced degree of cure since the tribological behavior observed was typical of contact between solids. Finally, the obtained friction values during the dwell region agreed with those reported in the literature for composites with advanced degree of cure, thus indicating that the testing rig was a reliable methodology to characterize tool-part friction force.

CHAPTER 4

CHARACTERIZATION OF TOOL-PART RESIDUAL SHEAR STRESS AT AUTOCLAVE MANUFACTURING CONDITIONS

4.1 Introduction

The shear stress of CFRP prepreg samples in contact with a metallic tool was characterized during cure using the testing rig described in chapter 3 (pp. 15) where the tool-part deformation mismatch was reproduced. The pull-out speed of the mobile plate (Figure 4c) was determined based on the CTE difference between the tool and the part (see Figure 12).

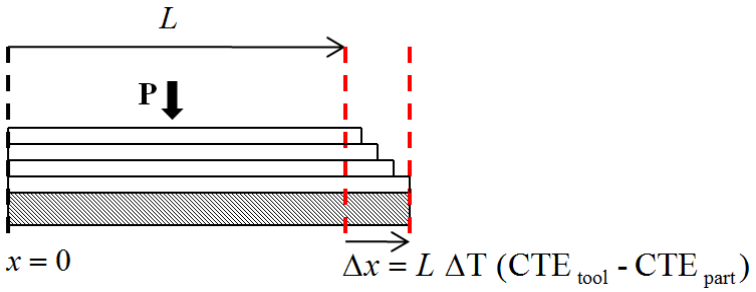

Figure 12. Tool-part deformation mismatch from the center ($x = 0$) to the edge ($x = L$) of the part

As mentioned before in Chapter 1 (pp. 2), a typical CTE value for an aluminum tool is 23.6 µm/(m·ºC) while for CFRP, the CTE could be -0.5 µm/(m·ºC) in fiber direction [3]. Hence, the relative displacement of the tool with respect to the part shown in Figure 12 was determined using equation (2):

$$v = x\frac{\Delta T}{\Delta t}\left(\mathrm{CTE}_{\mathrm{tool}} - \mathrm{CTE}_{\mathrm{part}}\right) \tag{2}$$

where v is the relative speed of the part with respect to the tool, and $\Delta T/\Delta t$ is the heat-up ramp of the cure cycle. $\mathrm{CTE}_{\mathrm{tool}}$ and $\mathrm{CTE}_{\mathrm{part}}$ are the coefficients of thermal expansion of tool and part,

respectively. The relative speed of the part with respect to the tool is zero in the center ($x = 0$) and it increases toward the edges ($x = L$) as follows [5]:

$$v_{\max} = L\frac{\Delta T}{\Delta t}(\mathrm{CTE}_{\mathrm{tool}} - \mathrm{CTE}_{\mathrm{part}}) \tag{3}$$

where L was half of the total length of the part and v was used as the tool-part relative displacement at the edges. Hence, a crosshead speed of v_{max} = 0.07 mm/min was obtained by considering a part length of L = 1 m, $\mathrm{CTE}_{\mathrm{tool}}$ = 23.6 μm/m·ºC, $\mathrm{CTE}_{\mathrm{part}}$ = -0.5 μm/m·ºC, and $\Delta T/\Delta t$ = 2.8ºC/min which was the heat up ramp of MRCC shown in Table 3. Note that equation (3) was a simplified expression of the tool-part relative displacement where effects such as chemical shrinkage of the resin were not included. Therefore, the tool-part shear stress was characterized using three different pull-out speeds (0.05, 0.10, and 0.15 mm/min) where the v_{max} = 0.07 mm/min was used as the reference value. With the aim of studying the static and dynamic COF, the displacement rate was held constant throughout the MRCC and its direction was not changed during cool-down.

4.2 Materials and Testing Parameters

4.2.1 Carbon Fiber Samples

Samples were made of carbon fiber-epoxy unidirectional prepreg (Cytec IM7/977-2 UD) with dimensions of 10 x 10 cm^2. The stacking sequence was $[0º]_2$, and the composite samples were placed on both sides of the mobile plate (see chapter 3, Figure 5a). The width of this plate was the same as the width of composite coupons in order to minimize changes in the contact area due to fiber spreading and resin flow. Tests were performed during the manufacturing MRCC of the prepreg IM7/977-2 UD (see Table 3), and a consolidation pressure of 550 kPa (80 psi) was used except in tests corresponding of section 4.3.9 where pressure was changed between 0.27 and 0.83 MPa.

TABLE 3

MANUFACTURER'S RECOMMENDED CURE CYCLE OF IM7/977-2 UD

Heating Ramp	2.8ºC/min
Dwell	3 hours at 177ºC

4.2.2 Tooling and Release Materials

The tools of the testing rig were made of aluminum 6061, which had a root-mean-squared surface roughness R_q = 0.18 μm after being conditioned with sand paper of 400 grit. This roughness corresponded to similar conditions as those found in industrial applications [16]. Notice that surface roughness was measured with a roughness tester Mitutoyo SJ-201.

Tool-part shear stress was characterized using three release methods between the tool and the part shown in Table 4:

TABLE 4

RELEASE SYSTEMS UTILIZED ON THE SURFACE OF THE TOOL

Release Method	Release Film (Airtech WL-5200)	Release Agent (Frekote 770NC)	Mold Sealer (Frekote B15)
1	✓	✓	✓
2		✓	✓
3	✓		

4.2.3 Testing Parameters for Continuous Shear Stress Measurements

An orthogonal DOE was implemented with the aim of identifying the relevance of different manufacturing conditions including surface roughness, pull-out rate, normal pressure, and stacking sequence on the tool-part shear stress. These factors were tested using the three levels shown in Table 5 (control parameters). Following the robust DOE proposed by Taguchi [59], a set of experiments was developed (Table 6) using an orthogonal array L_9. Note that the manufacturing parameters evaluated were assumed linearly independent, e.g. the change in

surface roughness did not depend on the stacking sequence, pull-out speed or normal pressure. Hence, the contribution of each testing factor was identified by averaging the shear stress results of samples from Table 6 that were tested using the same factors. For instance, the optimum tool surface condition was identified by comparing the stress average of experiments 1, 2, 3 (1.35 μm) with the average of experiments 4, 5, 6 (0.18 μm), and experiments 7, 8, 9 (0.18 μm + release agent). Similar methodology was used to determine the contribution of the other manufacturing parameters on shear stress. Therefore, orthogonal DOE was used to identify the optimum control parameters required to achieve the lowest tool-part frictional stress, which also represented the best manufacturing conditions. Notice that the scope of investigation did not include the analysis of signal-to-noise ratios since there were no specified assumptions about the effect of the control parameters on the shear stress.

TABLE 5

CONTROL PARAMETERS, WHICH REPRESENTED DIFFERENT VALUES (LEVELS) OF THE MANUFACTURING VARIABLES (FACTORS)

	Levels		
Factors	*1*	*2*	*3*
A. Surface Roughness (R_q) ***(release method)***	1.35μm* (*method 3*)	0.18μm** (*method 3*)	0.18μm + Release Agent *(method 1)*
B. Stacking Sequence	[0 / 0]	[0 / 90]	[45/-45]
C. Pull-out Rate (mm/min)	0.05	0.10	0.15
D. Pressure (kPa)	550	650	750

*120 grit sand paper

**400 grit sand paper

TABLE 6

ORTHOGONAL ARRAY L_9: SAMPLE CONFIGURATION

Sample Number	A. Tool surface condition (*release method*)	B. Stacking Sequence	C. Pull-out Rate (mm/min)	D. Pressure (kPa)
1	1.35 μm (*method 1*)	[0 / 0]	0.05	550
2	1.35 μm (*method 1*)	[0 / 90]	0.10	650
3	1.35 μm (*method 1*)	[45/-45]	0.15	750
4	0.18 μm (*method 1*)	[0 / 0]	0.10	750
5	0.18 μm (*method 1*)	[0 / 90]	0.15	550
6	0.18 μm (*method 1*)	[45/-45]	0.05	650
7	0.18μm + Release Agent (*method 3*)	[0 / 0]	0.15	650
8	0.18μm + Release Agent (*method 3*)	[0 / 90]	0.05	750
9	0.18μm + Release Agent (*method 3*)	[45/-45]	0.10	550

Once the strongest contributors to shear stress were identified, a study was performed to propose a mathematical approach to the tool-part interface using the samples shown in Table 7.

TABLE 7

SET OF EXPERIMENTS USED TO CHARACTERIZE SHEAR STRESS

Analysis	Test	Experiments	Results
Release film (*Method 1*)	During cure cycle	6	Figure 15
	Cool-down region	6	Figure 16
	Cured sample - release film	1	Figure 17
	Modulated temperature { With modulation	2	Figure 20
	Modulated temperature { Without modulation	2	Figure 20
	Shear stress-pressure test	5	Figure 24
Release agent (*Method 2*)	During cure cycle	6	Figure 18
	Modulated temperature { With modulation	2	Figure 21
	Modulated temperature { Without modulation	2	Figure 21
	Shear stress-pressure test	5	Figure 24
Surface roughness	1.35 μm (120 grit sand paper)	1	Figure 22
	0.18 μm (400 grit sand paper)	1	Figure 22
	0.18 μm and release agent	1	Figure 22
Rheology	Rheological analysis	1	Figure 19

4.2.4 Modulated Temperature Tests

Modulations of temperature were incorporated during the cure cycle to study the response of shear stress to temperature fluctuations. Using a LabVIEW interface, modulations were induced with an amplitude of ± 2ºC, which was in the same order of magnitude as that used by Twigg et al [14]. Additionally, the testing rig was modified to a high-deformation configuration by placing elastomeric bushings on the base of the rig, as shown in chapter 3, Figure 4e. This configuration increased the sensitivity of the system, thus allowing a distinction of the transition between static and dynamic friction force. Note that this high-deformation configuration was used only for modulated temperature tests because the additional deformation provided by the elastomeric bushings may result in tool-part displacement that does not correspond to the crosshead speed of the UTM machine.

4.3 Results

4.3.1 Continuous Shear Stress Characterization by Orthogonal DOE

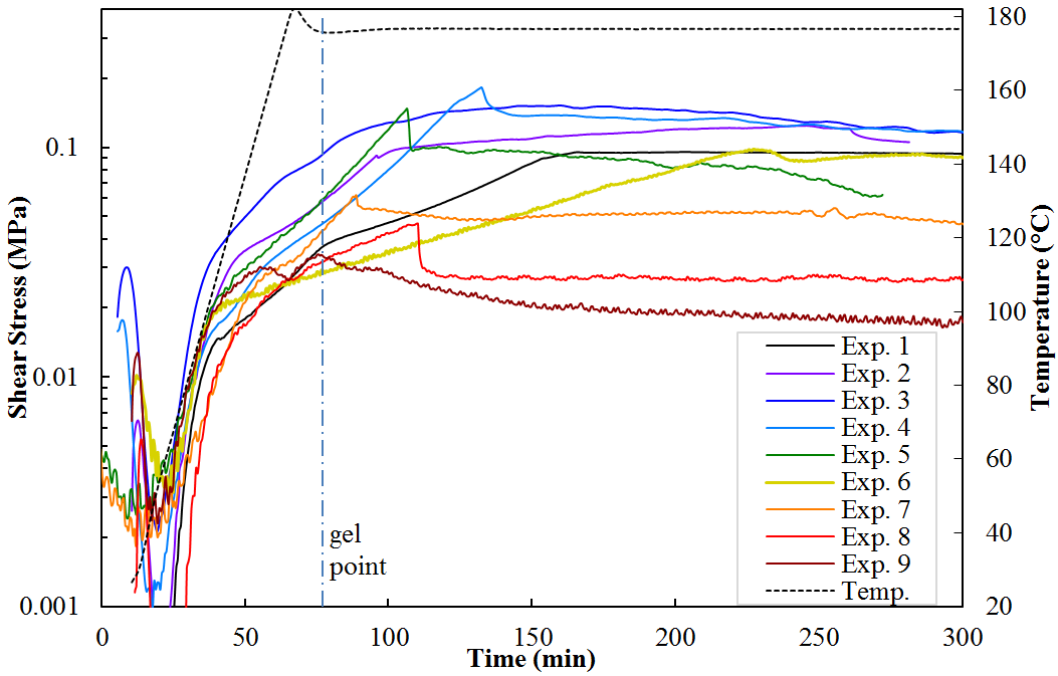

Figure 13. Shear stress obtained by continuous friction characterization.

A continuous friction characterization of the prepreg IM7/977-2 UD was carried out in order to identify the optimum manufacturing parameters among tool surface condition, sample stacking sequence, pull-out speed, and consolidation pressure. As mentioned in section 4.2.3, an orthogonal array L_9 was used and the experimental conditions were set up according to Table 6. The results of these experiments were illustrated in Figure 13, and the contribution of each factor on shear stress was determined at the plateau stress region (dynamic frictional interaction) in order to obtain an indicator of the relevance of each manufacturing factor on the tool-part interfacial shear stress. Results shown in Figure 14 (which were determined based on the graphs of appendix A) indicated that different tool surface conditions could change the shear stress up to 72%.

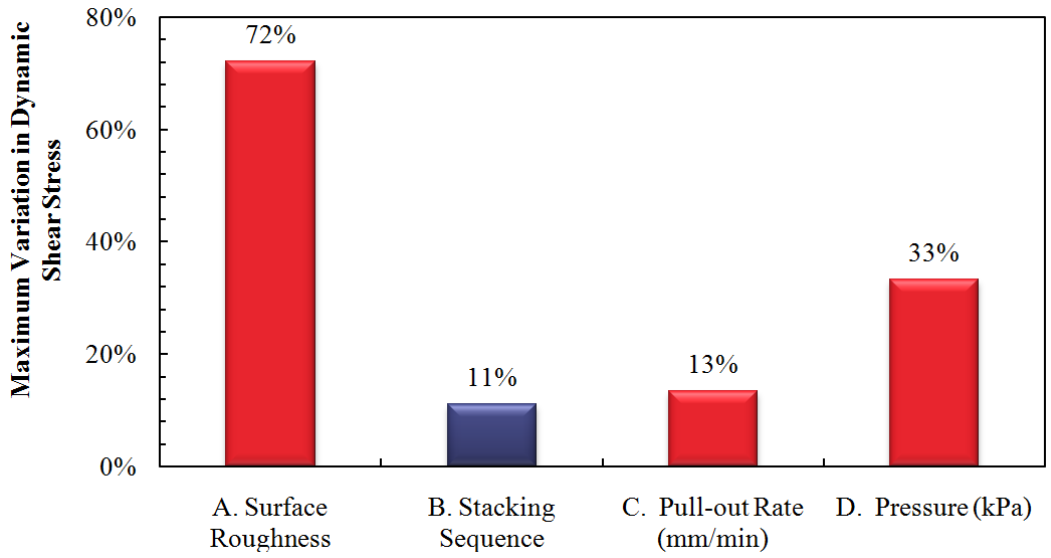

Figure 14. Relative factor interaction: Maximum difference in shear stress measured at the end of the plateau region

On the other hand, the stacking sequence showed changes in shear stress up to 10%. Note also that the experiments performed by R. Das et al. [29] indicated that composites can release a higher amount of process-induced residual stresses when the stacking sequence is different than

[0º]. Based on these results, a mathematical approach to the tool-part interaction was developed comprising the effects of tool surface conditions, pull-out speed, and consolidation pressure. Moreover, the influence of temperature on shear stress was studied, but different stacking sequences were not included in further tests.

4.3.2 Tool-Part Shear Stress: Release Film (Method 1)

During the cure cycle of the prepreg 977-2 UD, composite samples were tested at three pull-out speeds when using the release method 1 (Table 4) between the coupon and the tool. Results shown in Figure 15 illustrated the change in shear stress during the cure cycle (Figure 15a) and shear stress vs. temperature (Figure 15b). During the A–C region indicated in the figures, shear stress decreased until the point of maximum resin flow velocity was reached—that is, the point observed in Figure 15b around ~70ºC [60]. Subsequently, stress increased as the resin cured, thus indicating that the resin was developing its mechanical properties due to the cross linking reactions of the epoxy resin. This increase reached a limit at the point C (gel point, as shown in section 4.3.4—pp. 39) where the shear stress of the curve converged to a plateau value that was extended until the beginning of the cooling down region (point D). Thus, the shear stress increased during cure until the resin developed enough mechanical properties to bear the frictional force required to surpass the static COF and then the shear stress converged to a constant value corresponding to the dynamic friction force, which increased as temperature decreased during the cool down cycle (D–E region). Note also that these findings followed a similar trend than that of point-wise friction tests presented in section 3.5 (pp. 21).

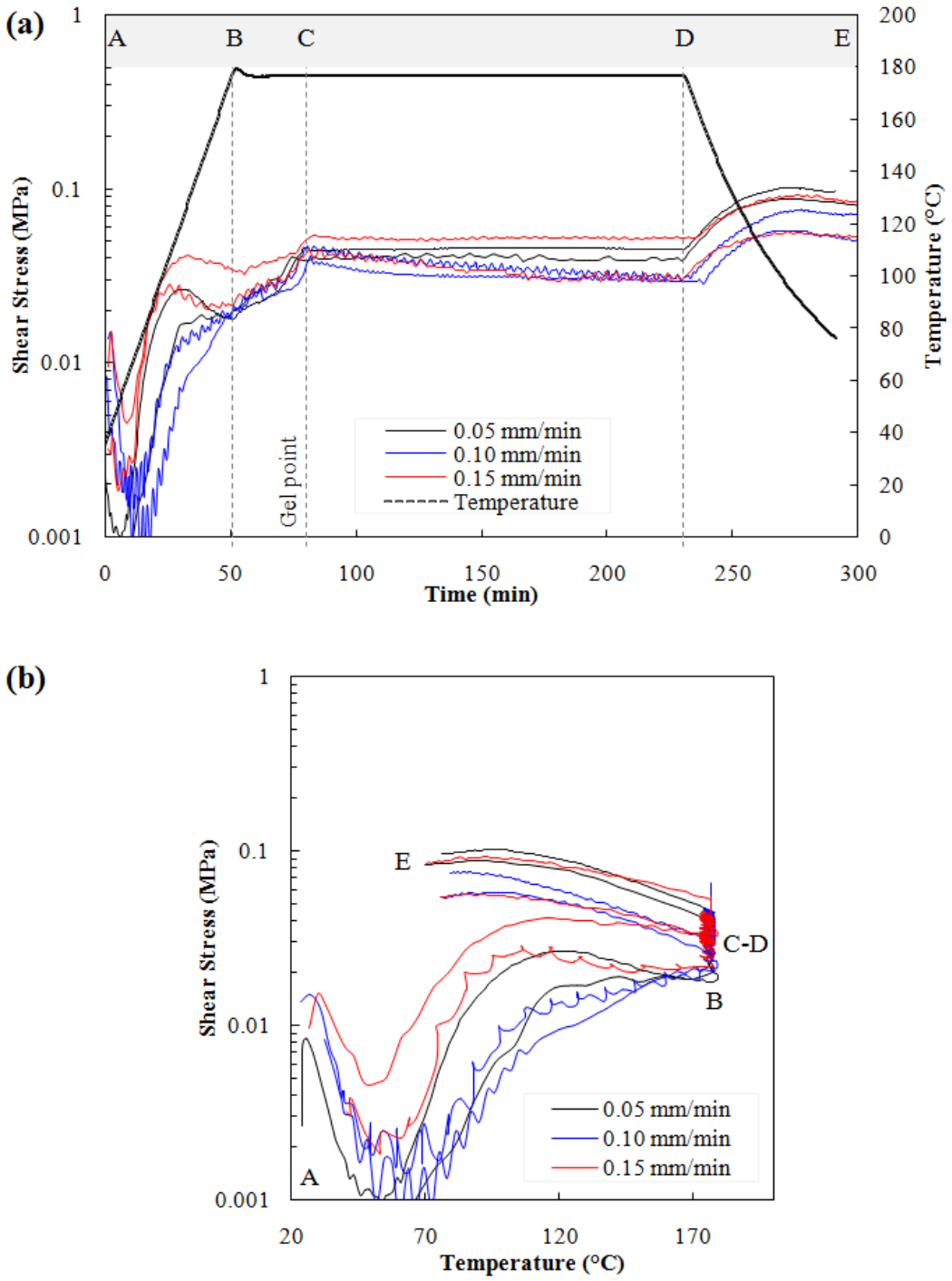

Figure 15. Release method 1: (a) Shear stress vs. time and (b) shear stress vs. temperature at pull-out speeds between 0.05 and 0.15 mm/min

Figure 16 showed the results of a study performed to determine the influence of temperature on shear stress, which was performed by analyzing the cool-down cycle (region D–E of Figure 15) in a linear scale. In this figure is shown that the stress-temperature curves displayed a linear trend ($R^2 \geq 0.99$) where slope values between -0.3 x 10^{-3} and -0.8 x 10^{-3} MPa/ºC were obtained.

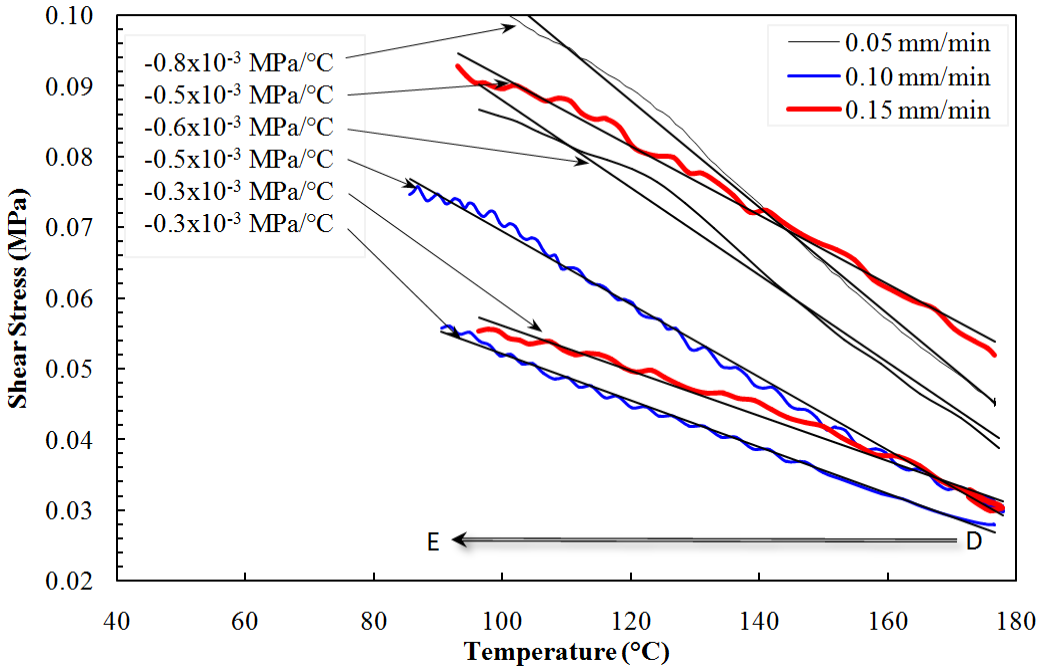

Figure 16. Cool down region (D–E) in linear scale at three different pull-out temperatures

Since the degree of cure of the samples was close to 1 during D–E region, the frictional behavior shown in Figure 16 could correspond only to the frictional interaction exerted by the release materials. This hypothesis was confirmed with an additional test where a release film (method 1) was placed on a fully cured composite, as shown in Figure 17a. For this test, the average speed utilized in Figure 16 was used (0.10 mm/min), and the release film was tested during the MRCC shown in Figure 15. Results indicated that for the heat-up (A–B) and cool-down (D–E) regions Figure 17b, stress-temperature slope values were between -0.3 x 10^{-3} and -0.4 x 10^{-3} MPa/ºC,

which were also within the range of the slopes depicted in Figure 16. Therefore, these findings indicated that the frictional interaction during the D–E region was governed by the release materials, and there was a strong dependence of temperature on shear stress.

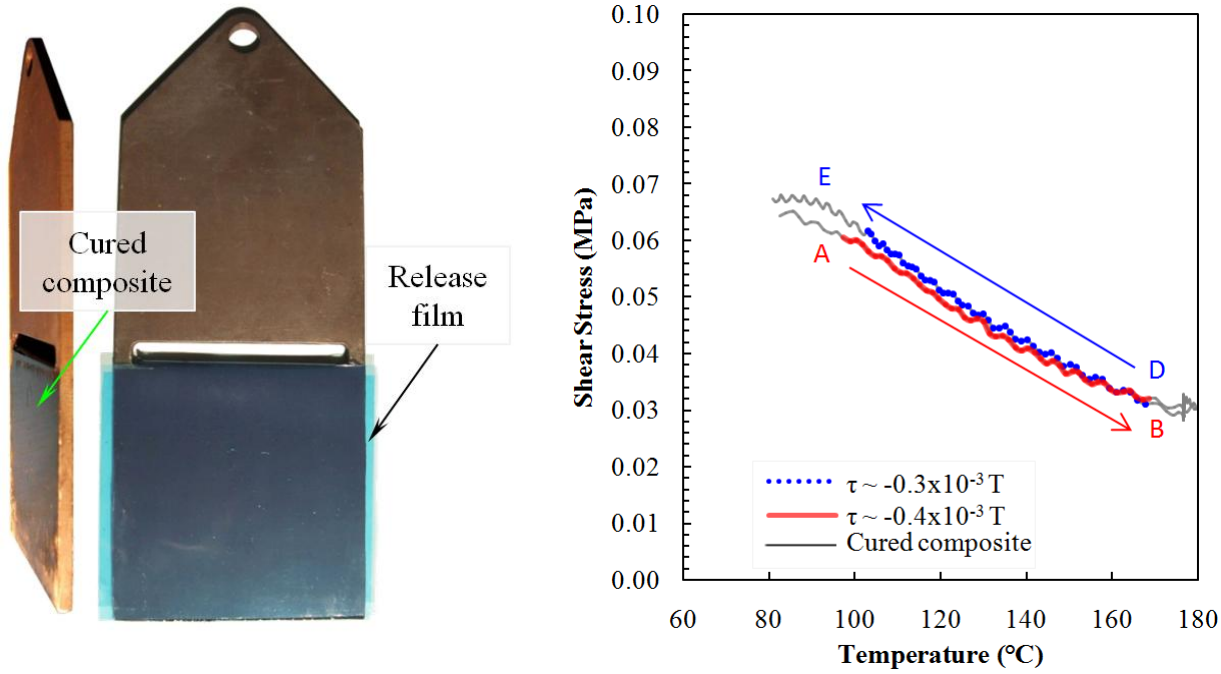

Figure 17. (a) Release film set-up on the mobile plate and (b) stress as a function of temperature for release film

4.3.3 Tool-Part Shear Stress: Release Agent (Method 2)

Since release materials portrayed an important role in tool-part interaction, the shear stress characterization was extended to testing composite coupons using a polymeric release agent, according to method 2 (Table 4). Unlike section 4.3.2, samples were tested without using a release film in order to study the frictional behavior of the release agent only. The results of Figure 18 showed that shear stress values were ~24% higher than those measured when using the release film (Figure 15) during the plateau region (C–D). A particular behavior was observed with tests performed at 0.05 mm/min where the stress curve depicted large peaks of more than

0.2 MPa, which indicated a strong adhesion between the sample and the tool. After an abrupt decrease in shear stress at the 150^{th} minute (tool-sample debonding), the stress converged to a plateau value similar to that measured when testing samples at 0.10 and 0.15 mm/min. Since equation (3) indicated that a pull-out speed of 0.05 mm/min corresponded to a part length of 0.70 m, these results implied that parts shorter than 0.70 m might remain adhered to the tool during manufacturing. In contrast, the lack of large stress peaks in samples tested at higher speed (equivalent to parts larger than 0.70 m) and parts tested with a release film (method 1) indicated that these samples surpassed the static frictional stress and slid on the surface of the tool. In summary, these findings indicated that parts processed using release method 2 might develop higher tool-part residual stress than parts where method 1 is used.

The change of shear stress as a function of temperature was also studied when using release method 2, as shown in Figure 18b. During the D–E region, samples tested without the release film showed in average a lower stress-temperature relation since the slopes measured during the cool-down region were between -0.3×10^{-3} and -0.4×10^{-3} MPa/ºC ($R^2 \leq 0.97$). Therefore, the shear stress was less sensitive to temperature when only the release agent was used.

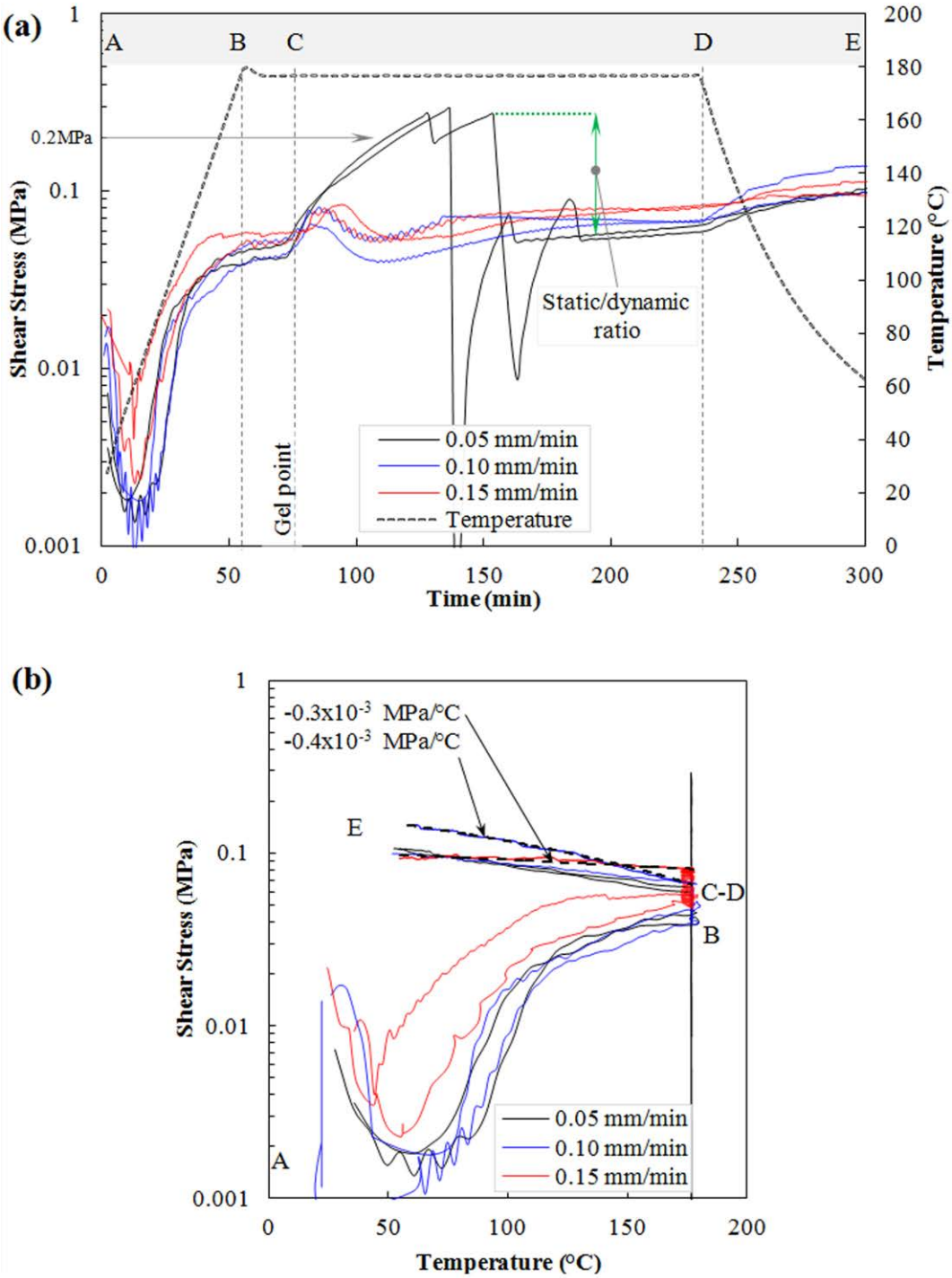

Figure 18. Release method 2: (a) Shear stress vs. time and (b) shear stress vs. temperature at pull-out speeds between 0.05 and 0.15 mm/min

4.3.4 Rheological Analysis

A rheological analysis (Figure 19) was performed to compare the viscoelastic behavior of the prepreg with the measured tool-part shear stress. During this analysis were identified two points of interest corresponding to the gel point and the minimum viscosity. The gel point was identified with the maximum value of loss tangent (Tan (δ)), according to ASTM D4473. Figure 19 showed a peak in Tan (δ) at the minute 74th, which agreed also with the gel point reported by Alavi-Soltani et al. [58]. Results indicated that the gel point matched the point C depicted in sections 4.3.2 and 4.3.3. Therefore, the gel point was the instant when composite coupons began to slide on the tool when method 1 was used (Figure 15), and the beginning of the peaks of shear stress (see Figure 18) when using method 2.

The second point of interest was the minimum viscosity of the prepreg, which was identified in Figure 19 around the 45th minute [61]. This point was compared with the results of sections 4.3.2 and 4.3.3, and it was found that it did not match the instant of minimum shear stress (20th minute of the cure cycle). Instead, minimum shear stress matched the point of maximum resin flow velocity reported by Ahmed [60]. The mismatch between minimum viscosity and maximum resin flow point was investigated by Dave et al. [62] who found that this phenomenon occurs because the fiber bed exerts a spring-like reaction force when the composite is subjected to compressive forces similar to those of autoclave processing. As the composite is consolidated, a sequential compaction is also carried out in which the autoclave pressure is gradually transferred to the fiber bed as the resin flows out (squeeze sponge effect). Consequently, the resin flow can cease before the point of minimum viscosity because the resin pressure drops as the consolidation pressure was transferred to the fiber bed. Based on these findings, it is suggested that the minimum shear stress measured at the 20th minute of the MRCC

was related to the point of maximum resin flow velocity, and not to the minimum viscosity of the resin.

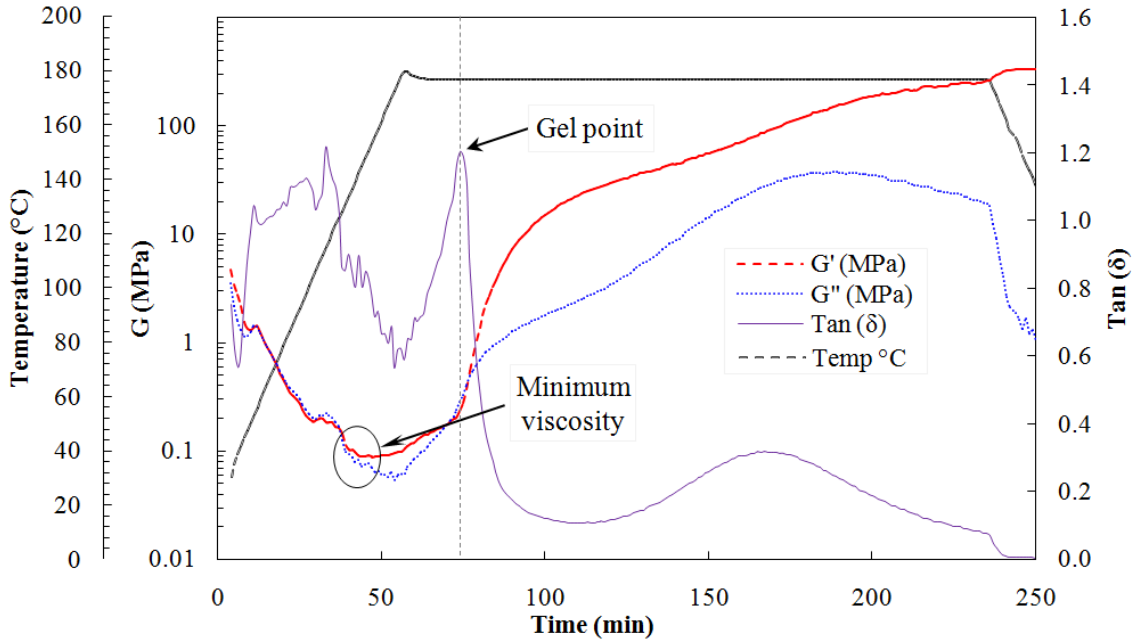

Figure 19. Rheological analysis of the prepreg during the MRCC

4.3.5 Shear Stress Characterization Using a Modulated Temperature Cycle

Modulated temperature tests were performed to identify the transition between static and dynamic shear stress. Moreover, the regions where the shear stress was highly dependent on temperature were identified. Notice that, as mentioned in section 5.2 (pp. 52), the testing rig was modified to a high deformation configuration in order to enhance the sensitivity of stress measurements, and the experiments were performed at 0.05 mm/min (see Table 7).

The shear stress measured with and without using a modulated temperature profile was portrayed in Figure 20 when using a release film (method 1, Table 4), and Figure 21 when using a release agent (method 2).

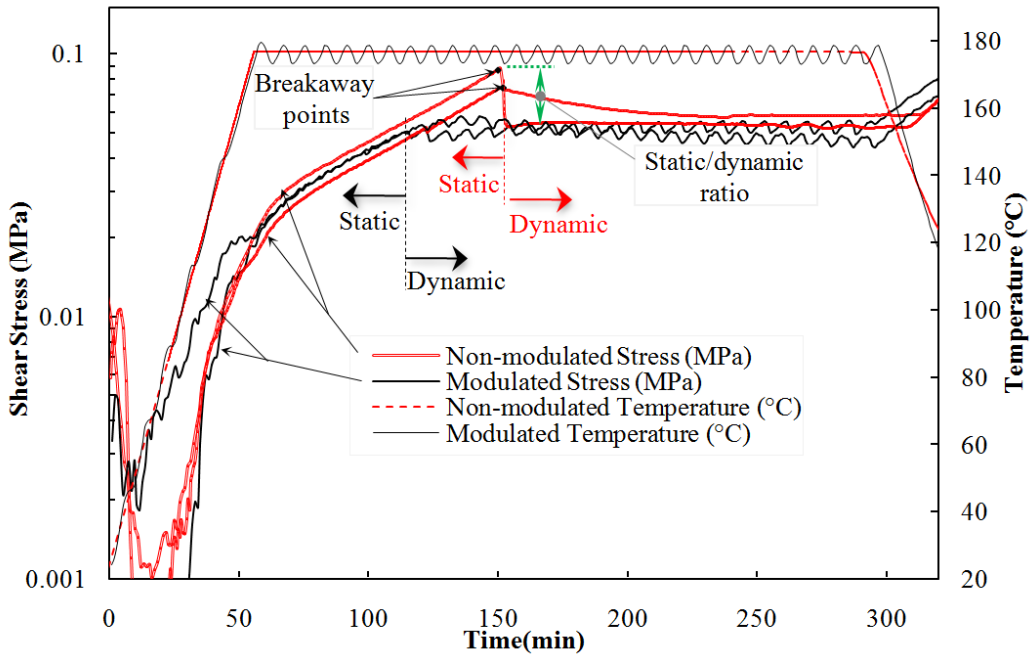

Figure 20. Modulated temperature tests for release film (method 1)

Results indicated that the shear stress response to temperature modulations could be used to identify the dynamic frictional interactions because, for both release methods, the temperature modulations induced oscillations of shear stress when the sample was moving on the tool. For instance, the modulated temperature results of Figure 20 depicted stress oscillations after the 120th minute of the tests, and Figure 21 showed stress oscillations in the region indicated in the graph. Since breakaway points were observed prior to the regions where stress modulations were shown, results implied that the shear stress was dependent on temperature only when the composite sample was sliding on the tool. Thus, modulated temperature tests were used to identify the transition between static and dynamic frictional stress.

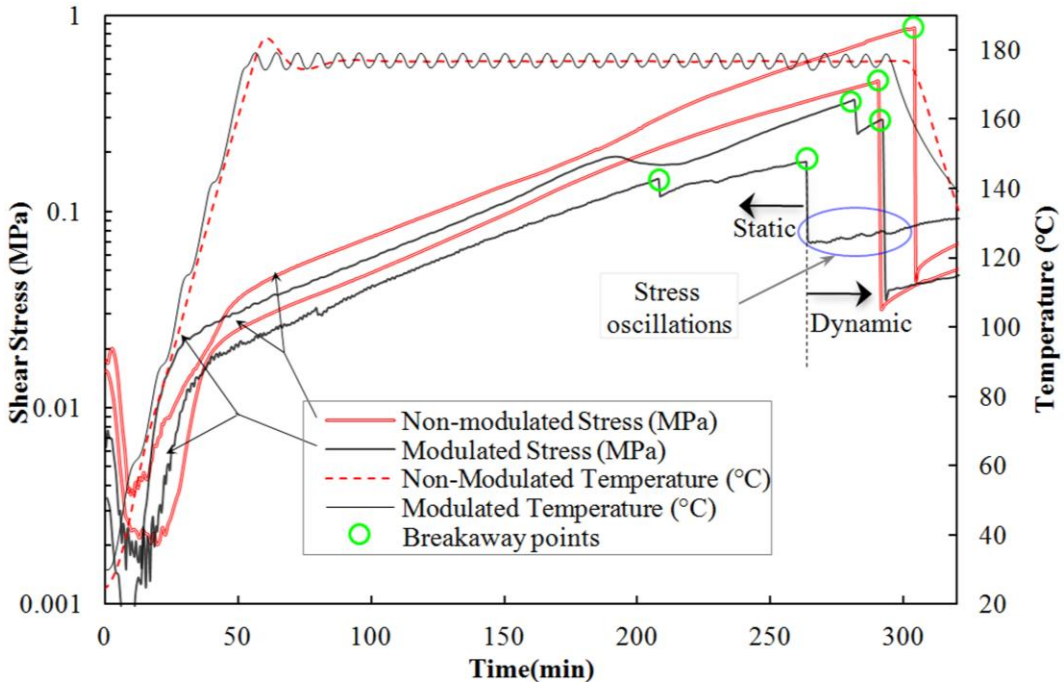

Figure 21. Modulated temperature test for release agent (method 2)

Modulations of temperature showed to be effective in reducing the static frictional tool-part interaction during manufacturing. It was observed in Figure 20 (method 1) that non-modulated tests depicted breakaway points (static friction stress) around the 145th minute of the test. However, these points were not noticed when using modulations in the temperature profile. A similar effect was observed in Figure 21 (method 2) where the magnitude of the breakaway points was 2.43 ± 0.13 times lower than the samples tested without modulations. The reduction in the magnitude of static frictional stress implied that the modulated temperature profile induced oscillations in thermal expansion at the tool-part interface, which reduced the static friction force and thus induced an earlier sliding of the sample on the tool.

4.3.6 Effect of Pull-Out Speed (Part Length) on Shear Stress

In previous sections, it was shown that the tool-part shear stress that was obtained for samples tested between 0.05 and 0.15 mm/min. These results indicated that the static COF depended on pull-out speeds only when using release method 2 (Figure 18) where the samples

tested at 0.05 mm/min showed a static/dynamic friction ratio of 5.29 ± 0.19. This ratio indicated a strong tool-part adhesion, and was considerably higher than those measured at speeds of 0.10 and 0.15 mm/min, which was 1.6 ± 0.10. Therefore, results indicated that parts with less than 0.7 m in length are likely to remain adhered to the tool, while longer parts could slide.

On the other hand, samples tested with a release film (method 1) did not depended on pull-out speed, and the stress ratio measured was 1 ± 0.01 (Figure 15). Furthermore, the dynamic COF, which was the shear stress measured after the breakaway point, did not depend on the pull-out speed for both release methods. These results agreed with the findings reported by Biswas et al. [18] who found that the dynamic COF of fluoropolymers was independent of speeds for values below 60 mm/min.

4.3.7 Effect of Tool Surface Conditions on Shear Stress

The influence of tool surface condition on shear stress was characterized by performing tests with different release materials and tool surface roughness. As such, two samples were tested using a release film (method 3, Table 4) and tools with surface roughness (R_q) of 1.35 μm and 0.18 μm that was obtained by polishing tools using sand paper of 120 and 400 grit, respectively. Results, which were portrayed in Figure 22, indicated that the shear stress decreased 10 – 27.1% when the surface roughness was 86% smoother. Then, a third sample was tested including a release agent (release method 1, Table 4) and a surface roughness of 0.18 μm where results showed a decrease in stress between 23.1 – 50.8% due to the use of this release method. Studies of friction in fluorocarbon based polymers—such as the release materials used in this research—indicated that their frictional interaction involved two mechanisms governed by the polymer hardness and surface energy [17], which are related to mechanical interlocking and thermodynamic interactions, respectively. Since the tool-part interaction was considerably

reduced when using a release agent without changing tool roughness, these results indicated, therefore, that thermodynamic interactions among release materials were more relevant to tool-part frictional stress than mechanical interlocking caused by the surface roughness of the tool.

In practical terms, these results suggested that composite manufacturers should find the most appropriated combination of release materials rather than enhancing the tool surface roughness. A very fine surface roughness might represent higher costs, while a coarser tool with the appropriate release materials could lead to a lower tool-part shear stress with an acceptable surface finishing.

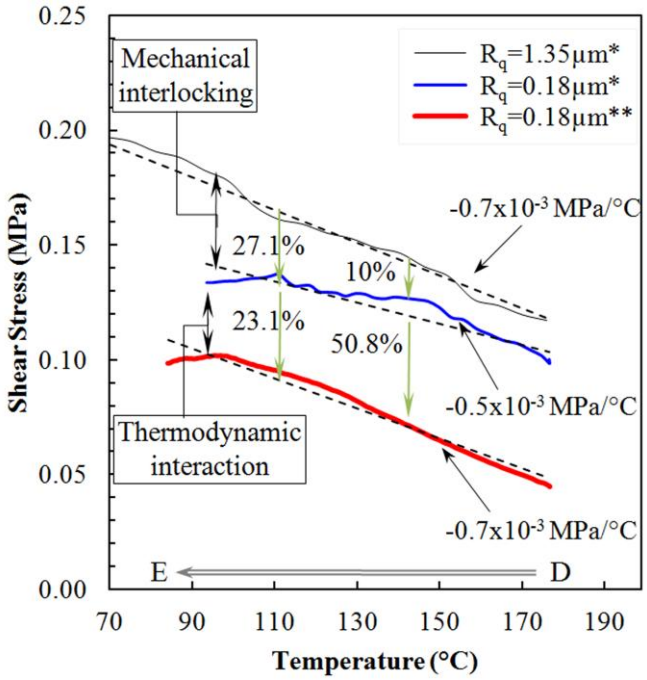

Figure 22. Shear stress measured during the D–E region (cool-down) using different tool surface conditions. Test pull-out speed: 0.05 mm/min.
**Release method 3. **Release method 1.*

4.3.8 Effect of Temperature on Shear Stress

Results obtained using modulated temperature profiles (section 4.3.6) indicated that the shear stress depended on temperature mainly when the composite sample was sliding on the tool.

Furthermore, the findings presented in section 4.3.7 showed that the shear stress encompassed two frictional modes corresponding to mechanical interlocking and thermodynamic interaction, which decreased linearly as a function of temperature (see Figure 22). These findings agreed with the literature where it was found that both mechanical interlocking [19, 20] and thermodynamic interactions [17] (surface energy [63]) might show a linear dependence with respect to temperature. Based on the physics of this frictional behavior, therefore, the dynamic frictional stress was approximated to a linear function of temperature, as shown in equation (4):

$$\tau = \mathrm{k}\,(\mathrm{c}\,\mathrm{T_c} - T) \tag{4}$$

where τ is the dynamic shear stress, and T is temperature. The terms k, c, and $\mathrm{T_c}$ were assumed constant in order to maintain a linear relation between stress and temperature, and $\mathrm{T_c}$ is an hypothetical critical temperature at which the polymer might degrade or melt [63]. Substituting equation (4) in the classical definition of COF equation (5), the dynamic COF (μ_k) was calculated using equation (6):

$$\mu = \frac{F_f}{F_N} = \frac{\tau}{\mathrm{P}} \tag{5}$$

$$\mu_k(T) = a\,T + b \tag{6}$$

where a and b are the constants shown in Table 8 which were obtained from the experimental results of section 4.3.2 and 4.3.3. The predicted μ_k was illustrated in Figure 23 and compared with the experimental results (normalized with respect to pressure) that showed the maximum and minimum dynamic shear stress values during the C–D region. Note that the study of parameters c, k, and T_c is beyond the scope of this study since μ_k was predicted with the constants a and b.

TABLE 8

CONSTANTS OBTAINED FOR μ_K IN EQUATION (6)

Release System	a	b
Release Film	$-0.95\times10^{-3}\pm0.35\times10^{-3}$	0.245 ± 0.08
Release Agent	$-0.60\times10^{-3}\pm0.1\times10^{-3}$	0.207 ± 0.02

Parameter *a* was obtained based on the results of Figure 16 and Figure 18b where the stress-temperature slope during the D–E region was normalized with respect the consolidation pressure (550 kPa), as indicated in equation (5). Since results of Figure 17 (section 4.2.3, pp. 28) indicated that the friction interaction of release materials was stable during the entire MRCC, the COF calculated during D–E region could be used to predict the COF in any other region. Results of Figure 23 proved this assumption since the shear stress did not exceed the predicted COF because the composite sample was adhered to the tool. The peaks observed in the vicinity of point C (Figure 23a) indicated that the threshold value corresponding to the static COF was reached, but after surpassing this point, the shear stress reached the predicted COF.

Parameter *b* was calculated with the value of COF measured at the beginning of the C–D region, which corresponded to the dynamic COF. As such, a considerable difference between measured and predicted friction coefficients was observed at the end of the C–D region in Figure 23 because the effects of wear and abrasion between the sample and the tool were neglected. The increase in measured COF observed during the C–D region was associated to the wear of the counter surfaces [64] while, in the case of release film, the slight negative slope observed was related to polymer deposition on the tool due to abrasion [65]. The difference obtained during the D–E was also attributed to these effects. However, these abrasive effects were not included in equation (6) because the tool-part deformation mismatch is reduced as the degree of cure of the resin advances during the C–D region.

Finally, the predicted COF values were compared with those reported in the literature for similar materials. The predicted μ_k for release film (which was calculated with equation (6)) indicated values of 0.07 ± 0.02 at 177ºC (point C) and 0.21 ± 0.07 at room temperature (point E). For the release agent, these values were 0.1 ± 0.005 at 177ºC and 0.20 ± 0.02 at point E. These values were in the same order of magnitude of μ_k obtained by Schön (μ_k = 0.3 – 0.6) who tested a carbon fiber-epoxy composite in contact with a metallic counter surface [64]. However, the μ_k reported herein was lower due to the use of release materials.

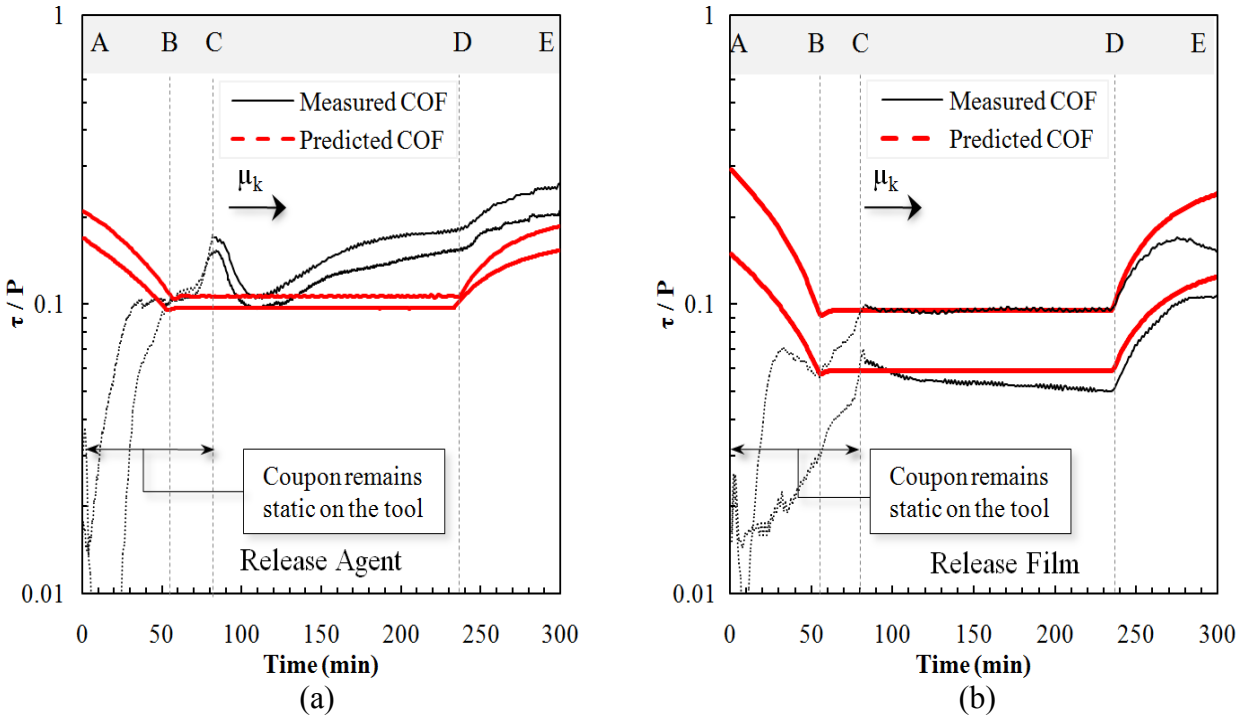

Figure 23. Measured and predicted COF when using (a) release agent and (b) release film between the tool and the sample

4.3.9 Effect of Pressure on Shear Stress

The tool-part shear stress was measured for method 1 (release film) and method 2 (release agent) when applying a consolidation pressure between 0.27 and 0.83 MPa, and results were illustrated in Figure 24. In this graph was observed that for both release methods, shear

stress showed a linear increase proportional to the pressure. This trend agreed with the classical definition of COF previously shown in equation (5) where it was indicated that the frictional force changed proportionally to the applied pressure.

In the literature, it was found that although materials used in this research might depict a linear dependence on applied pressure, it is also common to observe non-linear trends [12, 17]. As such, Bowden et al. [17] proposed an empirical model that was obtained for polymeric materials:

$$F_f(P) = k_1 \left(F_N\right)^{k_2} \tag{7}$$

where values of $k_2 \leq 1$. This model agreed with the results portrayed in Figure 24, in which the values of k_1 and k_2 were found approximately equal to μ and 1, respectively.

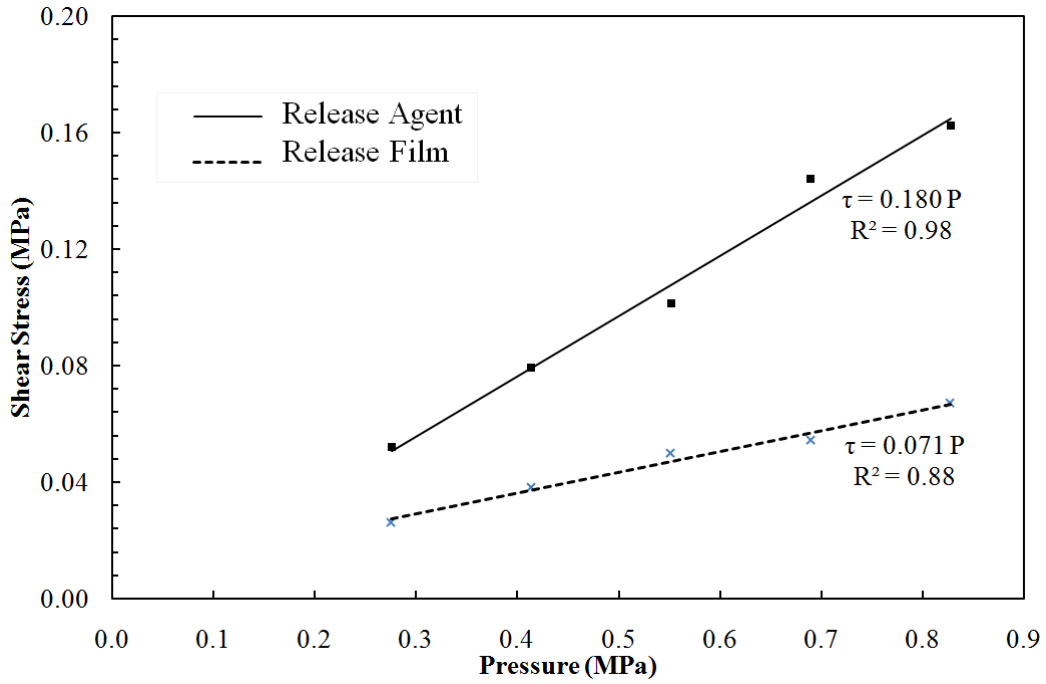

Figure 24. Tool-part shear stress as a function of pressure for release methods 1 and 2

4.3.10 Mathematical Approach to the Tool-Part Shear Stress

On the basis of the results presented in this research, a mathematical expression was proposed to predict the tool-part frictional interaction as a function of the main variables corresponding to autoclave manufacturing. This mathematical approach was based on Coulomb's friction model (equation (8)), which was modified to account for changes in frictional force as a function of temperature portrayed in equation (6).

$$F_f(P,T,t) = -F_N(P)\ \mu_k(T)\ \text{sign}(v(t)) \tag{8}$$

F_N was obtained from equation (5) and (11) and the kinetic COF as a function of temperature $\mu_k(T)$ was calculated from equation (6). The term *sign* ($v(t)$) represented the direction (not the magnitude) of the tool-part deformation mismatch. Finally, these substitutions were carried out, and the resulting mathematical approach to the tool-part shear stress was shown in equation (9).

$$F_f(P,T,t) = -\frac{P}{\text{A}}\ (\text{a}T + \text{b})\ \text{sign}(v(t)) \tag{9}$$

This expression should be complemented with the magnitude of the static COF where the static/dynamic friction ratio for method 1 (release film) was 1.05 ± 0.05. When method 2 (release agent) was used, the static/dynamic ratio was 5.29 ± 0.19 for parts shorter than 0.7 m and 5.29 ± 0.19 for longer parts.

The significance of the model shown in equation (11) was approached by analyzing the phenomenon of tool-part deformation mismatch. As shown in Figure 12, the shear stress is zero in the center of the part (x = 0) and it increases toward the edges as the deformation mismatch is developed during cure. Twigg et al. [14] showed that the transition point between static and dynamic stress migrates in the opposite direction from the edges toward the center of the part as a debonding front. In this context, the normal force (consolidation pressure) and the tool-part friction force induce a gradient of stress from the center of the part toward the edge. This

gradient reaches a limit corresponding to the threshold value of the static frictional stress. Therefore, the part remains adhered to the tool for small deformations that result in stresses lower than the maximum static shear stress indicated in equation (10a). Larger deformations that surpass the static shear stress might result in a tool-part interfacial stress that has a constant value corresponding to the dynamic shear stress shown in equation (10b).

$$\tau \leq \mu_s P \tag{10a}$$

$$\tau_k = \mu_k P \tag{10b}$$

4.4 Summary

In this chapter**,** the results of a continuous shear stress characterization when sliding composite samples on the surface of metallic tools at temperature and pressure typical of autoclave processing were shown. Initially, an orthogonal DOE was implemented to identify the most relevant manufacturing variables to the tool-part frictional stress. These preliminary findings indicated that pull-out speed (part length), consolidation pressure, and tool surface conditions were the most relevant parameters to the frictional stress.

Subsequently, samples were tested using a release film (method 1) and a release agent (method 2) between the tool and the part. Tests carried out using release method 1 showed lower values of static and dynamic coefficient of friction (COF) since the dynamic COF value for release film was 0.07 ± 0.02 while the use of the release agent only (method 2) increased this COF to 0.10 ± 0.005 (at 177ºC). Furthermore, the static/dynamic COF ratio obtained with method 1 was 1.1 while method 2 showed values up to 5.48 that indicated higher tool-part adhesion. Therefore, results implied that parts processed with a release film might develop lower geometrical distortion than parts where a release agent is used.

These samples were also tested at different temperatures, consolidation pressures, pull-out speeds, and tool surface roughnesses. As a result, a mathematical approach to the tool-part

frictional interaction was proposed based on a modification of Coulomb's friction model to account for the different manufacturing parameters. This mathematical expression was also validated with the mechanical and thermodynamic mechanisms found in the literature, which were related to the tool-part interaction.

CHAPTER 5

SHEAR STRESS CHARACTERIZATION OF SANDWICH STRUCTURES WHEN SUBJECTED TO TYPICAL AUTOCLAVE PROCESSING CONDITIONS

5.1 Introduction

A novel testing methodology was implemented to measure the shear strength of sandwich structures when subjected to combined conditions of temperature and pressure. For this purpose, the customized testing rig described in chapter 3 (pp. 15) was utilized. This study included an analysis of the shear stress of different materials that are commonly used for manufacturing of structural composite parts including aramid fiber honeycomb cores, epoxy adhesives, CFRP prepreg skins, and a combination of thereof in a sandwich structure. Furthermore, tests were focused on studying the shear strength of honeycomb cores in order to determine the amount of stress that cores can withstand before crushing due to the severe conditions exerted during autoclave processing [13]. This customized testing methodology was implemented because current standard test methods for sandwich structures (ASTM C273 [42]) do not include specifications to measure shear strength when samples are subjected to combined conditions of pressure and temperature. Therefore, it was imperative to develop a novel testing procedure to surpass these limitations.

5.2 Materials and Testing Parameters Used for Shear Stress Characterization of Sandwich Structures

Shear stress was measured using samples made of different composite materials typically used in sandwich structures (see Table 9). HRH-10 was chosen as the core of the sandwich structure since this material is commonly used in aerospace applications for structural and non-structural parts [66]. Hysol PL 7000 was used for co-curing the prepreg and the sandwich

structure because this epoxy adhesive has a curing temperature of ~180ºC [67], which is similar to that required for the prepreg IM7/977-2 UD. Therefore, samples were tested during the MRCC of this CFRP prepreg, which consisted in a ramp-up of 2.8ºC/min and a dwell time of 3 hours at 177ºC.

TABLE 9

MATERIALS USED FOR SHEAR STRESS CHARACTERIZATION OF SANDWICH STRUCTURES

Core	Aramid fiber/phenolic overexpanded honeycomb core HexWeb HRH-10-1/8-3.0 (by Hexcel)
Adhesive	Epoxy adhesive film Hysol PL 7000 (by Henkel)
Skin (face sheets)	Carbon fiber-epoxy prepreg IM7/977-2 UD (by Cytec)

Initially, the shear stress of the entire sandwich structure was characterized using a sample such as that illustrated in Figure 25. Then HRH-10 cores were tested at the pressures and temperatures mentioned in Table 10 with the aim of determining the effect of manufacturing conditions on shear strength in the principal directions—those are, ribbon and direction of expansion (see Figure 26). For these tests, squared samples (10 x 10 cm^2) of HRH-10 core were adhered to the pull-out plate of the testing rig (Figure 4b) and the heated metallic plates (Figure 4c) using a high-temperature epoxy adhesive, and a pull-out speed of 0.05 mm/min was utilized. The testing area of the rig was wrapped with super-insulating carbon aerogel (by McMaster-Carr) in order to maintain a constant temperature throughout the sample. Finally, the calculations of shear strength and core shear modulus were performed using the methodology suggested by ASTM C273.

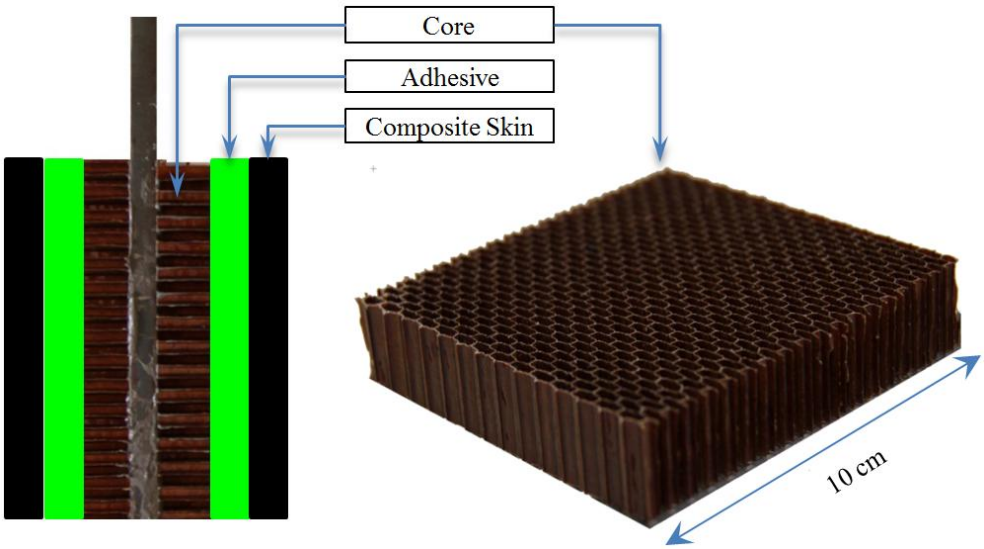

Figure 25. Sample used for shear stress characterization
of sandwich structures

TABLE 10

SAMPLES USED FOR CHARACTERIZATION OF SHEAR STRENGTH OF HONEYCOMB CORE HRH-10. UTM CROSSHEAD SPEED: 0.05 mm/min

Results	Direction	Pressure	Temperature
Figure 28	d11	310 kPa	23ºC
	d22	310 kPa	23ºC
Figure 29	d11	310 kPa	23ºC
	d11	550 kPa	23ºC
Figure 30	d22	310 kPa	23ºC
	d22	550 kPa	23ºC
Figure 31	d22	310 kPa	23ºC
	d22	310 kPa	60ºC
	d22	310 kPa	120ºC
	d22	310 kPa	177ºC

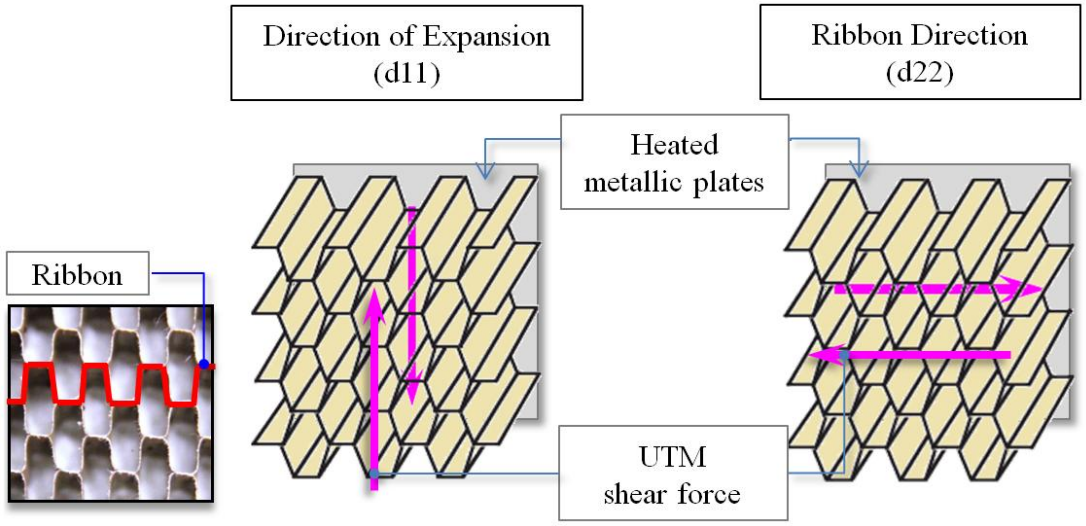

Figure 26. Principal directions of honeycomb cores: perpendicular to the ribbon or direction of expansion (d11) and ribbon direction (d22)

5.3 Shear Stress Characterization of Sandwich Structure

Tests were performed using the materials mentioned in Table 9 in order to study the shear stress behavior of a sandwich structure during co-curing CFRP face sheets with an aramid honeycomb core. Results, which were illustrated in Figure 27, indicated that the shear stress behavior of the entire sandwich structure depended on the mechanical properties of each of its constituent materials since the obtained stress curve showed a sudden increase in stress at the 70^{th} minute, which was associated with the gel point of the prepreg. Similarly, stress depicted a linear trend after the 90^{th} minute that was similar to the elastic behavior shown by the adhesive layer. This elastic behavior was extended until the minute 160^{th} where the elevated shear stress induced core crush. Therefore, results implied that the residual stresses transferred to the core during manufacturing strongly depend on the degree of cure of the CFRP skins and core-skin adhesive layer.

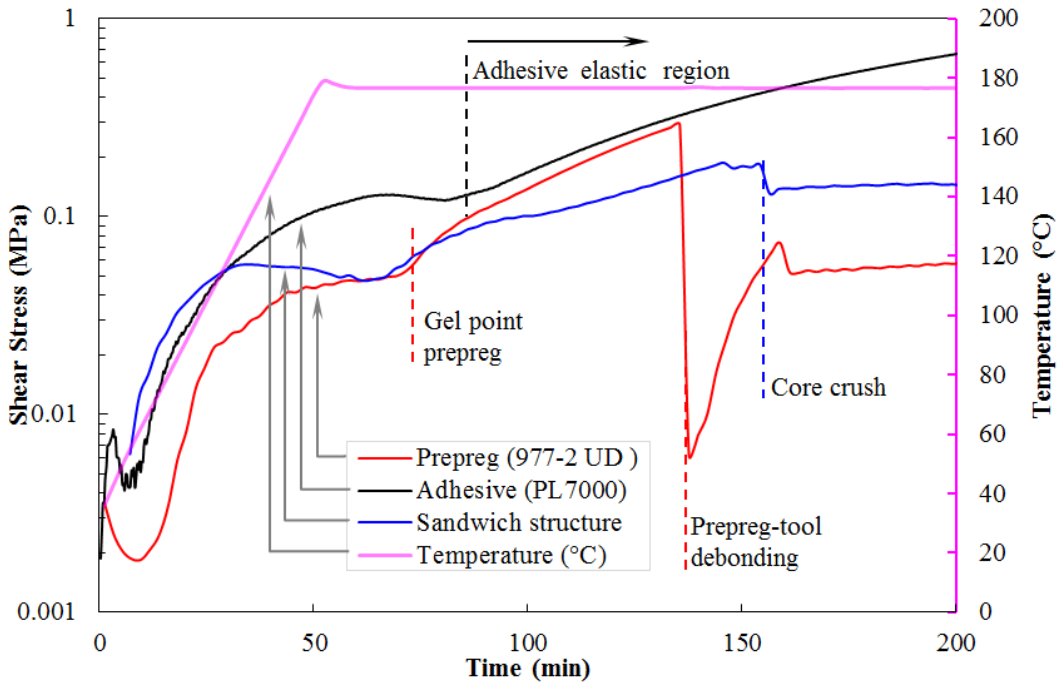

Figure 27. Shear stress characterization for carbon fiber-epoxy skin, adhesive, aramid core, and sandwich structure at 310 kPa

The transverse component of autoclave pressure could cause core crush, as previously mentioned in chapter 1, Figure 2 (b). As such, the findings portrayed in Figure 27 implied that cores might be vulnerable to these transverse pressures during the earlier stages of the cure cycle. In particular, transverse stresses could be transferred to the core around the 20th minute because, at this point, skins and adhesives showed the lowest shear resistance, and therefore had a weak capacity to bear the forces induced by the transverse component of manufacturing pressure. These findings agreed with the literature where it was mentioned that core crush could be influenced by resin viscosity, and prepreg-prepreg interlaminar interaction would determine the amount of residual shear stresses transferred to the core during manufacturing [6, 7, 13, 37]. However, a viscoelastic analysis previously performed to the prepreg skins (see pp. 36) indicated that this point of minimum shear stress did not match the point of minimum viscosity. Instead, shear stress was found related to the maximum resin flow point, which did not necessarily match

the point of minimum viscosity [62]. Therefore, these findings indicated that the point of maximum resin flow in the composite skins should be considered during the design of autoclave co-cured sandwich structures.

5.4 Influence of Ribbon Orientation in Shear Strength of Aramid Cores

Aramid honeycomb cores HRH-10 were subjected to shear forces in order to determine their strength at the pressures and temperatures mentioned in Table 10. Results corresponding to tests performed at 23ºC and 310 kPa were shown in Figure 28 for samples tested in the principal directions of the core (Figure 26): direction of expansion (d11) and ribbon direction (d22).

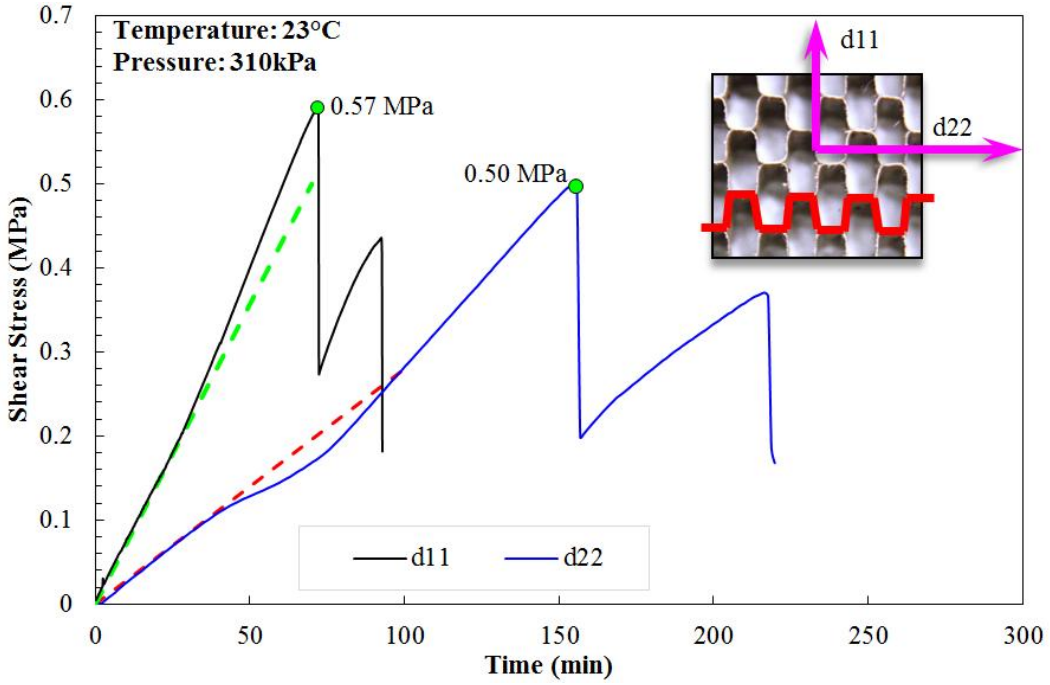

Figure 28. Shear stress characterization for HRH-10 honeycomb cores in d11 (direction of expansion) and d22 (ribbon direction) at 310 kPa and room temperature

Samples tested in d11 showed a constant increase in shear stress during the first 60 minutes of testing, which corresponded to elastic deformation of the core [41]. During this elastic region, two stages were observed in the stress curve. First, stress increased linearly during 30 minutes, and then the slope of the curve increased until the point of final failure. A similar behavior was

observed when testing samples oriented in d22 where a linear region was measured during the first 40 minutes, and subsequently a non-linear region was observed until the 74th minute where the curve continued with a linear trend until the point of final failure (150th minutes of the test). These changes in slope, which were more notorious in d22, could be related to reduction in mechanical properties. Furthermore, results also showed that the ultimate shear strength was 12% higher in d11 than d22, which implies, therefore, that HRH-10 cores would be more likely to fail in d22. Note that stronger mechanical properties in d11 agreed with the specifications reported by the manufacturer [66] where consolidation pressure was zero.

5.5 Influence of Consolidation Pressure on Shear Strength

The shear strength of honeycomb cores was measured when samples oriented in d11 were subjected to two different pressures with the aim of studying the effect of autoclave consolidation pressure in the structural integrity of the core. Results, which were illustrated in Figure 29, indicated that the consolidation pressure negatively affected the shear strength of samples tested in d11 because the ultimate shear strength decreased 22.4% when the pressure was increased from 310 kPa to 550 kPa. Then, the shear strength was plotted as a function of pressure where the strength value at 0 kPa was obtained from the literature [66] where it was observed that the strength vs. pressure curve followed an inverse exponential trend. Therefore, these results implied that chances of core crush would increase at elevated pressure due to two factors: the ultimate shear strength of the core decreases and the transverse component of autoclave pressure increases.

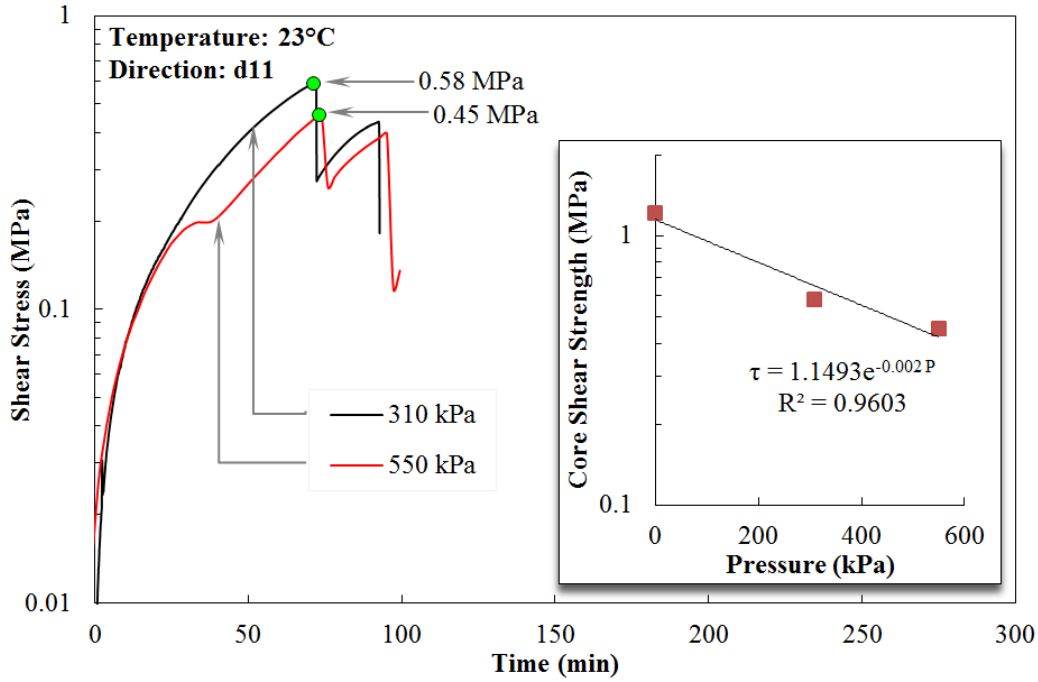

Figure 29. Shear stress characterization in d11 (direction of expansion) at 310 and 550 kPa

The HRH-10 core was also tested at different pressures in the ribbon direction (d22), and results were shown in Figure 30. The shear strength measured in d22 depicted a similar behavior than those tests performed in d11—that is, an inverse exponential trend of shear strength vs. pressure. However, results obtained in d11 indicated a higher decreased rate than those of d22, which implied that if results were extrapolated to ~800 kPa, there would be no difference between strength in d11 and d22. In the literature, Lee et al. [43] explained this phenomena as a decrease in degree of anisotropy (d11/d22 strength ratio) where the researchers identified a decrease in this strength ratio as temperature increased. Therefore, based on the results of Lee et al. (strength vs. temperature) and those portrayed in Figure 30 (strength vs. pressure), these findings implied the degree of anisotropy of honeycomb cores may decrease as both pressure and temperature increase.

Further, elastic elongation before failure was shown invariable for samples tested in d11 because the two curves shown in Figure 29 depicted the ultimate shear stress at the 65th minute of the test. On the other hand, samples tested in d22 (Figure 30) showed core failure at different points where tests performed at 550 kPa showed a failure point ~60 minutes earlier than that of the sample tested at 310 kPa. As such, these results indicated that consolidation pressure decreased the elongation of the core before failure only in d22.

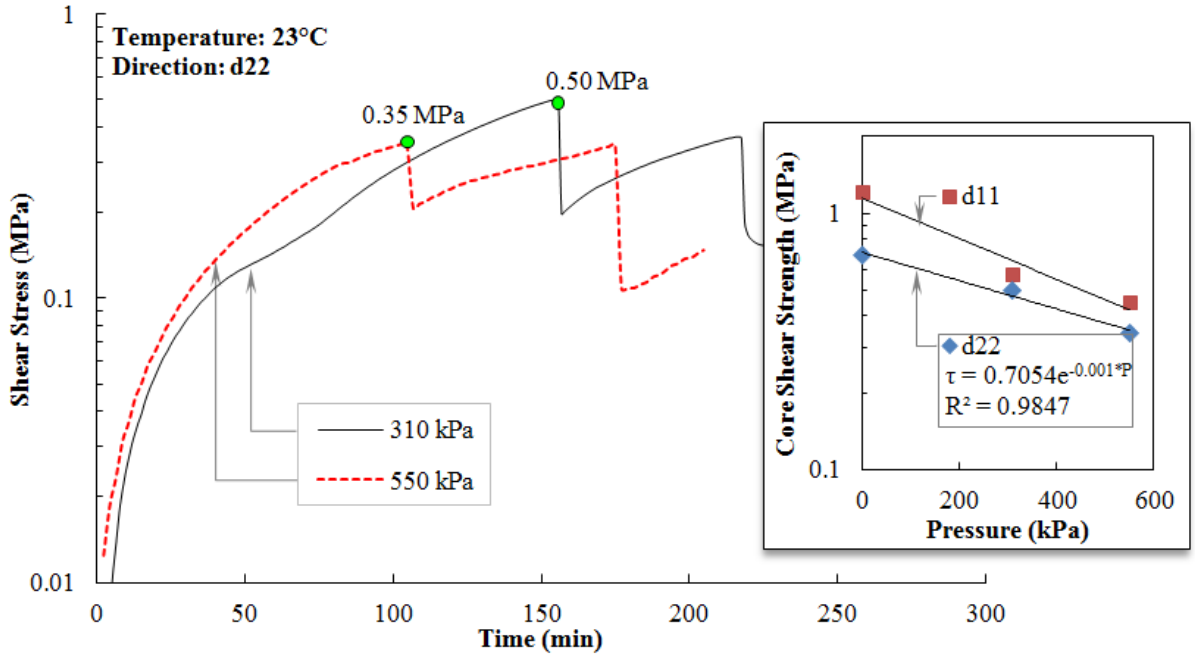

Figure 30. Shear stress characterization in d22 (ribbon direction) at 310 and 550 kPa

5.6 Influence of Temperature on Shear Strength

The effect of temperature in shear stress was characterized between 23ºC and 177ºC using a consolidation pressure of 310 kPa, which corresponded to a typical autoclave cycle, and results were shown in Figure 31. Note that samples of HRH-10 honeycomb core were tested only in the ribbon direction (d22) since previous results indicated that cores were weaker in d22. The maximum shear stress measured in Figure 31 was plotted as a function of temperature (see

Figure 32) where it was observed that the core shear strength decreased as temperature increased. These results complemented the findings of Lee et al. [43], who indicated that the shear strength of aramid honeycomb cores decreased when temperature increased without applying a consolidation pressure. The findings of Figure 32 evidenced that this decrease also occurred when samples were subjected to pressures of 310 kPa.

The curve shown in Figure 32 indicated an inverse exponential trend, which implied that the slope of such curve decreased as temperature increased. These findings differed from those reported by Lee et al. [43] because their results showed an increase in this slope. Notice that aramid cores used by Lee et al. had a hexagonal geometry that differed from samples utilized herein because the HRH-10 cells had an overexpanded shape. Therefore, these findings implied that cell architecture could affect the strength-temperature behavior.

Lastly, results of Figure 31 showed different failure mechanisms as temperature increased. At high temperatures (120 and 177ºC), tests depicted a sudden stress decrease at the failure point (160^{th} minute)**,** while samples tested at lower temperatures (23 and 60ºC) showed a progressive decrease after 120 minutes of testing. Hence, results indicated that temperature affected shear strength, failure mode, and elongation before failure.

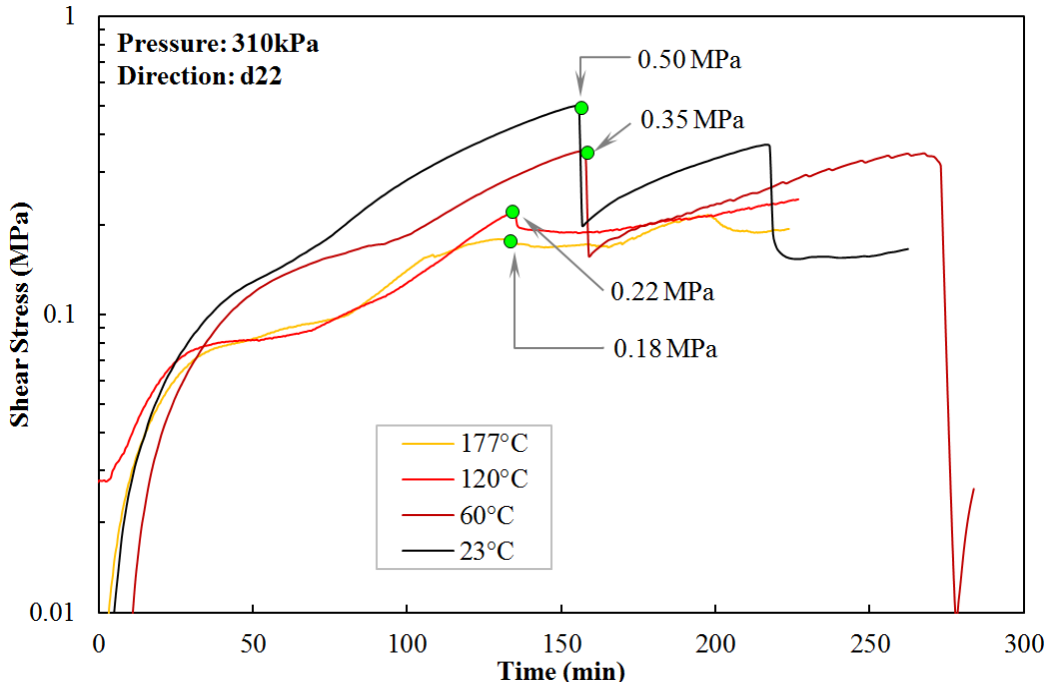

Figure 31. Shear stress characterization in d22 (ribbon direction) at different temperatures, when applying 310 kPa of pressure

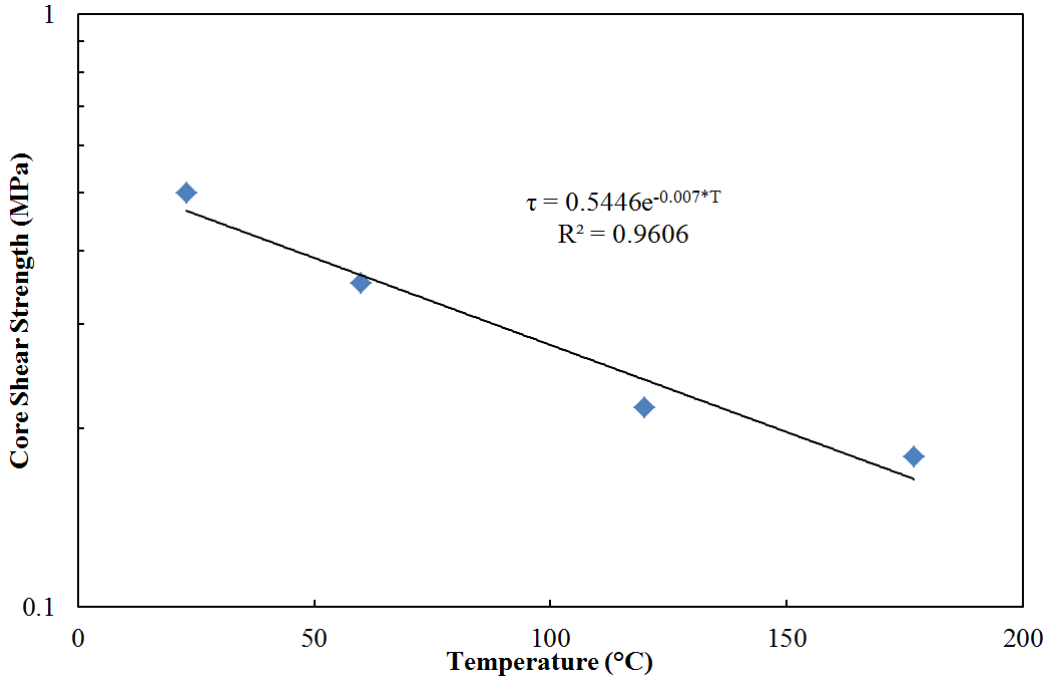

Figure 32. Ultimate shear strength as a function of temperature (consolidation pressure: 310kPa)

5.7 Conclusions

A novel testing methodology was proposed to characterize the shear stress of cores, adhesives, composite skins, and a combination of thereof in a sandwich structures while applying combined conditions of temperature and pressure. Initially, the whole sandwich structure was tested**,** and results indicated that the shear strength of the structure was influenced by the individual behavior of adhesive and prepreg. As such, the core might be vulnerable to transverse forces (exerted by the autoclave pressure) during the earlier stages of the cure cycle (around the 20^{th} minute) due to the low shear strength of skins and adhesive layer.

Subsequently, the aramid cores were tested in the direction of expansion (d11) and ribbon direction (d22) while applying pressures up to 550 kPa. These tests indicated that the shear strength decreased as pressure increased in both directions. Similarly, the strength anisotropy ratio (d11/d22) decreased as a function of pressure. Results showed that the weakest direction of the core was d22. Hence, samples were tested in d22 while applying combined conditions of temperature and pressure. The consolidation pressure was similar to that used for manufacturing of sandwich structures (310 kPa), and the temperature was changed from 23 to 177ºC. These results evidenced that temperature decreased the strength and elongation of the honeycomb cores before failure. Moreover, the trend of the strength-temperature curve was an inverse exponential, which was a similar trend to that measured in the curve of pressure vs. strength.

CHAPTER 6

INFLUENCE OF FIBER CONFIGURATION ON THERMAL PROPERTIES OF CFRP CHARACTERIZED USING THE LFA METHOD

6.1 Introduction

Thermal properties of composite materials depend on the amount and configuration of constituent materials because fibers and matrices have different thermal properties. In the case of carbon fiber-epoxy composites, fibers have considerably higher thermal conductivity (24.0 W/(m·K) [68]) than resins (0.17 – 0.79 W/(m·K) [69]), which implies that fabric weave configuration and fiber volume fraction (V_f) may affect the thermal properties of composite parts [46]. These thermal properties are crucial during manufacturing because CFRP are commonly heat-cured using ovens or autoclaves where the predominant heat transfer methods are shown in Figure 33: autoclave/oven convection and tool-part conduction. Note that although tools are commonly heated by convection, the tool-part heat transfer mechanism is conduction due to the higher thermal mass (thermal inertia) of the tool. Hence, the combination of these heat transfer mechanism along with the internal heat generation caused by the exothermic curing reactions typical of epoxy resins may induce gradients in heat flow and irregular curing throughout the part. These curing gradients might also reduce the mechanical properties and create geometrical distortion [47]. Since these defects are not easily reversible, curing gradients can be predicted using numerical methods which require several submodels including thermal properties of the materials [25, 70].

In this chapter, it was investigated the influence of fabric weave configuration on thermal properties including thermal diffusivity, specific heat (C_p), thermal expansion (density), and thermal conductivity using cured samples made of carbon fiber-epoxy prepregs. These samples

were made of autoclave resin systems, out-of-autoclave resin systems, and three different prepreg fiber fabrics.

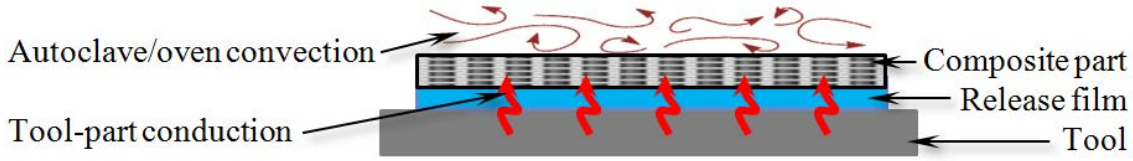

Figure 33. Heat transfer mechanisms during composite processing

The methodology utilized was Light Flash Analysis, which demonstrated reduced testing times for a large number of samples compared with other methods of thermal analysis [55]. In addition, thermal properties of a tetrafluoroethylene (TFE) release film were measured to determine the thermal conductivity at the tool-part interface and to quantify the error induced by graphite coatings on both CFRP and TFE samples.

6.2 Methodology: Light Flash Analyzer

Thermal properties of composite materials were measured utilizing a light flash analyzer (LFA, Nanoflash 447 by Netzsch), following the ASTM E1461. As shown in Figure 34, this analyzer operated a xenon flashlight that induced a pulse of energy on the bottom side of the sample. Such pulse increased the sample temperature, and an indium antimonide (InSb) infrared detector (on the top side of the sample) measured the temperature response time to this pulse of energy. The response time was utilized to calculate thermal diffusivity using different models that are mentioned in section 6.2.1 (pp. 66).

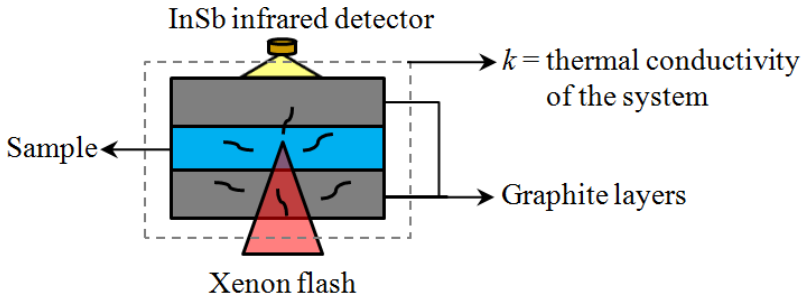

Figure 34. Operational principle of the LFA

For instance, the thermal diffusivity could be calculated using the Parker/adiabatic method (ideal case) as follows [51]:

$$\alpha = 0.13879 \cdot \frac{l^2}{t_{1/2}} \tag{11}$$

where α is the thermal diffusivity, l is the sample thickness, and $t_{1/2}$ is half of the response time. Then, the thermal conductivity k was calculated by multiplying α, specific heat (C_p), and the sample density (ρ):

$$k(T) = \alpha(T) \cdot C_p(T) \cdot \rho(T) \tag{12}$$

6.2.1 Thermal Diffusivity

Using the software Proteus LFA Analysis v. 4.8.5 (by Netzch), the post-processing of data acquired with the LFA was performed, and the thermal diffusivity was calculated by solving the Fourier equation for heat conduction in one dimension [71]:

$$\dot{T}(z,t) = \alpha \cdot \nabla^2 T(z,t) \tag{13}$$

where $T(z,r)$ represents the difference between sample and surrounding temperatures. α in equation (13) was calculated using four mathematical models of thermal diffusivity: adiabatic/Parker model (ideal case) [51], heat loss correction/Cowan model [72], radiation-diathermic/Mehling et al. model [73], and Cape-Lehman model [74]. Subsequently, thermal

diffusivity was recalculated for all samples using the model that showed the lowest standard deviation with respect to the temperature response obtained with the infrared sensor.

The flash pulse length used was 350 μs, since Always-Cooper et al. [55] indicated that using a pulse of ~400 μs for samples with a thermal conductivity of ~10 W/(m·K) would induce a negligible error due to the temperature dependency of thermal properties. Additionally, the voltage applied was 304 V and no optical filters were used.

6.2.2 Density

The change in density of composite materials used in this research was calculated with equations (14) and (15) where the anisotropy effect caused by the thermal expansion was considered. Note that the CTE of fiber-reinforced composites might be affected by fiber orientation and fabric configuration [27]. As such, using the procedure described in Appendix B, the following equations for density as a function of temperature were used:

$$\rho(T) = \frac{\rho_o}{\left(1+\frac{\Delta L_{11}(T)}{L_{o_{11}}}\right)\cdot\left(1+\frac{\Delta L_{33}(T)}{L_{o_{33}}}\right)^2} \qquad \text{for unidirectional laminates} \qquad (14)$$

$$\rho(T) = \frac{\rho_o}{\left(1+\frac{\Delta L_{11}(T)}{L_{o_{11}}}\right)^2\cdot\left(1+\frac{\Delta L_{33}(T)}{L_{o_{33}}}\right)} \qquad \text{for plain and satin weaved fabrics} \qquad (15)$$

where L_{oij} is the sample length measured at 23ºC (room temperature). The thermal strain $\Delta L_{ij}(T)/L_{o_{ij}}$ was measured in directions d11 and d33 utilizing a thermomechanical analyzer (TMA, Q400 by TA instruments), where ASTM E831 [75] was used as a reference. These tests consisted in equilibrating the sample at 0ºC and then measuring the dimensional change up to 180ºC during a temperature ramp of 2ºC/min (probe contact force of 50 mN).

The density at room temperature ρ_o was obtained using the *Test Method A*—testing solid plastics in water—of the ASTM D792 [76]. The weight of the sample in air w and its weight when submerged in water w_w were measured with a scale Mettler Toledo XS205, and the sample density was calculated by the Archimedes principle:

$$\rho_o^{23°C} = \frac{w_w \cdot \rho_{water}^{23°C}}{w_w - w} \tag{16}$$

where the density of the water was 0.998 g/cm^3 at 23ºC.

6.2.3 Specific Heat (C_p)

Using the mentioned Proteus LFA Analysis v. 4.8.5 software, C_p was calculated by measuring the temperature change of the samples and a reference material when subjected to the same pulse of energy as follows:

$$\Delta T_s = \left(\frac{Q}{\rho l C_p} \right)_S \qquad \Delta T_r = \left(\frac{Q}{\rho l C_p} \right)_r \tag{17}$$

where Q is the energy corresponding to a light pulse of 350 μs of the LFA flash lamp, l is sample thickness, ΔT is temperature change, and suffixes *s* and *r* are sample and reference, respectively. The reference material used for this purpose was Pyrex 7740 Borosilicate glass, provided by Netzsch. This material was chosen because preliminary tests indicated that Pyrex had similar C_p to that measured in composite materials (~0.75 J/(g·K) at room temperature). Moreover, the thermal conductivity of Pyrex 7740 is ~1.0 W/(m·K) at room temperature, which was a value between the thermal conductivity of the composite in d11 (2 – 3 W/(m·K)) and d33 (0.5 – 0.6 W/(m·K)) [46].

Since Q was the same for sample and reference (light pulse of 350 μs), C_p of sample was calculated as follows:

$$C_{p_S}^{*} = \frac{\rho_r l_r C_{p_r} \Delta T_r}{\rho_s l_s \Delta T_s} \tag{18}$$

where $C_{p_s}^{*}$ was the specific heat calculated by the software, in which an isotropic density was assumed. Then, $C_{p_s}^{*}$ was multiplied for a correction factor where the anisotropic thermal expansion (Appendix B) of the sample was considered. Hence, the sample C_p was calculated with equations (19) and (20):

$$C_{p_S} = C_{p_s}^{*} \cdot \left[\frac{\left(1 + \frac{\Delta L_{11}(T)}{L_{o_{11}}}\right)^3}{\left(1 + \frac{\Delta L_{11}(T)}{L_{o_{11}}}\right) \cdot \left(1 + \frac{\Delta L_{33}(T)}{L_{o_{33}}}\right)^2} \right] \text{ for unidirectional laminates} \tag{19}$$

$$C_{p_S} = C_{p_s}^{*} \cdot \left[\frac{\left(1 + \frac{\Delta L_{11}(T)}{L_{o_{11}}}\right)^3}{\left(1 + \frac{\Delta L_{11}(T)}{L_{o_{11}}}\right)^2 \cdot \left(1 + \frac{\Delta L_{33}(T)}{L_{o_{33}}}\right)} \right] \text{ for plain and satin weave laminates} \tag{20}$$

LFA results were compared with tests performed using a differential scanning calorimeter (DSC, Q2000 by TA instruments), which is a method commonly used to measure specific heat by the ASTM 1269 [77]. DSC samples consisted of squares of approximately 2 x 2 x 1 mm^3.

6.3 Materials

The characterization of thermal properties by the LFA method was performed using the materials mentioned in Table 11, which had the fiber configurations illustrated in Figure 35: unidirectional tape (UD), eight-harness satin weave (8HS), and plain weave (PW). Initially,

panels of 300 x 300 mm^2 were cured using the manufacturing cycles shown in Figure 36 where those made of 5320 resin system were vacuum bag cured in an oven while panels made of the resin system 977-2 were cured in an autoclave. One panel was manufactured for each fiber configuration for a total of five panels: two panels of 977-2 resin system (UD and PW fiber configuration) and three panels of 5320 (UD, 8HS, and PW). Then these panels were machined to obtain samples for LFA testing in the fiber direction (d11), which consisted of five strips of 10 x 2 mm^2 with 2 mm in thickness. Similarly, squared samples of 10 x 10 mm^2 with 2 mm in thickness were used for through-the-thickness (d33) tests. Lastly, squared samples of 10 x 10 mm^2 were used to determine the thermal conductivity of a TFE release film (WL-5200 blue by Airtech). In order to avoid variations due to emissivity of the surfaces [78, 79], samples were coated with a dry graphite film dgf-123 by Miracle Power, as depicted in Figure 34. Notice that the characterization of diffusivity, C_p, density, and conductivity was performed at temperatures between 25 to 180ºC, and three samples were tested for each material.

TABLE 11

CARBON FIBER-EPOXY MATERIALS UTILIZED FOR CHARACTERIZATION OF THERMAL PROPERTIES

Resin system	Cycom 977-2 Epoxy (autoclave resin)		Cycom 5320 Epoxy (out of autoclave resin)		
Fiber type	IM7	IM7	T650	T650	T650
Fiber configuration	Unidirectional	Plain weave	Unidirectional	Eight-harness satin weave	Plain weave
Fibers per tow	Tape	3000	Tape	3000	3000

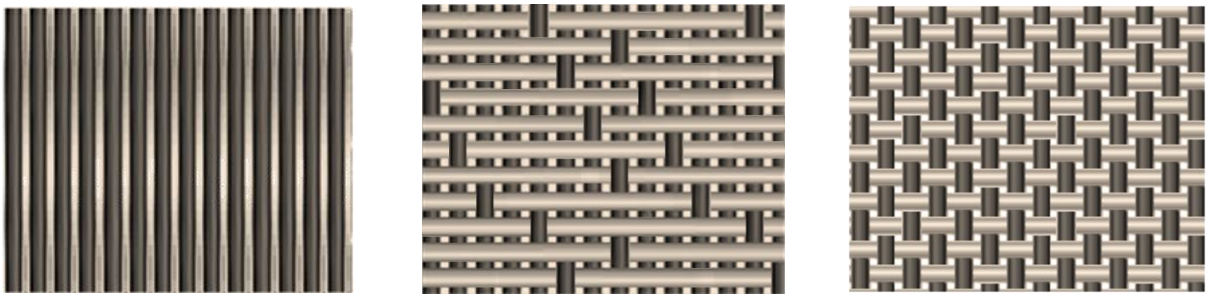

(a) (b) (c)

Figure 35. Fabric configuration: (a) unidirectional tape, (b) eight-harness satin weave, and (c) plain weave [80]

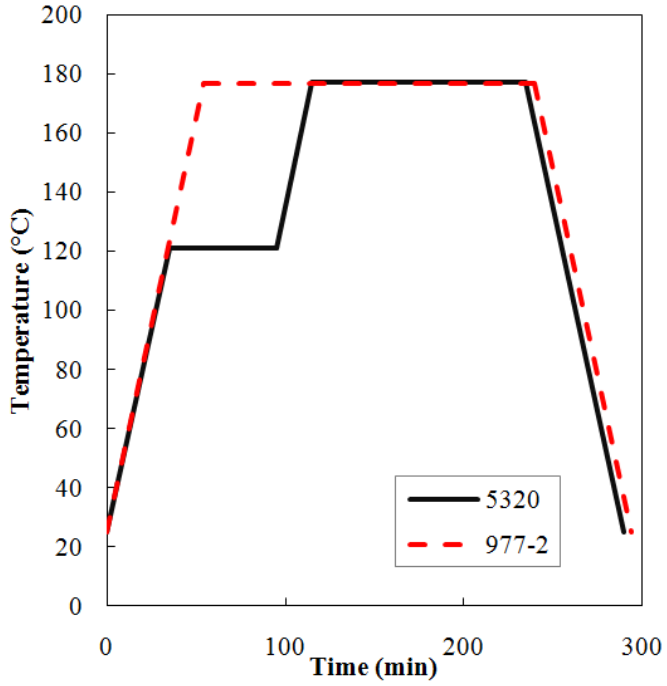

5320 system (oven cured)	
Debulking	12 hours
Ramp-up	2.8ºC/min (5ºF/min)
Dwell	121ºC (250ºF) for 60 min
Ramp-up	2.8ºC/min (5ºF/min)
Dwell	177ºC (350ºF) for 120 min
Cool-down	2.8ºC/min (5ºF/min)

977-2 system (autoclave)	
Debulking	6 hours
Ramp-up	2.8ºC/min (5ºF/min)
Dwell	177ºC (350ºF) for 120 min
Cool-down	2.8ºC/min (5ºF/min)
Autoclave pressure	550kPa (80 psi)

Figure 36. Manufacturer's recommended cure cycle for 5320 and 977-2 resin systems

Samples of resin only (without fibers) were made of 977-2 and 5320 resin systems to determine its density (see results in Table 12). The procedure to manufacture these samples consisted in dissolving the prepreg resin in acetone and then this mixture was filtered to separate the fibers. Subsequently, the filtered solution of acetone-resin was deposited in aluminum molds and dried while applying a vacuum at room temperature (23ºC) for 48 hours to evaporate the

acetone from the solution. Finally, the remaining resin was cured in an oven using the MRCC, and resin samples were obtained.

6.4 Results

6.4.1 Density

Density was measured at room temperature for the composites mentioned in Table 11 to obtain the term $\rho_o^{23°C}$ of equation (13) and (14). Results, shown in Figure 37, indicated that different weave configurations affected the composite density because samples made of woven fabrics (PW and 8HS) showed lower density values than those measured in UD samples. Since the density of epoxy resins was ~27% lower than that of carbon fibers (see Table 12), these findings implied that samples with higher density would contain a larger amount of fibers—that is, high fiber volume fraction (V_f). Therefore, results indicated that fiber configuration influenced both density and V_f of the different materials tested, which agreed with the literature where it was found that V_f values for unidirectional composites were higher (V_f = 50 – 70% [81]) than those for woven fabrics (V_f = 35 – 55% [82, 83]).

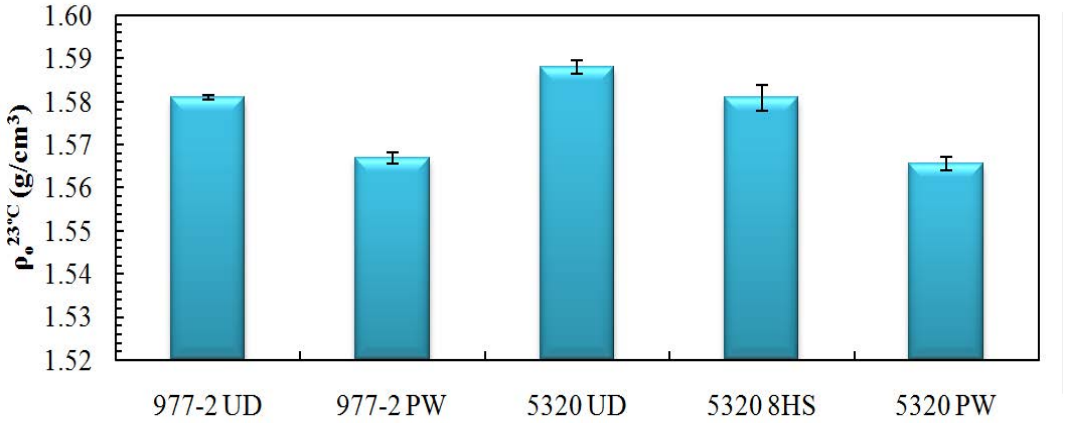

Figure 37. Density of the different carbon fiber-epoxy composite materials at room temperature

TABLE 12

DENSITY OF EPOXY RESIN AND CARBON FIBERS

Material		Density (g/cm^3)
Epoxy resin	Cycom 977-2	1.299
	Cycom 5320	1.292
Carbon Fiber [80]	IM7	1.78
	T650	1.76

Once the density was characterized at room temperature, the next step was to measure the thermal expansion $\Delta L(T)/L_0$ of composite samples oriented in fiber direction (d11) and through-the-thickness (d33) using a TMA in order to obtain the remaining terms of equation (13) and (14). Figure 38a showed that in d33, composites made of 977-2 resin had higher thermal expansion than those made of 5320 resin. Moreover, UD tapes depicted lower thermal expansion than woven fabrics when the same resin system was used. Hence, results implied that thermal expansion in d33 was governed by the epoxy resin where 977-2 showed higher thermal expansion than 5320.

Figure 38a also indicated that thermal expansion in d33 was considerably higher than d11, which agreed with results reported in the literature [27]. Results of samples tested in d11 were portrayed in Figure 38b where the curves were shown grouped with respect to the sample fiber configuration. Woven fabrics depicted a positive thermal expansion whereas UD tapes indicated a slightly negative expansion. Note that curves of PW and 8HS samples were overlapped regardless of the resin formulation. Therefore, these findings indicated that in d11 fiber configuration was the predominant factor**,** while in d33 the thermal expansion was dominated by the resin.

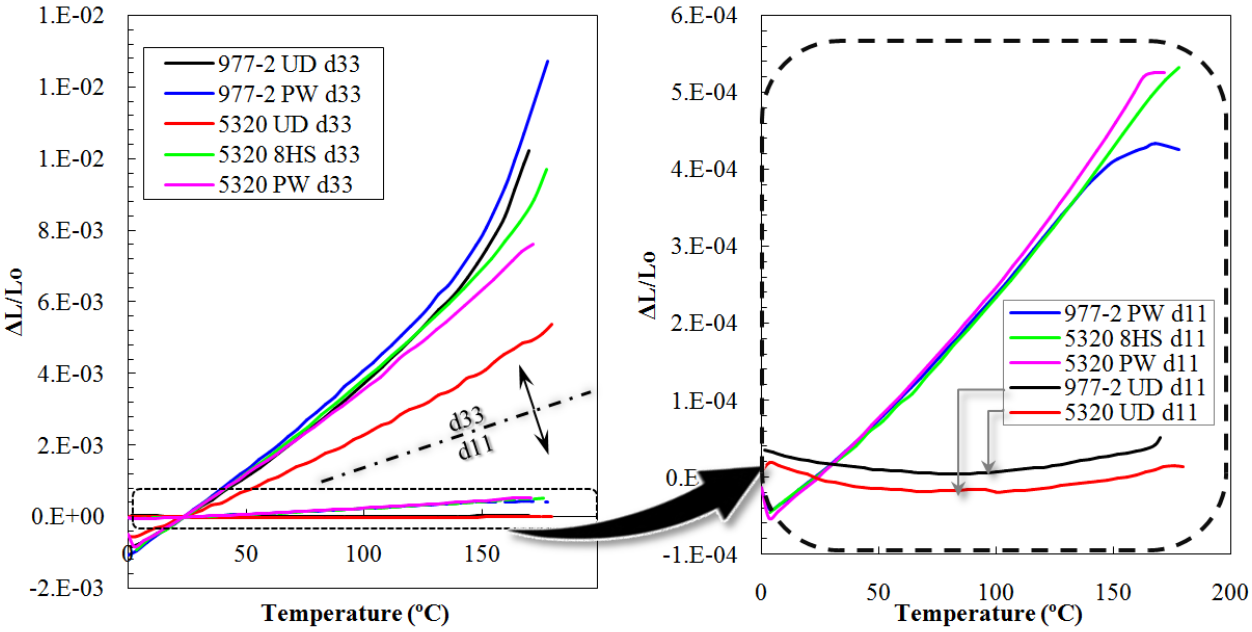

(a) (b)

Figure 38. Thermal expansion $\Delta L(T)/L_o$ of composite materials measured by TMA

The results obtained of $\rho_o^{23°C}$ and $\Delta L(T)/L_o$ in this section was organized in a spreadsheet that was later used to calculate the thermal conductivity and C_p using equations (12) and (18), respectively. Notice that tests in d22 direction were not performed due to the assumptions showed in Appendix B, equations (26) and (27).

6.4.2 Specific Heat (C_p)

The specific heat was characterized for materials shown Table 11 using the LFA method (Figure 39a), and results were compared with those obtained utilizing a DSC (Figure 39b). In these graphs it was observed that C_p curves were similar for all the CFRP samples tested since at room temperature (20ºC), C_p was measured around 900 J/(kg·K) while at 180ºC was ~1300 J/(kg·K). Furthermore, C_p increased linearly proportional to temperature for all the samples where the linear regression results (depicted in Table 13) indicated R^2 values of 0.90 ± 0.09. Similarly, the regression parameters *m* and *b* were 2.66 ± 0.82 and 844 ± 84 respectively, thus

indicating that C_p did not vary considerably when different resins, carbon fibers, and fabric configurations were tested.

In Figure 39a (LFA) and Figure 39b (DSC) was observed that C_p measured by LFA showed higher dispersion than that obtained with DSC. Moreover, the R^2 values (Table 13) obtained for DSC method were between 0.98 and 0.99, while those obtained for LFA were 0.81 – 0.90, thus implying lower experimental noise for DSC results. Nevertheless, the main advantage observed of using LFA was the testing time because a C_p measurement performed by DSC took around 30 minutes, while the same test in the LFA could take ~2 minutes. Based on these results, it is recommended using DSC method when higher data accuracy is required**,** while LFA may be used when testing time is an issue e.g. as an initial qualitative analysis when there are numerous tests to be performed.

TABLE 13

COEFFICIENTS CORRESPONDING TO THE LINEAR REGRESSION OF C_P vs. TEMPERATURE FOR RESULTS SHOWN IN Figure 39a AND Figure 39b (LINEAR REGRESSION: $y=mx+b$)

DSC	*m*	*b*	R^2
977-2 UD	2.612	869.3	0.997
977-2 PW	2.598	863.8	0.979
5320 UD	2.462	891.8	0.998
5320 PW	2.263	904.5	0.996
5320 8HS	2.059	929.4	0.993

LFA	*m*	*b*	R^2
977-2 UD	2.344	774.6	0.829
977-2 PW	2.849	782.3	0.807
5320 UD	3.126	807.7	0.909
5320 PW	3.481	851.4	0.876
5320 8HS	2.813	774.0	0.901

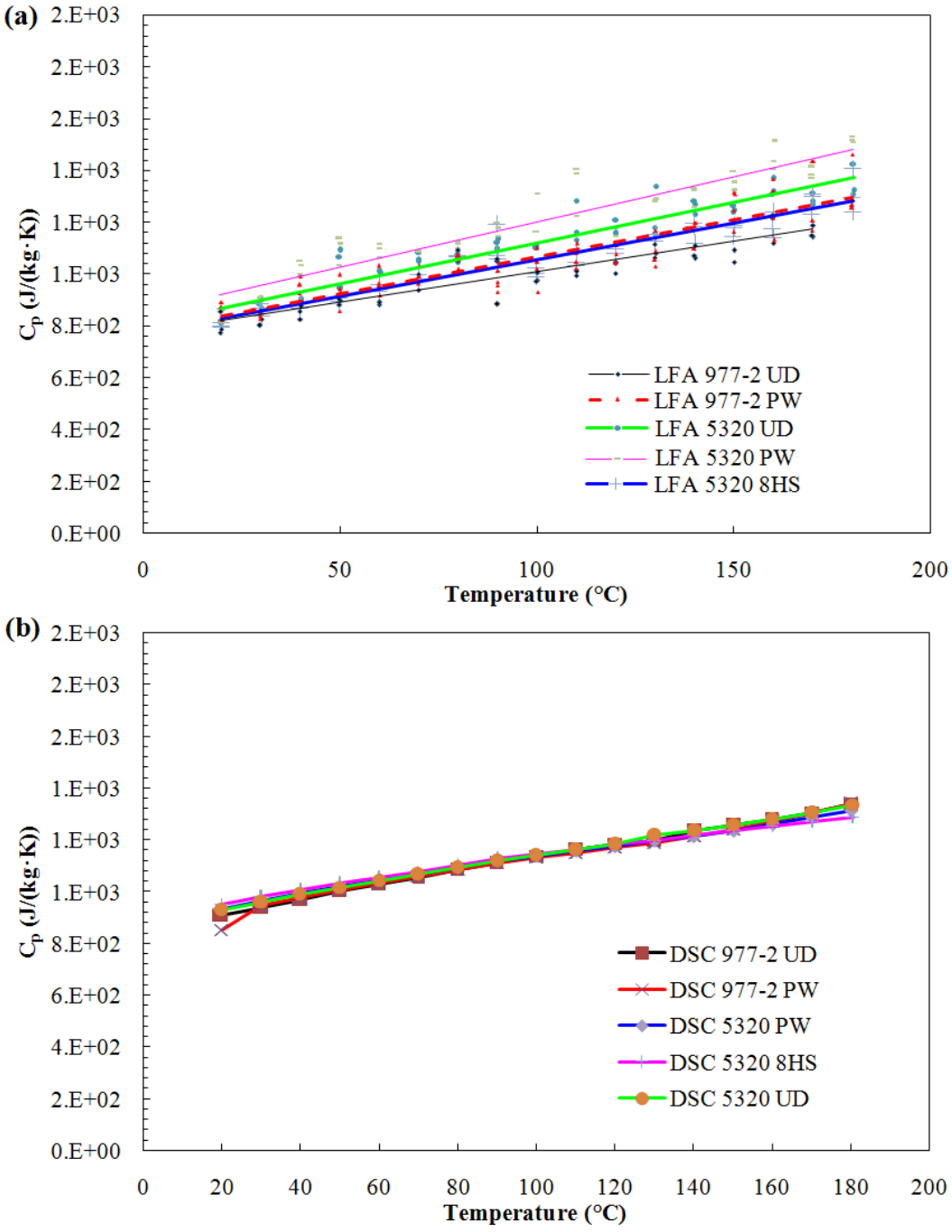

Figure 39. C_p obtained as a function of temperature utilizing LFA (a) and DSC (b) methods

6.4.3 Thermal Diffusivity Model

The thermal diffusivity of CFRP samples was calculated using the mathematical models included in the software Proteus LFA Analysis v. 4.8.5 (by Netzch), which are adiabatic/Parker (ideal case) [51], heat loss correction/Cowan [72], and Cape-Lehman [74]. The radiation-diathermic/Mehling et al. model [73] was also included in the software, but an analysis of the theory for this approach indicated that it should not be used for CFRP of Table 11. The Mehling et al. model was developed for semi-transparent materials that showed a diathermic behavior such as the one depicted in Figure 40 [73]. However, CFRP samples behaved as non-transparent materials (as shown in the figure) because a diathermic effect was not observed during testing. Hence, the Parker, Cowan, and Cape-Lehman models were subjected to a statistical analysis using Pareto diagrams in order to identify the model that showed the lowest standard deviation with respect to the time-temperature curve measured for the composite samples. Notice that the standard deviation was calculated with Proteus LFA software.

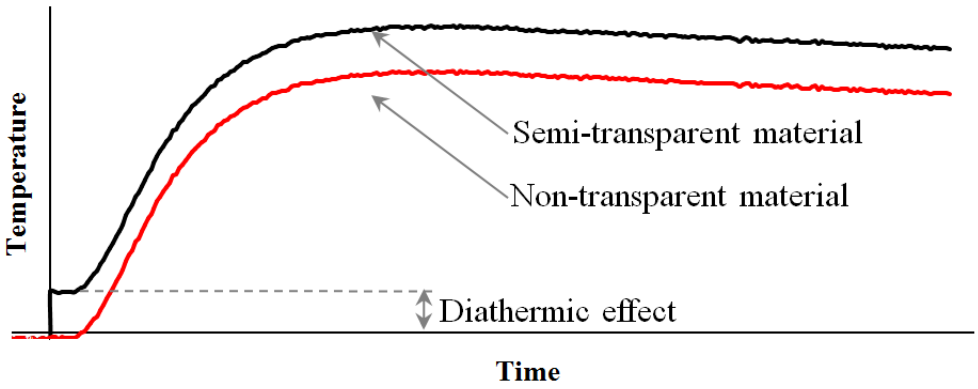

Figure 40. Time-temperature behavior for semi-transparent and non-transparent materials during LFA testing

The relative frequency (number of occurrences divided by total number of samples) in which each model showed the lowest standard deviation was determined for each material using the Pareto diagrams shown in Figure 41.

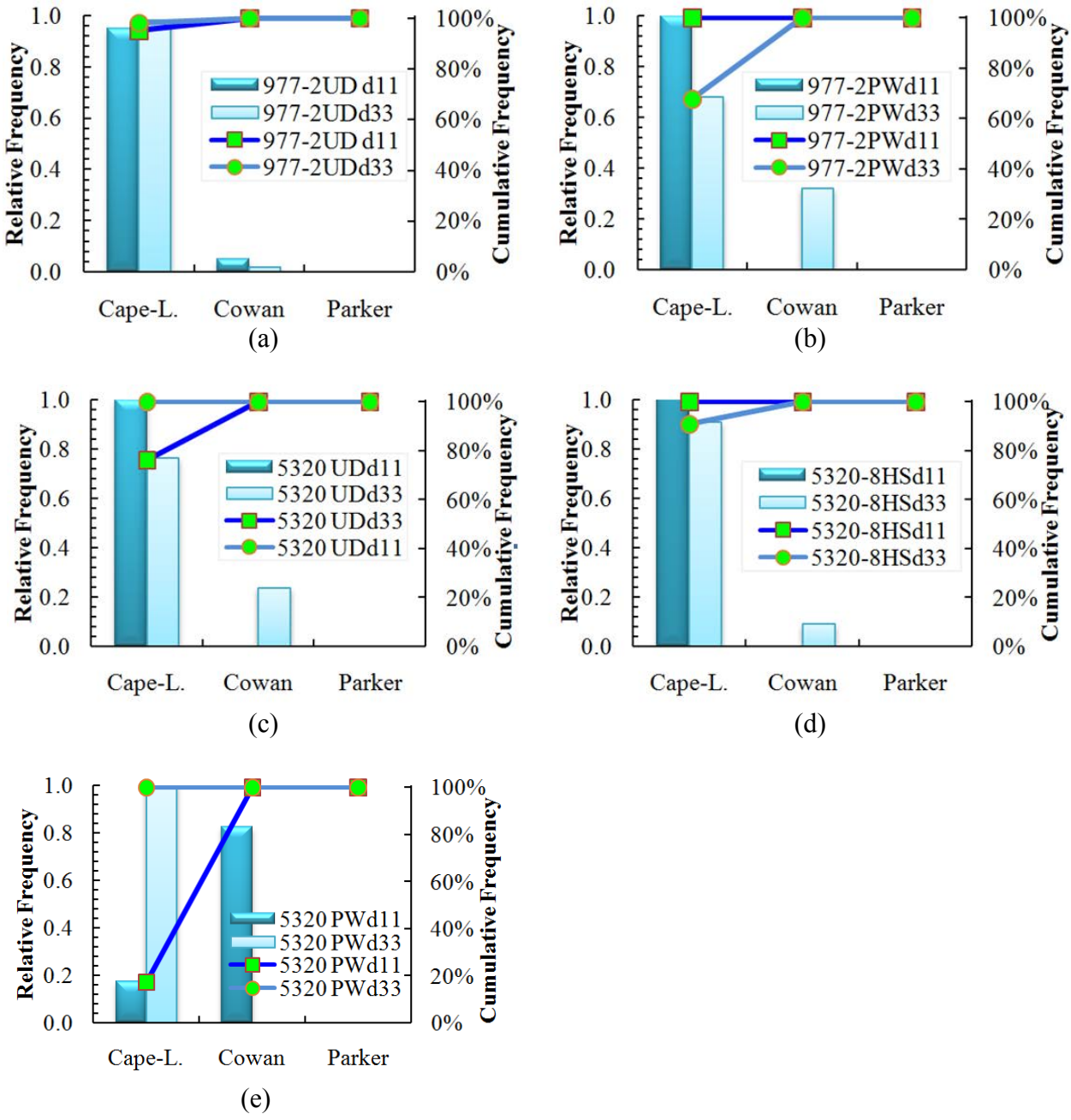

Figure 41. Pareto analysis for the relative frequency where each model showed the lowest standard deviation for (a) 977-2 UD, (b) 977-2 PW, (c) 5320 UD, (d) 5320 8HS, and (e) 5320 PW

Results of Figure 41a indicated that Cape-Lehman model showed the lowest standard deviation for 95% of the 977-2 UD samples tested in d11 and 98% of the samples tested in d33. A similar trend was observed for all the materials except for samples made of 5320 PW where Cowan

model was the best fitting model in d11. Therefore, all the measurements were recalculated using the Cape-Lehman model to determine thermal diffusivity since this model was identified as the best fit for most of the samples.

Note that the occurrence of the Parker model was zero for all the materials where this model assumed a perfect scenario (adiabatic boundaries)—that is, all the heat of the flash lamp is diffused throughout the sample and detected by the IR sensor as an increase in temperature. Hence, considerations included in Cape-Lehman and Cowan model related to heat loss radiation with the boundaries indicated a closer approach to the real case scenario.

6.4.4 Thermal Diffusivity and Conductivity of CFRP

Thermal diffusivity of CFRP samples (Figure 42) was obtained using the Cape-Lehman model, and tests were performed between 20ºC and 180ºC. Further, thermal conductivity (Figure 43) was calculated using equation (12), which was solved with a VBA algorithm that compiled the previous thermal properties: density/thermal expansion, C_p (calculated by DSC method), and diffusivity.

Results of Figure 42 and Figure 43 indicated that both thermal diffusivity and conductivity were highly influenced by fiber configuration because samples made of UD tapes depicted diffusivity and conductivity twice as high as those made of woven fabrics when tested in d11 (see Figure 42a and Figure 43a). Moreover, 8HS samples showed higher diffusivity and conductivity than those made of PW fabrics when samples made of 5320 resin were tested. These findings implied that the V_f of the samples might influence the thermal properties due to the fact that samples made of UD fibers typically have lower resin content than those made of woven fabrics (8HS and PW), as previously mentioned in section 6.4.1 (pp. 72). Since the resin conductivity (0.17 – 0.79 W/(m·K) [69]) was lower than that of carbon fibers (24.0 W/(m·K)

[68]) fabrics rich in resin might depict lower thermal conductivity. Note that the thermal conductivity values obtained in these tests agreed with literature since Sweeting et al. [46] reported conductivity of 2 – 3 W/(m·K) in d11 for plain weaved CFRP and 0.5 – 0.6 W/(m·K) in d33, which matched those values obtained for 977-2 and 5320 PW.

Additionally, Figure 42 and Figure 43 showed that the thermal diffusivity and conductivity in d33 were not strongly influenced by the fabric configuration. Results depicted typical values of thermal conductivity for epoxy resin [69], which implied that the thermal properties in through-the-thickness direction were governed mainly by the resin. Furthermore, the samples did not show relevant differences regarding the thermal behavior of the two epoxy resin systems tested despite the fact that 977-2 was formulated for autoclave processing while 5320 was an out-of-autoclave resin.

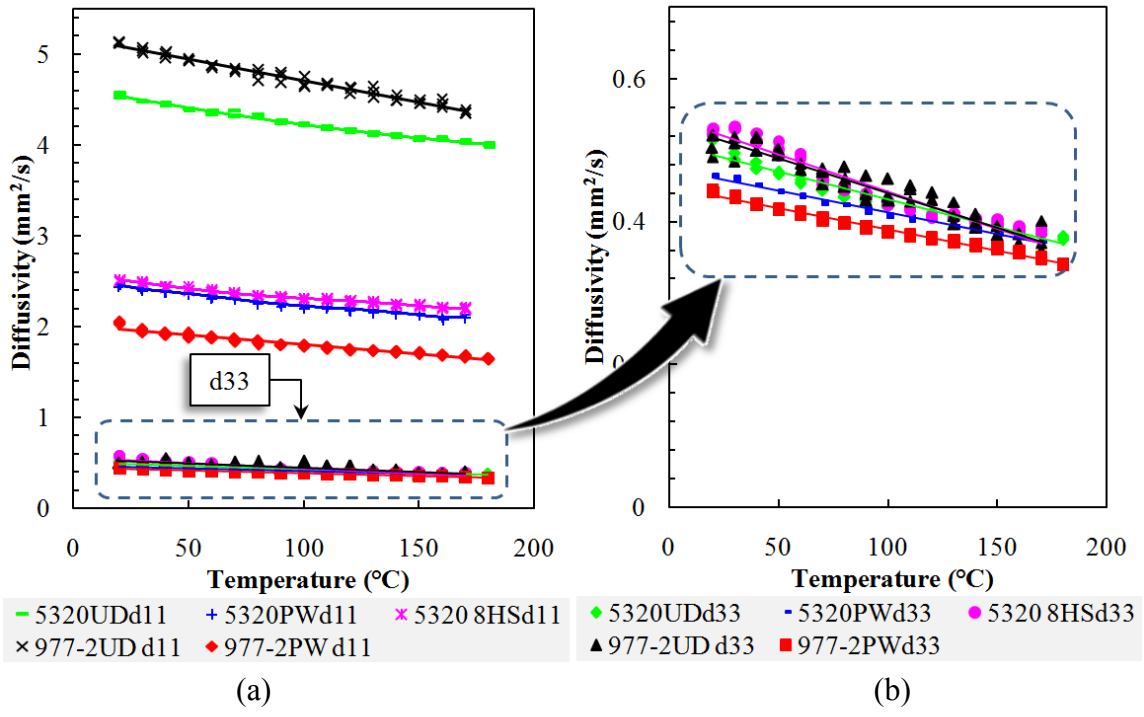

Figure 42. Thermal diffusivity measured between 20ºC and 180ºC in (a) fiber direction (b) through-the-thickness direction

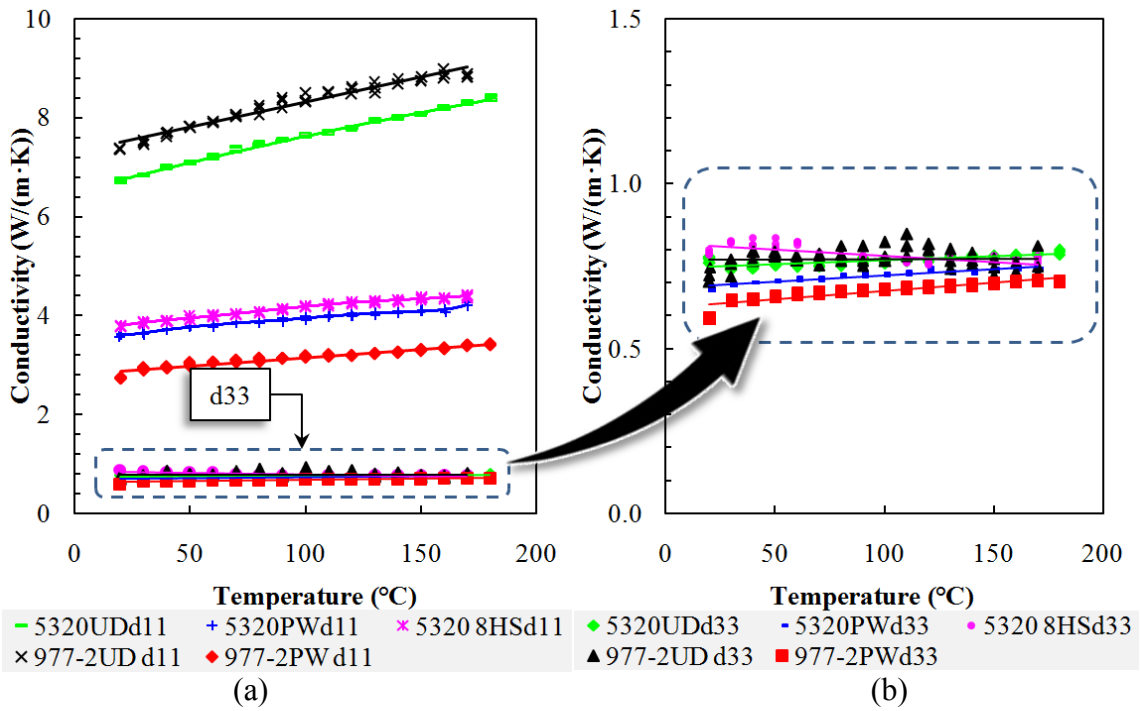

Figure 43. Thermal conductivity measured between 23ºC and 180ºC in (a) fiber direction (b) through-the-thickness direction

6.4.5 Thermal Conductivity of TFE Release Film

Thermal conductivity of a TFE release film was measured using a gravimetric method. A graphite coating was deposited on the top and bottom surfaces of the sample in order to reduce the transparency of the material since the LFA testing requires that the sample absorb the energy emitted by the flash lamp to increasing its temperature. However, this coating represented up to 20% of the sample total weight since the thickness of the film was 50 µm. Hence, samples with five different amounts of graphite (1.5 and 5.58 mg) were tested and the thermal conductivity was obtained by extrapolation.

Results, which were illustrated in Figure 44, showed a linear trend of thermal conductivity as a function of the graphite coating mass (R^2 of 0.95). This trend line was extrapolated in order to determine what would be the thermal conductivity of the sample with no graphite. These findings indicated a conductivity value of 0.23 – 0.24 W/(m·K) of the TFE film

which agreed with the theoretical values of fluoropolymers: 0.25 W/(m·K) [84]. Additionally, these experiments were replicated at temperatures between 30 and 100ºC where results did not depict a considerable variation in conductivity as a function of temperature. Therefore, these values of thermal conductivity implied that the release film could be an important factor of thermal lag at the tool-part interface during composites manufacturing since the thermal conductivity of the film was more than two times lower than the values calculated through-the-thickness (d33) of composites (d33) in section 6.4.4.

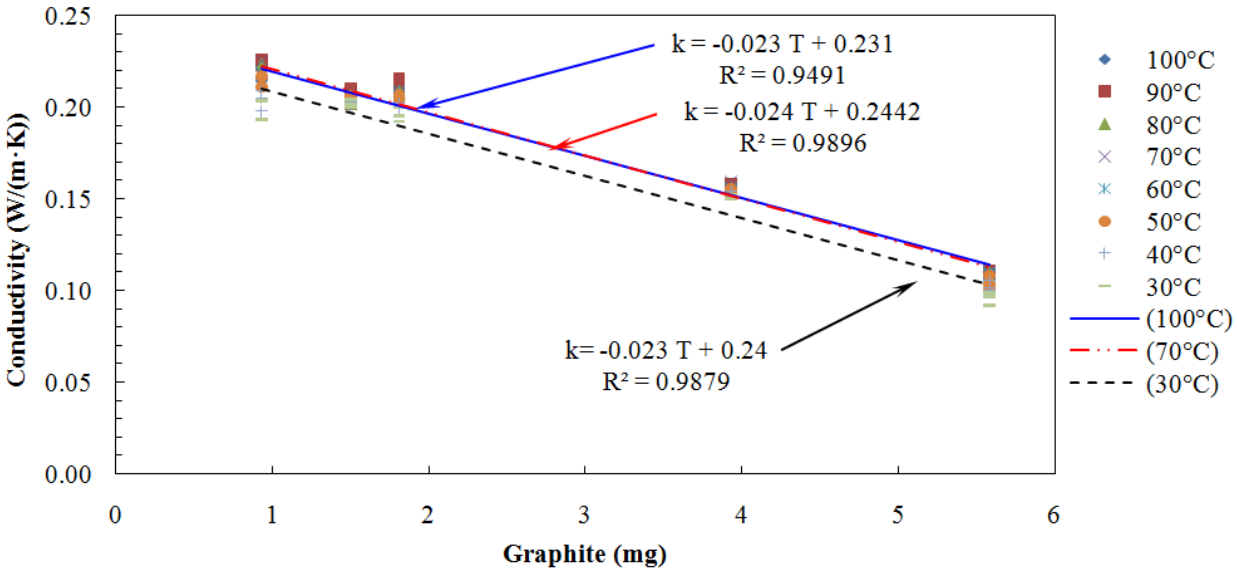

Figure 44. Thermal conductivity of TFE film measured by gravimetric method

Note also that samples with 20% wt. (~5.5 mg) of graphite showed an error up to 0.15 W/(m·K) with respect to the theoretical thermal conductivity. Therefore, these results indicated that the error induced by the graphite layers—mentioned in [55] as Δt_g—was negligible for thicker samples (2 mm in thickness) such as the aforementioned CFRP because the thin graphite layers that were used (~2 mg) would represent less than 1% of the total sample weight. Notice

that in the literature it was reported that similar coatings could influence materials with higher thermal conductivities (100 – 1000 W/m·K) and V_f lower than 0.2 [55].

6.5 Summary

Thermal properties of different autoclave and out-of-autoclave CFRP were characterized using the LFA method in order to determine the influence of fabric configuration in thermal conductivity, diffusivity, C_p, and density. Initially, the density of composite samples was measured at room temperature where findings indicated that unidirectional samples had higher density than woven fabrics because UD tapes indicated higher fiber volume fraction (V_f) than woven fabrics. Similarly, it was observed that thermal expansion of samples depended on fiber configuration since woven fabrics expanded at a higher rate than UD tapes. This phenomenon was attributed to V_f since samples epoxy resins commonly have considerably higher CTE than carbon fibers.

Subsequently, specific heat (C_p) was obtained using LFA and DSC methods where C_p increased linearly with respect to temperature. However, it was observed that this property did not change considerably when samples with different fabric configuration or resin formulation were tested. These results also indicated that tests performed using a DSC showed less dispersion in the data obtained, thus implying higher accuracy for these tests. Nevertheless, results obtained by the LFA method were still acceptable, and LFA was 10 times faster than DSC. Therefore, LFA could be used when large amount of samples is required while DSC should be used for tests that require high accuracy.

Then a model to calculate thermal diffusivity for composite samples was identified. Three thermal diffusivity models that are commonly used by the LFA method were subjected to a statistical analysis where it was found Cape-Lehman model as the best fit for most of the

samples tested. Hence, all the measurements were recalculated using such model and the thermal diffusivity was obtained.

Further, the thermal conductivity was calculated by multiplying diffusivity, density and C_p where results indicated that both diffusivity and conductivity were considerably affected by fabric configuration. Unidirectional fiber samples showed up to two times higher diffusivity and conductivity in d11 thus indicating that fiber volume fraction could affect the heat propagation within composite parts mainly in the direction of the fibers. Nevertheless, it was not evidenced that the resin formulations changed diffusivity or conductivity since measurements in d33 showed similar values for both 5320 and 977-2 prepregs.

Lastly, tests carried out using TFE samples lead to three main conclusions: First, the thermal conductivity of release materials was significantly lower than composites, which might create a thermal lag between tools and parts. Second, the error induced by graphite layers applied on the surface of CFRP samples was negligible for thick samples (2 mm in thickness)**,** while for thin samples such as TFE film (0.05 mm in thickness) coating could considerably influence the measurement of thermal properties.

CONCLUSIONS

During the manufacturing of structural composite materials, several setbacks have been found due to geometrical distortion and irregular mechanical properties caused by tool-part interaction, low transverse strength in sandwich structures, and uneven heat flow. As such, this research portrayed an experimental study of these manufacturing issues in order to provide a better understanding of autoclave manufacturing of composites.

A customized testing rig was designed to measure tool-part frictional stress and shear strength of sandwich structures when subjected to temperatures and pressures typical of autoclave processing. This testing methodology was aimed at overcoming different limitations of pressure, temperature, and speed that were found in current standard methods. The design of this apparatus included the development of control and monitoring systems for temperature and pressure. Moreover, several algorithms were implemented to compile the data of the monitoring systems and that of a universal testing machine, which quantified the shear stress required for deforming or moving a sample lodged in the rig. Similarly, computer codes were developed to create a user-friendly interface. Preliminary tests were performed to validate the functioning of the rig, which indicated that this testing rig was a reliable apparatus to calculate tool-part interaction since results agreed with the friction values reported in literature and the friction points corresponding to static/dynamic force were clearly identified when testing CFRP prepregs at different temperatures and degrees of cure.

Using this rig, a study was performed to develop a mathematical expression to predict the tool-part contact force. As such, experiments were carried out to characterize the frictional interaction between CFRP prepreg coupons and metallic tools while samples were subjected to customized temperature and pressure cycles that reproduced autoclave manufacturing conditions.

Moreover, the effect of main manufacturing conditions was studied including temperature, consolidation pressure, part length (pull-out speed), and tool surface roughness when using three different combinations of release materials. Samples were tested in the customized rig where results indicated that friction force was governed by mechanical interlocking and atomic interaction of the counter surfaces. Based on the theoretical behavior of this frictional interaction, a mathematical model was proposed comprising Coulomb's friction model, which was modified to account for temperature and non-linear normal forces.

These tests indicated that samples tested using a TFE release film (method 1) between tools and parts could have lower frictional interaction than those where a polymeric release (method 2) agent was used. Coefficient of friction (COF) values obtained for method 1 were 0.05 – 0.09 at 177°C whereas tests performed with method 2 showed higher values in the range of 0.09 – 0.10. Moreover, the static/dynamic friction ratios obtained for the release film were 1.0 – 1.1 while those obtained for the release agent were 5.29 ± 0.19 at pull-out speeds of 0.05 mm/min and 1.6 ± 0.1 at higher speeds. In practical terms, these findings indicated that tools might induce less residual stresses to parts during manufacturing when using release films instead of release agents.

Additionally, tests were performed to identify the optimum tool surface conditions that would minimize the tool-part frictional interaction. For this purpose, tests were performed using a TFE release film and tools with two different surface roughnesses. These results indicated a decrease in shear stress of 19 ± 9% when reducing tool surface roughness by 86% (from 1.35 to 0.18μm). Then a polymeric release agent was applied on the tool with a surface roughness of 0.18μm where it was measured up to 51% additional decrease in shear stress. These results

implied, therefore, that tool-part interaction could be more effectively reduced by a using an appropriate combination of release materials rather than using finer surface finishing on tools.

Further, the testing rig was used to characterize the shear strength of sandwich structures and honeycomb cores when subjected to typical autoclave conditions of temperature and pressure. The shear stress measured in sandwich structures indicated that the structural integrity of the core depended on the degree of cure of prepreg skins and adhesives. Furthermore, tests were performed using honeycomb core samples tested in the principal in-plane directions. These results indicated that both temperature and pressure reduced the shear strength following an inverse exponential trend. These results would serve as design parameters for autoclave manufacturing of sandwich structures.

Lastly, the thermal properties of CFRP including thermal expansion, diffusivity, conductivity, and specific heat were characterized using the LFA method, and the influence of temperature, fabric architecture, and resin formulation on thermal properties was studied. Initially, an analysis of anisotropic thermal expansion of the different CFRP samples was performed in order to determine the change in density as a function of temperature. This analysis was used to develop correction factors required to calculate C_p since this property depended on sample density. Then a statistical analysis was performed among three models commonly used for characterization of thermal diffusivity in order to obtain the best fit for CFRP. As such, the Cape-Lehman model showed the lowest standard deviation in most of the tests, and results of thermal diffusivity were obtained with this model. Then thermal conductivity was calculated at different temperatures using the results obtained for diffusivity, density, thermal expansion, and C_p. These results indicated that the fiber volume fraction (V_f) of the samples influenced the density, diffusivity, and conductivity of samples. Density values of 1.59 and 1.58 g/cm^3 for

unidirectional samples were obtained while plain weaved ones, which had lower V_f, showed density around 1.56 g/cm^3. This effect was more notorious when thermal diffusivity and conductivity were determined since unidirectional samples showed more than two times higher thermal diffusivity and conductivity in fiber direction than those made of weaved carbon fibers. Nevertheless, C_p did not change considerably regardless of resin formulation and fiber architecture.

REFERENCES

REFERENCES

[1] Huang, X., Gillespie, J.W., and Bogetti, T., "Process Induced Stress for Woven Fabric Thick Section Composite Structures," *Composite Structures*, Vol. 49, No. 3, 2000, pp. 303-312.

[2] White, S.R. and Hahn, H.T., "Process Modeling of Composite Materials: Residual Stress Development during Cure. Part II. Experimental Validation," *Journal of Composite Materials*, Vol. 26, No. 16, 1992, pp. 2423-2453.

[3] Callister, W.D., *Materials Science and Engineering: An Introduction*. John Wiley & Sons, 2007.

[4] Zarrelli, M., Partridge, I.K., and D'Amore, A., "Warpage Induced in Bi-Material Specimens: Coefficient of Thermal Expansion, Chemical Shrinkage and Viscoelastic Modulus Evolution during Cure," *Composites Part A: Applied Science and Manufacturing*, Vol. 37, No. 4, 2006, pp. 565-570.

[5] Ersoy, N., Potter, K., Wisnom, M.R., and Clegg, M.J., "An Experimental Method to Study the Frictional Processes During Composites Manufacturing," *Composites Part A: Applied Science and Manufacturing*, Vol. 36, No. 11, 2005, pp. 1536-1544.

[6] Hsiao, H.-M., Lee, S., and Buyny, R., "Core Crush Problem in the Manufacturing of Composite Sandwich Structures: Mechanisms and Solutions," *AIAA Journal*, Vol. 44, No. 4, 2006, pp. 901-907.

[7] Renn, D.J., Tulleau, T., Seferis, J.C., Curran, R.N., and Ahn, K.J., "Composite Honeycomb Core Crush in Relation to Internal Pressure Measurement," *Journal of Advanced Materials*, Vol. 27, No. 1, 1995, pp. 31-40.

[8] Flanagan, R., "The Dimensional Stability of Composite Laminates and Structures," PhD thesis, Queen's University of Belfast. 1998.

[9] Joven, R., Tavakol, B., Rodriguez, A., Guzman, M., and Minaie, B., "Characterization of Shear Stress at the Tool-Part Interface during Autoclave Processing of Prepreg Composites," *Journal of Applied Polymer Science*, No., 2013.

[10] Joven, R., Tavakol, B., Rodriguez, A., and Minaie, B. "Experimental Investigation of Tool/Part Interface during Curing of Composites," *SAMPE 2010 Conference and Exhibition "New Materials and Processes for a New Economy," May 17, 2010 - May 20, 2010*. Soc. for the Advancement of Material and Process Engineering, Seattle, WA, United states, 2010, pp. Seattle and Eastern Canada SAMPE Chapters.

[11] Joven, R., Tavakol, B., Rodriguez, A., and Minaie, B. "Study of Parameters Affecting Friction Shear Stress at Tool-Part Interface for Autoclave Composites Processing," *2011 SAMPE Spring Technical Conference and Exhibition - State of the Industry: Advanced Materials, Applications, and Processing Technology, May 23, 2011 - May 26, 2011*. Soc. for the Advancement of Material and Process Engineering, Long Beach, CA, United states, 2011, pp. SAMPE Orange County Chapter.

[12] Kaushik, V. and Raghavan, J., "Experimental Study of Tool-Part Interaction during Autoclave Processing of Thermoset Polymer Composite Structures," *Composites Part A: Applied Science and Manufacturing*, Vol. 41, No. 9, 2010, pp. 1210-1218.

[13] Martin, C.J., Seferis, J.C., and Wilhelm, M.A., "Frictional Resistance of Thermoset Prepregs and its Influence on Honeycomb Composite Processing," *Composites Part A: Applied Science and Manufacturing*, Vol. 27, No. 10, 1996, pp. 943-951.

[14] Twigg, G., Poursartip, A., and Fernlund, G., "An Experimental Method for Quantifying Tool-Part Shear Interaction during Composites Processing," *Composites Science and Technology*, Vol. 63, No. 13, 2003, pp. 1985-2002.

[15] Twigg, G., Poursartip, A., and Fernlund, G., "Tool-Part Interaction in Composites Processing. Part I: Experimental Investigation and Analytical Model," *Composites Part A: Applied Science and Manufacturing*, Vol. 35, No. 1, 2004, pp. 121-133.

[16] Sloan, J., "Proper Mold Care: Mandatory!," *Composites Technology*, 2011 [cited 2012 August 8]; Available from: http://www.compositesworld.com/articles/proper-mold-care-mandatory.

[17] Bowden, F.P. and Tabor, D., *The Friction and Lubrication of Solids, Part XIII: The Friction Deformation of Polymeric Materials*. Oxford. pp. 214-220, 1964.

[18] Biswas, S. and Vijayan, K., "Friction and Wear of PTFE—A Review," *Wear*, Vol. 158, No. 1-2, 1992, pp. 193-211.

[19] Rae, P.J. and Brown, E.N., "The Properties of Poly(tetrafluoroethylene) (PTFE) in Tension," *Polymer*, Vol. 46, No. 19, 2005, pp. 8128-8140.

[20] Fote, A.A., Wildvank, A.H., and Slade, R.A., "Coefficient of Friction of PTFE-Impregnated Porous Bronze Versus Temperature," *Wear*, Vol. 47, No. 2, 1978, pp. 255-261.

[21] Johnston, A., Vaziri, R., and Poursartip, A., "A Plane Strain Model for Process-Induced Deformation of Laminated Composite Structures," *Journal of Composite Materials*, Vol. 35, No. 16, 2001, pp. 1435-1469.

[22] Fernlund, G., Rahman, N., Courdji, R., Bresslauer, M., Poursartip, A., Willden, K., and Nelson, K., "Experimental and Numerical Study of the Effect of Cure Cycle, Tool Surface, Geometry, and Lay-Up on the Dimensional Fidelity of Autoclave-Processed Composite Parts," *Composites Part A: Applied Science and Manufacturing*, Vol. 33, No. 3, 2002, pp. 341-351.

[23] Zeng, X. and Raghavan, J., "Role of Tool-Part Interaction in Process-Induced Warpage of Autoclave-Manufactured Composite Structures," *Composites Part A: Applied Science and Manufacturing*, Vol. 41, No. 9, 2010, pp. 1174-1183.

[24] Roozbehjavan, P., Das, R., Joven, R., and Minaie, B. "Experimental and Numerical Investigation of Distortion of L-Shaped and U-Shaped Carbon Fiber-Reinforced Composite," *SAMPE 2012 Conference and Exhibition , October 22, 2012 - October 25, 2012*. Soc. for the Advancement of Material and Process Engineering, Charleston, SC, United states, 2012.

[25] Tavakol, B., "Prediction of Residual Stresses and Distortion of Carbon Fiber/Epoxy Composites due to Curing Process," in *Mechanical Engineering*, Wichita State University: Wichita, KS. 2011.

[26] Tavakol, B., Roozbehjavan, P., Ahmed, A., Das, R., Joven, R., Koushyar, H., Rodriguez, A., and Minaie, B., "Prediction of Residual Stresses and Distortion in Carbon Fiber-Epoxy Composite Parts due to Curing Process Using Finite Element Analysis," *Journal of Applied Polymer Science*, No., 2012, pp. 941–950.

[27] Ahmed, A., Tavakol, B., Das, R., Joven, R., Roozbehjavan, P., and Minaie, B. "Study of Thermal Expansion in Carbon Fiber-Reinforced Polymer Composites," *SAMPE 2012 Conference and Exhibition , October 22, 2012 - October 25, 2012*. Soc. for the Advancement of Material and Process Engineering, Charleston, SC, United states, 2012.

[28] Das, R., "Stress Relaxation Behavior of Carbon Fiber-Epoxy Prepreg Composites During and After Cure," in *Mechanical Engineering*, Wichita State University: Wichita, KS. 2012.

[29] Das, R., Joven, R., Roozbehjavan, P., and Minaie, B. "Stress Relaxation of Carbon Fiber-Reinforced Thermosetting Polymer Composite Material," *SAMPE 2012 Conference and Exhibition , October 22, 2012 - October 25, 2012*. Soc. for the Advancement of Material and Process Engineering, Charleston, SC, United states, 2012.

[30] Joven, R., Das, R., Roozbehjavan, P., Ahmed, A., and Minaie, B. "Thermal Properties of Carbon Fiber-Epoxy Composites with Different Fabric Weaves," *SAMPE 2012 Conference and Exhibition, October 22, 2012 - October 25, 2012*. Soc. for the Advancement of Material and Process Engineering, Charleston, SC, United states, 2012.

[31] Grove, S.M., Popham, E., and Miles, M.E., "An Investigation of the Skin/Core Bond in Honeycomb Sandwich Structures Using Statistical Experimentation Techniques," *Composites Part A: Applied Science and Manufacturing*, Vol. 37, No. 5, 2006, pp. 804-812.

[32] Yuan, C., Li, M., Zhang, Z., and Gu, Y., "Experimental Investigation on the Co-Cure Processing of Honeycomb Structure with Self-Adhesive Prepreg," *Applied Composite Materials*, Vol. 15, No. 1, 2008, pp. 47-59.

[33] Kohli, D., "High Performance Adhesive Compositions," WO Patent WO/2011/025,873. 2011.

[34] Corbett, D.H. and Smith, S.A., "Tiedown Ply for Reducing Core Crush in Composite Honeycomb Sandwich Structure," US Patent 5,895,699. 1999.

[35] Hopkins, W.B. and Hartz, D.E., "Adhering Tiedown Plies in Composite Construction," US Patent 5,685,940. 1997.

[36] Erickson, D.G., George, P.E., Mortensen, R.C., and Smith, S.A., "Mandrel and Method for Manufacturing Composite Structures," US Patent 7,138,031. 2006.

[37] Martin, C.J., Putnam, J.W., Hayes, B.S., Seferis, J.C., Turner, M.J., and Green, G.E., "Effect of Impregnation Conditions on Prepreg Properties and Honeycomb Core Crush," *Polymer Composites*, Vol. 18, No. 1, 1997, pp. 90-99.

[38] Hsiao, H.M., Lee, S.M., Buyny, R.A., and Martin, C.J., "Core-Crush Resistant Fabric and Prepreg for Fiber Reinforced Composite Sandwich Structures," US Patent 6,663,737. 2003.

[39] Schneider, T.L. and Pelton, T.L., "Composite Prepreg Material Form with Improved Resistance to Core Crush and Porosity," EP Patent 1,001,063. 2005.

[40] Pan, S.-D., Wu, L.-Z., and Sun, Y.-G., "Transverse Shear Modulus and Strength of Honeycomb Cores," *Composite Structures*, Vol. 84, No. 4, 2008, pp. 369-374.

[41] Pan, S.-D., Wu, L.-Z., Sun, Y.-G., Zhou, Z.-G., and Qu, J.-L., "Longitudinal Shear Strength and Failure Process of Honeycomb Cores," *Composite Structures*, Vol. 72, No. 1, 2006, pp. 42-46.

[42] ASTM-C273/C273M, "Standard Test Method for Shear Properties of Sandwich Core Materials," ASTM International: West Conshohocken, PA. 2011.

[43] Lee, H.S., Hong, S.H., Lee, J.R., and Kim, Y.K., "Mechanical Behavior and Failure Process during Compressive and Shear Deformation of Honeycomb Composite at Elevated Temperatures," *Journal of Materials Science*, Vol. 37, No. 6, 2002, pp. 1265-1272.

[44] Tavman, I. and Akinci, H., "Transverse Thermal Conductivity of Fiber Reinforced Polymer Composites," *International communications in heat and mass transfer*, Vol. 27, No. 2, 2000, pp. 253-261.

[45] Yamane, T., Katayama, S.i., Todoki, M., and Hatta, I., "Thermal Diffusivity Measurement of Single Fibers by an AC Calorimetric Method," *Journal of Applied Physics*, Vol. 80, No. 8, 1996, pp. 4358-4365.

[46] Sweeting, R.D. and Liu, X.L., "Measurement of Thermal Conductivity for Fibre-Reinforced Composites," *Composites Part A: Applied Science and Manufacturing*, Vol. 35, No. 7–8, 2004, pp. 933-938.

[47] Scott, E.P. and Beck, J.V., "Estimation of Thermal Properties in Carbon/Epoxy Composite Materials during Curing," *Journal of Composite Materials*, Vol. 26, No. 1, 1992, pp. 20 - 36.

[48] Friis-Pedersen, H.H., Pedersen, J.H., Haussler, L., and Storm, B.K., "Online Measurement of Thermal Diffusivity during Cure of an Epoxy Composite," *Polymer Testing*, Vol. 25, No. 8, 2006, pp. 1059-1068.

[49] Ångström, A.J., "New Method of Determining the Thermal Conductivity of Bodies," *Philosophical Magazine*, Vol. 25, No., 1863, pp. 130-142.

[50] Garnier, B. and Sommier, A., "Thermal Property Measurements during Curing of Thermoset Resins Using Steady Periodic Conditions," *Journal of Reinforced Plastics and Composites*, Vol. 21, No. 13, 2002, pp. 1193-1203.

[51] Parker, W.J., Jenkins, R.J., Butler, C.P., and Abbott, G.L., "Flash Method of Determining Thermal Diffusivity, Heat Capacity, and Thermal Conductivity," *Journal of Applied Physics*, Vol. 32, No. 9, 1961, pp. 1679-1684.

[52] Rolfes, R. and Hammerschmidt, U., "Transverse Thermal Conductivity of CFRP Laminates: A Numerical and Experimental Validation of Approximation Formulae," *Composites Science and Technology*, Vol. 54, No. 1, 1995, pp. 45-54.

[53] Ng, H.Y., Lu, X., and Lau, S.K., "Thermal Conductivity, Electrical Resistivity, Mechanical, and Rheological Properties of Thermoplastic Composites Filled With Boron Nitride and Carbon Fiber," *Polymer Composites*, Vol. 26, No. 1, 2004, pp. 66-73.

[54] Hwang, I.U., Yu, H.N., Kim, S.S., Lee, D.G., Suh, J.D., Lee, S.H., Ahn, B.K., Kim, S.H., and Lim, T.W., "Bipolar Plate Made of Carbon Fiber Epoxy Composite for Polymer Electrolyte Membrane Fuel Cells," *Journal of Power Sources*, Vol. 184, No. 1, 2008, pp. 90-94.

[55] Alway-Cooper, R.M., Theodore, M., Anderson, D.P., and Ogale, A.A., "Transient Heat Flow in Unidirectional Fiber–Polymer Composites during Laser Flash Analysis: Experimental Measurements and Finite Element Modeling," *Journal of Composite Materials*, No., 2012.

[56] ASTM-G115, "Standard Guide for Measuring and Reporting Friction Coefficients," ASTM International: West Conshohocken, PA. 2010.

[57] ISO-6601:2002, "Plastics—Friction and wear by sliding—Identification of Test Parameters," International Organization for Standardization. 2002.

[58] Alavi-Soltani, S., Sabzevari, S., Koushyar, H., and Minaie, B., "Thermal, Rheological, and Mechanical Properties of a Polymer Composite Cured at Different Isothermal Cure Temperatures," *Journal of Composite Materials*, Vol. 46, No. 5, 2012, pp. 575-587.

[59] Taguchi, G., Chowdhury, S., and Wu, Y., *Taguchi's Quality Engineering Handbook*. John Wiley & Sons, 2005.

[60] Ahmed, A., "Resin Flow Velocity Measurement of Carbon Fiber-Epoxy Composites in Autoclave Processing," Wichita State University: Wichita, KS. 2012.

[61] Alavi-Soltani, S., "Thermal, Rheological, and Mechanical Properties of a Polymer Composite Cured at Staged Cure Cycles," in *Mechanical Engineering*, Wichita State University: Wichita, KS. 2010.

[62] Dave, R., Kardos, J.L., and Duduković, M.P., "A Model for Resin Flow during Composite Processing: Part 1—General Mathematical Development," *Polymer Composites*, Vol. 8, No. 1, 1987, pp. 29-38.

[63] Eötvös, R., "Ueber den Zusammenhang der Oberflächenspannung der Flüssigkeiten mit Ihrem Molecularvolumen," *Annalen der Physik*, Vol. 263, No. 3, 1886, pp. 448-459.

[64] Schön, J., "Coefficient of Friction for Aluminum in Contact with a Carbon Fiber Epoxy Composite," *Tribology International*, Vol. 37, No. 5, 2004, pp. 395-404.

[65] Yang, E.L., Hirvonen, J.P., and Toivanen, R.O., "Effect of Temperature on the Transfer Film Formation in Sliding Contact of PTFE with Stainless Steel," *Wear*, Vol. 146, No. 2, 1991, pp. 367-376.

[66] Hexcel, "Product Data Sheet of HexWeb HRH-10 Aramid Fiber/Phenolic Resin Honeycom," 2012 10/10/2012]; Available from: http://www.hexcel.com/Resources/DataSheets/Honeycomb-Data-Sheets/HRH_10_us.pdf.

[67] Henkel Corporation, A., "Product Data Sheet of Hysol PL 7000: Epoxy Film Adhesive," 2012 [cited 2012 10/10/12]; Available from: http://www.hysolpl7000.com/assets/downloads/Hysol_PL_7000.pdf.

[68] MatWeb, "Graphite, Carbon, C," 2012 May, 2012]; Available from: http://www.matweb.com/search/DataSheet.aspx?MatGUID=3f64b985402445c0a5af911135909344&ckck=1.

[69] MatWeb, "Epoxy, Cast, Unreinforced," 2012 May, 2012]; Available from: http://www.matweb.com/search/DataSheet.aspx?MatGUID=1c74545c91874b13a3e44f400cedfe39&ckck=1.

[70] Bogetti, T.A. and Gillespie, J.W., "Two-Dimensional Cure Simulation of Thick Thermosetting Composites," *Journal of Composite Materials*, Vol. 25, No. 3, 1991, pp. 239-273.

[71] Pinto, C.S.C., Massard, H., Couto, P., Orlande, H.R.B., Cotta, R.M., and Ambrosio, M.C.R., "Measurement of Thermophysical Properties of Ceramics by the Flash Method," *Brazilian Archives of Biology and Technology*, Vol. 49, No., 2006, pp. 31-40.

[72] Cowan, R.D., "Pulse Method of Measuring Thermal Diffusivity at High Temperatures," *Journal of Applied Physics*, Vol. 34, No. 4, 1962, pp. 926 - 928.

[73] Mehling, H., Hautzinger, G., Nilsson, O., Fricke, J., Hofmann, R., and Hahn, O., "Thermal Diffusivity of Semitransparent Materials Determined by the Laser-Flash Method Applying a New Analytical Model," *International Journal of Thermophysics*, Vol. 19, No. 3, 1998, pp. 941-949.

[74] Cape, J.A. and Lehman, G.W., "Temperature and Finite Pulse-Time Effects in the Flash Method for Measuring Thermal Diffusivity," *Journal of Applied Physics*, Vol. 34, No. 7, 1963, pp. 1909-1914.

[75] ASTM-E831, "Standard Test Method for Linear Thermal Expansion of Solid Materials by Thermomechanical Analysis," ASTM International: West Conshohocken, PA. 2012.

[76] ASTM-D792, "Standard Test Method for Density and Specific Gravity (Relative Density) of Plastics by Displacement," ASTM International: West Conshohocken, PA. 2008.

[77] ASTM-E1269, "Standard Test Method for Determining Specific Heat Capacity by Differential Scanning Calorimetry," ASTM International: West Conshohocken, PA. 2011.

[78] Albers, A.P.F., Restivo, T.A., Pagano, L., and Baldo, J.B., "Effect of Testing Conditions on the Laser Flash Thermal Diffusivity Measurements of Ceramics," *Thermochimica acta*, Vol. 370, No. 1, 2001, pp. 111-118.

[79] Cernuschi, F., Lorenzoni, L., Bianchi, P., and Figari, A., "The Effects of Sample Surface Treatments on Laser Flash Thermal Diffusivity Measurements," *Infrared physics & technology*, Vol. 43, No. 3, 2002, pp. 133-138.

[80] Hexcel, "Reinforcements for Composites," in *Technical Fabrics Handbook,* 2012.

[81] Koushyar, H., Alavi-Soltani, S., Minaie, B., and Violette, M., "Effects of Variation in Autoclave Pressure, Temperature, and Vacuum-Application Time on Porosity and Mechanical Properties of a Carbon Fiber/Epoxy Composite," *Journal of Composite Materials*, No., 2011.

[82] *Department of Defence, MIL-HDBK-17-1F Composite Materials Handbook* Vol. 1. Polymer matrix composites guidelines for characterization of structural materials. 2002.

[83] Sun, B., Liu, F., and Gu, B., "Influence of the Strain Rate on the Uniaxial Tensile Behavior of 4-Step 3D Braided Composites," *Composites Part A: Applied Science and Manufacturing*, Vol. 36, No. 11, 2005, pp. 1477-1485.

[84] Duncan M. Price, M.J., "Thermal Conductivity of PTFE and PTFE Composites," in *Proceedings of the Twenty-Eight Conference of the North American Thermal Analysis Society*: Orlando, FL. 2000.

APPENDICES

APPENDIX A

AVERAGE OF SHEAR STRESS MEASURED FOR THEMANUFACTURING CONDITIONS SHOWN IN THE ORTHOGONAL ARRAY L_9

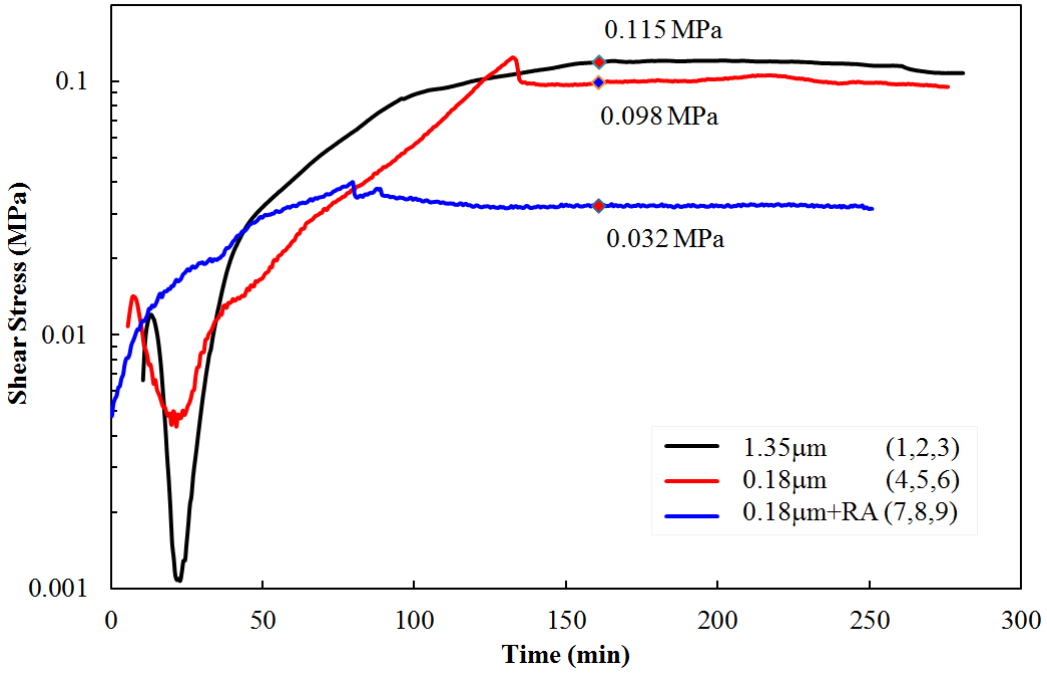

Figure A.1. Effect of surface conditions on the frictional stress. Samples 1, 2, and 3 (1.35µm surface roughness); 4, 5, and 6 (0.18µm surface roughness); and 7, 8, and 9 (0.18µm surface roughness plus release agent).

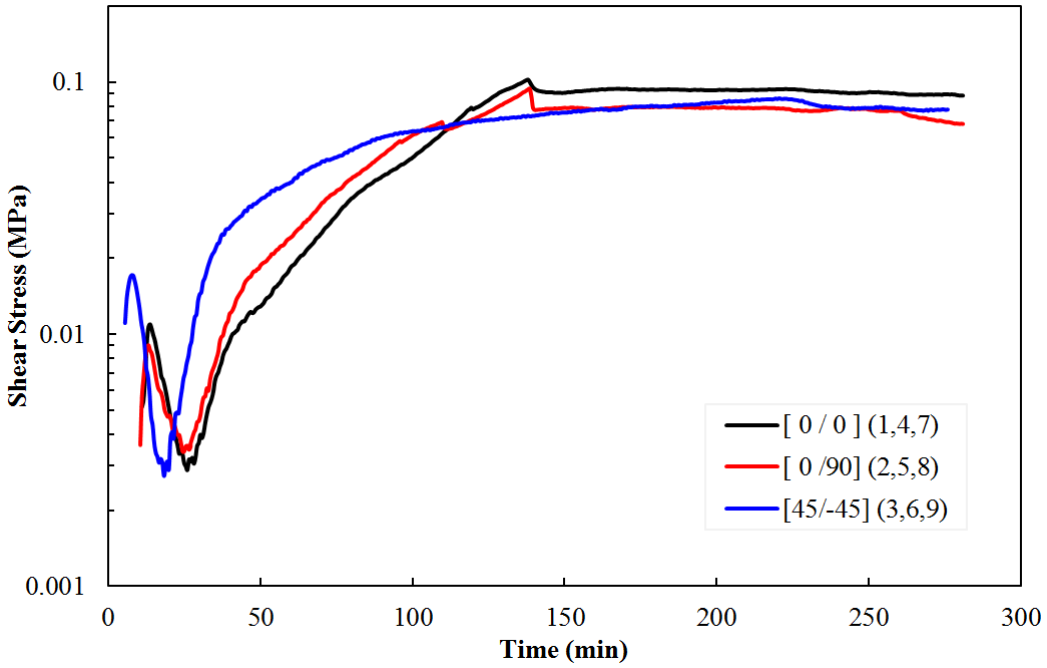

Figure A.2. Friction stress calculated for different layup configuration: samples 1, 4, and 7 have unidirectional layup; 2, 5, and 8 are [0/90]; and 3, 6, and 9 are [45/45]

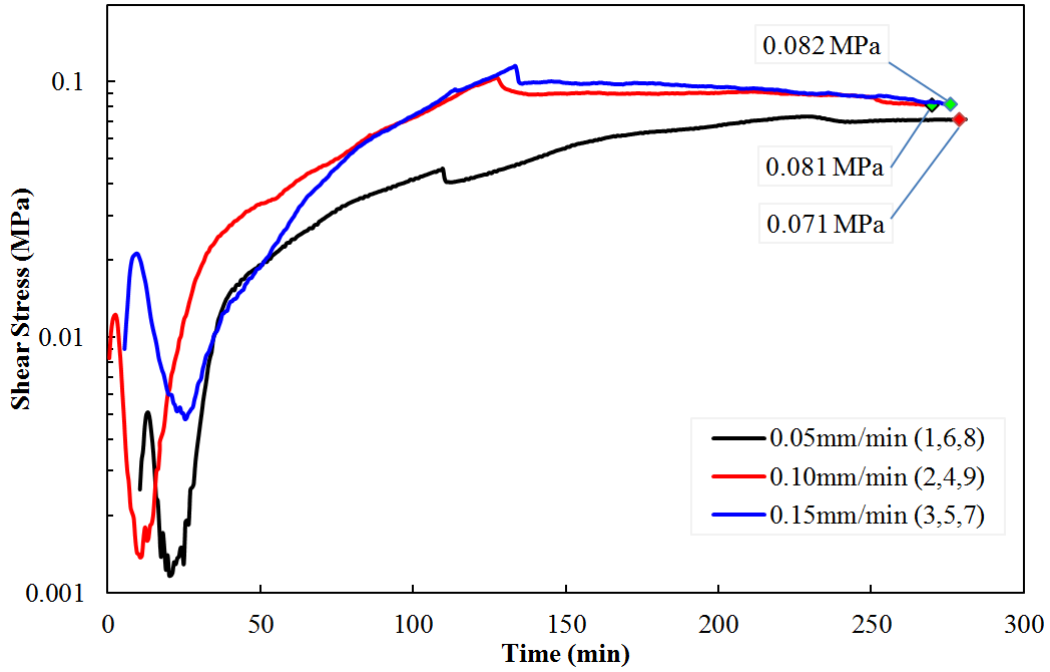

Figure A.3. Influence of pull-out speed in the friction stress: samples 1, 6, and 8 were pulled out at 0.05 mm/min; 2, 4, and 9 at 0.10 mm/min; and 3, 5, and 7 at 015 mm/min.

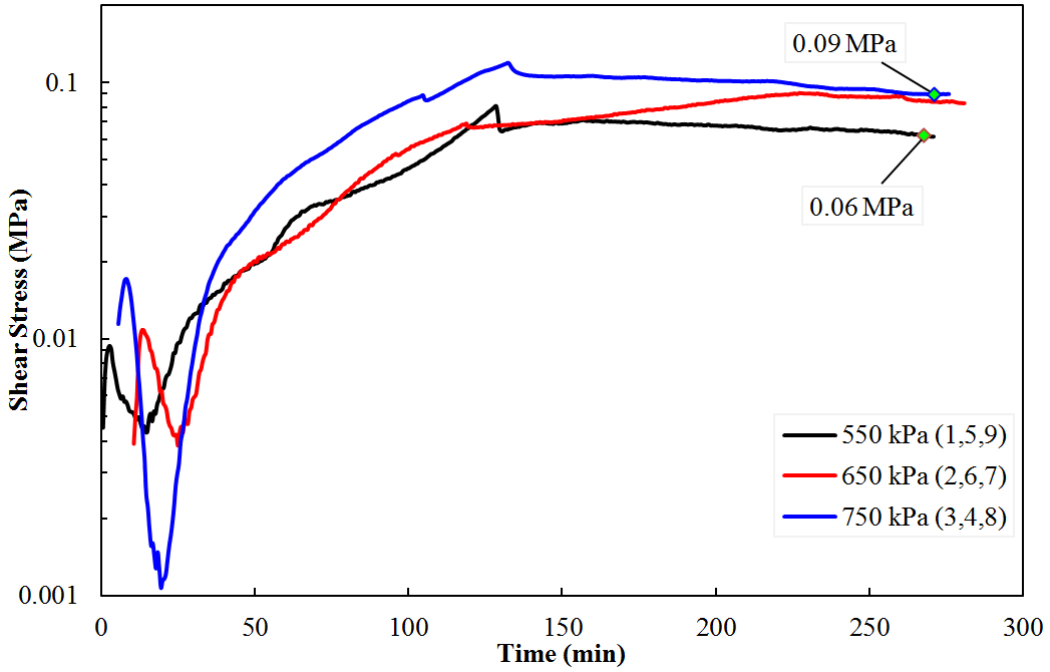

Figure A.4. Normal force (autoclave pressure): 550kPa applied to samples 1, 5, and 9; 650kPa to samples 2, 6, and 7; and 750kPa to samples 3, 4, and 8.

APPENDIX B

MATHEMATICAL EXPRESSIONS USED TO DETERMINE THE ANISOTROPIC CHANGE OF DENSITY IN COMPOSITES

The density $\rho(T)$ of composite materials changes with temperature as the composite develops volumetric thermal expansion $V_o + \Delta V(T)$:

$$\rho(T) = \frac{m}{V_o + \Delta V(T)} \tag{21}$$

where m is mass which can be related to the initial density of the sample as $m = V_o \cdot \rho_o$, which results in:

$$\rho(T) = \frac{\rho_o}{1 + \frac{\Delta V(T)}{V_o}} \tag{22}$$

where

$$1 + \frac{\Delta V(T)}{V_o} = \left(1 + \varepsilon_{11}(T)\right) \cdot \left(1 + \varepsilon_{22}(T)\right) \cdot \left(1 + \varepsilon_{33}(T)\right) \tag{23}$$

The thermal strain $\varepsilon_{ij}(T)$ is related to the initial length $L_{o_{ij}}$ and the dimension change $\Delta L_{ij}(T)$ as follows:

$$\varepsilon_{ij}(T) = \frac{\Delta L_{ij}(T)}{L_{o_{ij}}} \tag{24}$$

where $L_{o\ ij}$ was the sample length measured at 23ºC (room temperature). As well, $\varepsilon_{ij}(T)$ for anisotropic materials is given by:

$$\varepsilon_{ij}(T) = \alpha_{ij}(T - T_o) \tag{25}$$

where the CTE tensor α_{ij} for composites with fiber orientation of [0º] or [0º/90º] is:

$$\alpha_{ij} = \begin{bmatrix} \alpha_{11} & 0 & 0 \\ 0 & \alpha_{22} & 0 \\ 0 & 0 & \alpha_{33} \end{bmatrix}$$

The following relations of α_{ij} were used for the different fiber configuration:

$\alpha_{11} < \alpha_{22} \approx \alpha_{33}$ for unidirectional laminates (26)

$\alpha_{11} \approx \alpha_{22} < \alpha_{33}$ for plain and satin laminates (27)

Hence, $\rho(T)$ was calculated as follows:

$$\rho(T) = \frac{\rho_o}{\left(1 + \frac{\Delta L_{11}(T)}{L_{o_{11}}}\right) \cdot \left(1 + \frac{\Delta L_{33}(T)}{L_{o_{33}}}\right)^2}$$ for unidirectional laminates (28)

$$\rho(T) = \frac{\rho_o}{\left(1 + \frac{\Delta L_{11}(T)}{L_{o_{11}}}\right)^2 \cdot \left(1 + \frac{\Delta L_{33}(T)}{L_{o_{33}}}\right)}$$ for plain and satin weave laminates (29)